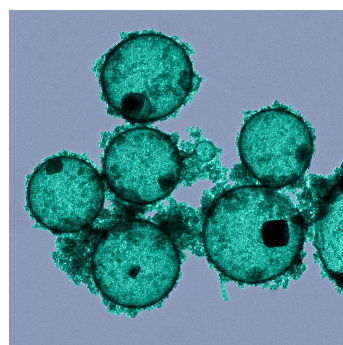
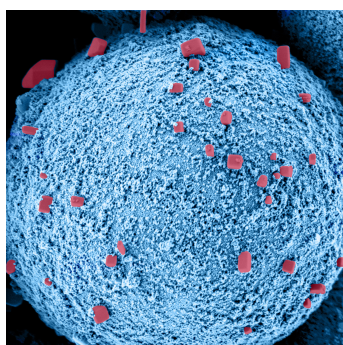
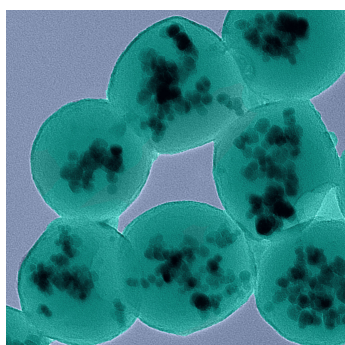




Structure Control in Polymer/Inorganic Hybrid Nanomaterials



Dissertation

zur Erlangung des Grades
„Doktor der Naturwissenschaften“
im Promotionsfach Chemie
am Fachbereich Chemie, Pharmazie und Geowissenschaften
der Johannes Gutenberg-Universität Mainz
D77 - Mainzer Dissertation

vorgelegt von

Alexander Schoth

geboren in Limburg



MAX-PLANCK-GESELLSCHAFT

Mainz, im November 2015

Dekan:

1. Berichterstatterin:
2. Berichterstatter:

Tag der mündlichen Prüfung:

Contents

1. Motivation	1
2. Theoretical Background	3
2.1. Stability of Emulsions	3
2.1.1. Stabilization by Surfactants	5
2.1.2. Miniemulsions	6
2.1.3. Stabilization with Particles – Pickering Emulsions	7
2.2. Nanocapsule Formation in Miniemulsion	8
2.2.1. Capsule Formation via Phase Separation	8
2.2.2. Capsule Formation via Interfacial Reactions	10
2.3. Synthetic Strategies for the Formation of Inorganic Nanoparticles	11
2.3.1. General Overview of Different Bottom-Up Strategies	11
2.3.1.1. Redox Reactions	11
2.3.1.2. Metathesis Reactions	12
2.3.1.3. Acid/Base Reactions	12
2.3.2. Synthesis of Silica Nanoparticles – The Stöber Process	12
2.3.3. Synthesis of Superparamagnetic Magnetite Nanoparticles	13
2.3.4. Surface Functionalization of Inorganic Nanoparticles	14
2.3.4.1. Surface Functionalization with Surfactants	14
2.3.4.2. Surface Functionalization with Substrate-Specific Groups	14
2.3.4.3. Core-Shell Particles	15
2.3.4.4. Silanization as Versatile Functionalization Technique	15
2.4. Synthetic Routes Towards Polymer/Inorganic Hybrid Nanomaterials	16
2.4.1. General overview	16
2.4.2. Hybrid Nanomaterials in Miniemulsion	17
2.4.3. The Structure of Hybrid Materials in Miniemulsion	19
2.4.4. Hybrid Materials via Pickering Emulsions	21
3. Characterization Techniques	23
3.1. Electron Microscopy	23
3.1.1. Transmission Electron Microscopy	23
3.1.2. Scanning Electron Microscopy	23
3.2. Dynamic Light Scattering	24
3.3. Thermal Analysis	25
3.3.1. Thermogravimetric Analysis	25
3.3.2. Differential Scanning Calorimetry	25

3.4. Infrared Spectroscopy	25
3.5. Calorimetric Methods	25
3.5.1. Reaction Calorimetry	25
3.5.2. Isothermal Titration Calorimetry	26
4. Results and Discussion	27
4.1. Structure Control in PMMA/Silica Hybrid Nanoparticles	28
4.1.1. Hydrophobization of Silica Particles	28
4.1.2. Encapsulation of Hydrophobized Silica Particles	30
4.1.3. Measurement of the Polymerization Kinetics	36
4.1.4. Hybrid Particles via the Solvent Evaporation Approach	37
4.1.5. Conclusions	37
4.2. Encapsulation of Magnetic Nanoparticles	39
4.2.1. Surface Functionalization of Magnetite Nanoparticles	40
4.2.2. Composition of Hybrid Materials	42
4.2.3. Structure of the Hybrid Nanoparticles	45
4.2.4. Conclusions	49
4.3. Polymer/Silica Hybrid Nanoparticles and their Structure in Coatings	49
4.3.1. Synthesis of Hybrid Particles	49
4.3.2. Physical Properties of Hybrid Particles	52
4.3.3. Film Formation	54
4.3.4. Conclusions	54
4.4. Encapsulation of Hydrophobic Liquids in the Presence of Silica Nanoparticles	57
4.4.1. Nanocapsules via Polymerization in Miniemulsion	57
4.4.2. Nanocapsules via Solvent Evaporation in Miniemulsion	59
4.4.3. Conclusions	59
4.5. Pickering-Stabilized Nanoparticles in Direct Miniemulsion	61
4.5.1. Stabilization Using Laponite Clay	61
4.5.2. Stabilization Using Silica	61
4.5.3. Conclusions	63
4.6. Pickering-Stabilized Nanocapsules in Inverse Miniemulsion	64
4.6.1. Stabilization of the Emulsions	64
4.6.2. Capsule Formation	65
4.6.3. Encapsulation of Organic Compounds	65
4.6.4. Encapsulation of Inorganic Salts	68
4.6.5. Conclusions	69
4.7. General Discussion	71

5. Experimental Part	75
5.1. Experimental Details for Section 4.1	76
5.1.1. Modification of Silica Particles with CTMA-Cl	76
5.1.2. Functionalization of Silica Particles with Trimethoxysilane Compounds	76
5.1.3. Preparation of PMMA/Silica Hybrid Particles via Polymerization . .	76
5.1.4. ITC measurements	77
5.1.5. Preparation of PMMA/Silica Hybrid Particles via Solvent Evaporation	77
5.2. Experimental Details for Section 4.2	77
5.2.1. Synthesis of Acid-Functionalized Magnetite Nanoparticles	77
5.2.2. Synthesis of Silanized Magnetite Nanoparticles	78
5.2.3. Synthesis of Hybrid Nanoparticles	78
5.3. Experimental Details for Section 4.3	78
5.3.1. Silica Functionalization	78
5.3.2. Miniemulsion Polymerization	79
5.4. Experimental Details for Section 4.4	79
5.4.1. Functionalization of Silica Particles	79
5.4.2. Preparation of Nanocapsules via Polymerization	79
5.4.3. Preparation of Nanocapsules via Solvent Evaporation	79
5.5. Experimental Details for Section 4.5	80
5.5.1. Particles Stabilized by Laponite Clay	80
5.5.2. Particles Stabilized by Ludox TMA Silica	80
5.6. Experimental Details for Section 4.6	80
5.6.1. Functionalization of Silica Particles	80
5.6.2. Preparation of Nanocapsules in Inverse Miniemulsion	80
5.6.3. Sample Preparation for Fluorescence Measurements	81
5.7. Analytical Tools	81
5.7.1. Transmission Electron Microscopy	81
5.7.2. Scanning Electron Microscopy	81
5.7.3. Dynamic Light Scattering	81
5.7.4. Thermogravimetric Analysis	82
5.7.5. Differential Scanning Calorimetry	82
5.7.6. Reaction Calorimetry	82
5.7.7. Isothermal Titration Calorimetry	82
5.7.8. Gel Permeation Chromatography	82
5.7.9. Infrared Spectroscopy	82
5.7.10. UV/Vis Spectroscopy	83
6. Summary and Outlook	85

7. Zusammenfassung und Ausblick	89
8. References	92
A. List of Figures	101
B. List of Tables	103
C. Abbreviations and Symbols	104
D. Acknowledgments	105
E. Curriculum Vitae	106
F. Scientific Contributions	107
F.1. Publications	107
F.2. Presentations	108

1. Motivation

The combination of substances with different properties is crucial in the development of functional materials. In nature, several examples of hybrid materials with distinctive properties can be found. Magnetotactic bacteria, for example, are able to produce magnetite nanoparticles and use them to align themselves in magnetic fields.^[1] Bones and teeth in the human body are formed by a combination of hydroxylapatite and peptides.^[2] The result is a composite material that combines the high modulus of the inorganic material by overcoming its brittleness. The same principle can also be applied for technical applications. In the automotive industry, tires have to meet several requirements. Besides providing good contact and grip to the street, they need to be stable enough to carry the high weight of the vehicle. This combination of requirements is fulfilled by using a combination of different materials. The main compound is natural rubber, which is very sticky and flexible. Carbon black is added to the mixture to reach mechanical stability and to suppress abrasion.

An important parameter for the performance of hybrid materials is their homogeneity. In order to reach a homogeneous product, the different materials forming the hybrid have to be mixed in an at least microscopic, better nanoscopic range. If this condition is fulfilled, the properties of the material are, in macroscopic dimensions, homogeneous. Materials with at least one dimension in the size range of nanometer are usually referred to as colloids.^[3] Colloidal materials can show unique properties that are not known for macroscopic systems. Magnetite particles with a size under 10 nm, for example, may show so-called superparamagnetism. Due to their small size, these particles consist only of one magnetic domain and show a much higher magnetization than ferromagnetic particles.^[4] These uncommon properties make inorganic nanoparticles highly interesting for a broad field of technical applications. Beside the aforementioned magnetic particles, famous examples are the use of inorganic materials as catalysts^[5] or as UV active components.^[6] Also in the biomedical field inorganic nanomaterials are of big interest as possible candidates for innovative strategies in imaging^[7] and drug delivery.^[8]

In all the previous fields it may be problematic to use the pure inorganic materials, as they are often toxic, not sufficiently dispersible or chemically unstable. In many of those cases it can be helpful to use hybrid nanomaterials to overcome these problems. The inorganic particles can be combined with polymers to obtain polymer/inorganic hybrid nanomaterials. Waterborne systems for the synthesis of these hybrid materials are highly demanded, as they are environmentally friendly and safe to operate. Different techniques are known for the synthesis of these systems, such as seeded emulsion or dispersion polymerization.^[9] With these techniques, the number of available structures is limited by the underlying reaction mechanisms. One way to enlarge the number of possible morphologies is the use of miniemulsion systems. Here, the structures are mostly determined by self-assembly processes inside the

droplets. The systems are governed by a minimization of the overall interfacial energy, which can be manipulated by change or chemical modification of the different materials.

This thesis focuses on strategies that help to control the structure of polymer/inorganic hybrid nanomaterials in miniemulsion. Hybrid particles are synthesized with different inorganic materials and varying polymer compositions. The synthetic approaches cover different techniques in direct (oil-in-water) and inverse (water-in-oil) systems. Furthermore, nanocapsules with a polymer shell and a liquid core are prepared in the presence of inorganic nanoparticles. The central parameter is the surface functionalization of the inorganic nanoparticles which is investigated regarding its influence on structure control. Different functionalization techniques are compared to find a way to overcome the thermodynamically controlled self-assembly process in favor of kinetic control. The work presents a versatile toolbox of strategies which can help to tune the structure of polymer/inorganic hybrid nanomaterials. It is, therefore, useful for a broad range of materials as well as synthetic strategies.

2. Theoretical Background

Colloidal systems are known with many different materials and states of matter and have been studied extensively over the last decades. Dispersions, for example, consist of solid particles that are dispersed in a continuous liquid phase. Polymers as well as metals or other inorganic materials are well-known as components for dispersed particles. They can be dispersed in water or a broad range of organic liquids. The colloidal mixture of two immiscible liquids is called an emulsion. Plenty of combinations of hydrophilic and hydrophobic liquids can form emulsions, and also combinations of solid particles in emulsions are well-established.

All of these systems have in common their size in the range of a few nanometer up to several microns. Due to this small size, colloidal systems have a very large inner surface that needs to be stabilized.^[3] In this chapter, some of the basic principles of colloidal systems will be explained. Section 2.1 gives an introduction to different stabilization strategies for emulsions. Besides the stabilization mechanisms of surfactants, the basic principles of miniemulsions are discussed. Furthermore, the stabilization of emulsions by solid particles, the so-called Pickering stabilization, is introduced briefly. The basic principles for the formation of nanocapsules are explained in section 2.2. Examples for the encapsulation of aqueous as well as hydrophobic liquids in polymeric and inorganic shells are presented.

In the following section 2.3, different strategies for the synthesis of inorganic nanoparticles are discussed. The synthesis of silica particles using the Stöber method^[10] as well as the synthesis of superparamagnetic iron oxide nanoparticles are focused on in detail, as these particles have been used extensively in the experiments described in this dissertation. Furthermore, several methods for the surface functionalization of inorganic particles are introduced as a fundamental prerequisite for the synthesis of hybrid materials.

The last part of this chapter, section 2.4, deals with the different types of polymer/inorganic hybrid materials. After a general overview of the field, a special attention will be paid to methods in miniemulsions as well as on Pickering emulsions.

2.1. Stability of Emulsions

Systems where droplets are dispersed in another liquid phase are called emulsions. Generally, emulsions can be divided in three main types: macro-, micro- and miniemulsions.^[3,11] These three types differ in terms of size and stability of the dispersed droplets. All these types have in common the necessity of a surfactant in order to ensure stability over a certain period. For most of the systems, energy input is required to reach small droplet sizes. This energy can be inserted for instance by stirring, ultrasonication or the use of high pressure homogenizers.^[11] Emulsions can also be classified by the properties of their continuous and dispersed phases. Oil-in-water emulsions (O/W) are referred to as direct emulsions, while water-in-oil (W/O) systems are called inverse emulsions.^[3] Direct emulsions are of great importance for industrial

applications, as water is environmentally friendly and can help to avoid the use of organic solvents.^[12] Inverse emulsions are beneficial for example for the synthesis of core-shell systems with aqueous cores, which are hard to synthesize by other techniques.^[13]

Emulsions with droplet sizes of 0.1–10 μm are referred to as macroemulsions. They usually contain a high amount of surfactant and are created by fast stirring. Macroemulsions are kinetically stabilized by the surfactant, but are not thermodynamically stable. Droplet growth occurs over time, leading to a relatively fast phase separation.^[3]

In contrast to macroemulsions, microemulsions are thermodynamically stable. The surfactant concentration is clearly above the critical micellar concentration (cmc). In addition to the surfactant, a so-called co-surfactant is added. These molecules assemble in between the surfactant molecules at the interface and help to further lower the interfacial tension. A typical example for such a system is the combination of sodium dodecyl sulfate (SDS) as surfactant and pentanol as co-surfactant.^[14] As microemulsions are thermodynamically stable, they form spontaneously and do not need further homogenization. Typical droplet sizes for microemulsions are in the range of 5–100 nm.^[3]

The third type of emulsions is the miniemulsion with droplet sizes of about 50–500 nm. As the macroemulsion, it is kinetically stabilized and not thermodynamically stable. The surfactant concentration is below the cmc, but stabilization is improved by the addition of an osmotic agent.^[15] This approach is explained in detail in section 2.1.2.

In general, there are two main reasons for the growth of droplets in emulsions: coalescence and Ostwald ripening.^[16] These mechanisms are shown schematically in Figure 2.1. Coalescence is caused by collisions of droplets with each other. Due to stirring or Brownian motion, the droplets move and, therefore, collide. These collisions can lead to fusion of the droplets and end up in larger droplets.^[3] Coalescence can be suppressed by the addition of a surfactant, which is described more in detail in section 2.1.1. Ostwald ripening describes the diffusion of material from a small droplet to a larger one. Suppression of Ostwald ripening can be reached by the addition of an osmotic agent.^[16] This approach is discussed in section 2.1.2.

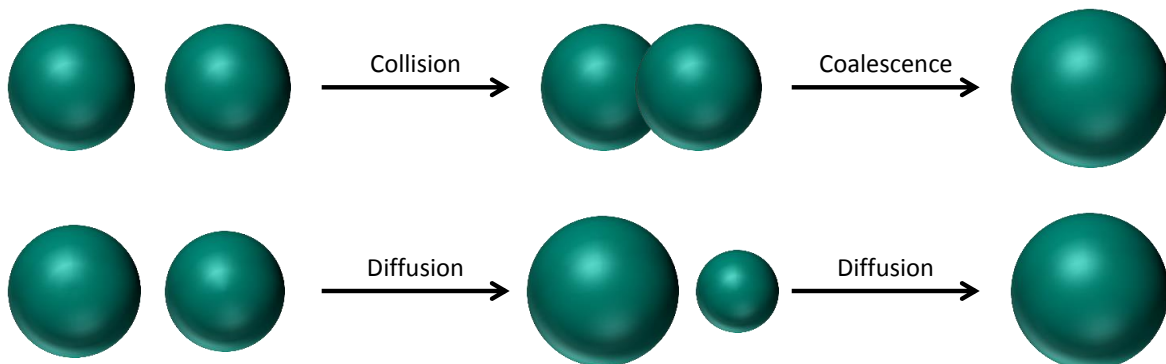


Figure 2.1: Coalescence and diffusion (Ostwald ripening) lead to a growth of the average droplet diameter and diminish the number of droplets.^[3]

2.1.1. Stabilization by Surfactants

Surfactants play an overall important role in the stabilization of emulsions. They help to prevent droplet collisions and, therefore, keep the droplet size small and homogeneous. This effect is reached by two mechanisms, which are shown schematically in Figure 2.2.

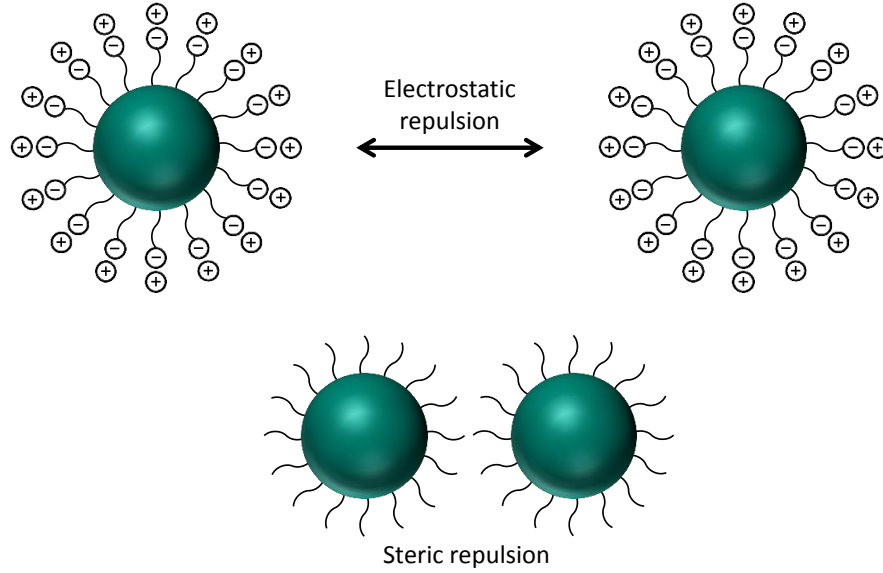


Figure 2.2: Surfactants prevent the collision of droplets by electrostatic and steric stabilization.^[3]

The first strategy is *electrostatic stabilization*. Many surfactants carry charged groups. Typical examples are sulfate or phosphate groups for anionic and ammonium groups for cationic surfactants. When the surfactants are assembled at the liquid/liquid interface and two droplets approach each other, the identical surface charges repel each other due to Coulomb repulsion and avoid droplet collision.^[3] This effect depends on the conditions in the continuous phase. For example, the pH has to be suitable to keep the surfactants charged. Furthermore, the salt concentration has to be low in order to allow electrostatic interaction of the droplets over a sufficient distance.^[17]

The second mechanism is *steric stabilization*. This effect also plays a role for ionic surfactants, but it is the predominant mechanism for non-ionic surfactants, such as block copolymers. As two droplets approach each other, the polymer chains of the surfactants get in contact and interact. In this case, two effects have to be taken into account that cause repulsion of the droplets. Firstly, the mobility of the chains is reduced due to the reduction of free space. In consequence, the number of possible chain configurations and, therefore, the entropy of the system is reduced.^[17] As second effect, the higher number of polymer chains between the droplets leads to a concentration gradient. This gradient causes an osmotic pressure between the droplets and they repel each other.^[3]

2.1.2. Miniemulsions

Besides the suppression of coalescence by the use of surfactants, a second strategy is necessary to keep miniemulsions stable over a longer time. As coalescence plays only a minor role in the destabilization of miniemulsions,^[18] Ostwald ripening needs to be suppressed effectively. The reason for Ostwald ripening, as it is shown in Figure 2.1, is the Laplace pressure p_L . It can be calculated using the interfacial tension γ between the two phases and the radius r of the droplet:^[3]

$$p_L = \frac{2 \cdot \gamma}{r} \quad (2.1)$$

The Laplace pressure is caused by the interfacial tension and describes the pressure difference between the inside and the outside of a curved surface.^[19] According to equation (2.1), p_L is higher for smaller droplets. In consequence, small differences in droplet size lead to a diffusion of material from the smaller to the bigger droplet. At the end, the small droplet is completely transferred to the bigger one.^[16] In miniemulsions, an osmotic agent is added to suppress this diffusion. This agent should be well soluble in the dispersed phase, but insoluble in the continuous phase. Typical examples are hexadecane for direct systems and inorganic salts, such as sodium chloride, for inverse systems.^[20] The effect of these agents is shown in Figure 2.3. When diffusion occurs, the concentration of the osmotic agent in the shrinking droplet increases. The higher concentration causes a rise of the osmotic pressure Π_{osm} in the droplet, which can be calculated using equation (2.2):^[19]

$$\Pi_{\text{osm}} = \frac{R \cdot T \cdot c}{M} \quad (2.2)$$

In this equation, R is the universal gas constant, T the temperature, c the concentration of the osmotic agent and M its molecular weight. The osmotic pressure counteracts the Laplace pressure and hinders inter-droplet diffusion. In consequence, reactions like polymerization or crystallization occur within each droplet, which makes them usable as nanoreactors.^[16] Due to the combination of surfactant and osmotic agent, coalescence as well as Ostwald ripening are effectively suppressed in miniemulsions, leading to a kinetically stabilized system for up to several months.^[21]

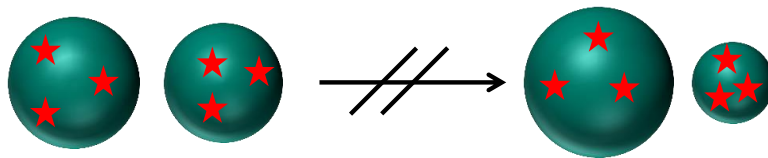


Figure 2.3: Suppression of Ostwald ripening by the addition of an osmotic agent.

2.1.3. Stabilization with Particles – Pickering Emulsions

An alternative way to stabilize emulsions is to use a layer of adsorbed particles instead of surfactants. This type of stabilization is named after S.U. Pickering, who firstly described this effect in 1907.^[22,23] Stabilization of emulsions is possible with particles formed of many different materials such as metal oxides, polymers or organic compounds.^[3] One of the most common materials are clay minerals. Due to their platelet structure, these materials provide a good coverage of the droplet surface and form a stable film.^[24] This is also the basic principle of Pickering stabilization: particles adsorb to the liquid/liquid interface and form a mechanically stable layer. This layer protects the droplets when they collide with each other and, therefore, effectively suppresses coalescence.^[3]

In contrast to the stabilization with surfactants, there are two major differences in particle-stabilized systems. Firstly, the particles are irreversibly attached to the liquid/liquid interface. There is no adsorption/desorption equilibrium as it is observed for surfactants. Secondly, adsorbed particles do not influence the interfacial tension between the two liquid phases.^[25] Due to the stabilization with a mechanically stable film, Pickering emulsions are very robust towards outer influences. The emulsions usually do not break in the presence of high amounts of salts or under acidic or basic conditions. Generally, the composition of the continuous phase does not have a big influence on the stability of the emulsion.^[3]

The stability of Pickering emulsions depends directly on the ability of the particles to form a film at the liquid/liquid interface. This ability is described by the adsorption energy ΔE , which can be calculated using equation (2.3):^[26]

$$\Delta E = \pi \cdot r^2 \cdot \gamma \cdot (1 - \cos(\Theta))^2 \quad (2.3)$$

Besides the radius r of the particles, ΔE depends on the interfacial tension γ between the two liquid phases and on the contact angle Θ of the particles at the liquid/liquid interface.^[27] The contact angle Θ has to be close to 90° to make the particles wettable in both liquid phases. Only this both-sided wettability enables film formation at the liquid/liquid interface.^[28,29] The influence of the contact angle on the stabilized system is shown schematically in Figure 2.4.

The exact adjustment of the contact angle determines which kind of emulsion a system of particles and two liquids will form. In general, particles can stabilize the liquid phase in which they have a lower wettability.^[30] As shown in Figure 2.4, systems with a contact angle $\Theta < 90^\circ$, this means with slightly hydrophilic particles, will form direct emulsions. Hydrophobic particles with a contact angle of $\Theta > 90^\circ$ stabilize inverse emulsions.^[29] In the very rare case of $\Theta = 90^\circ$, theoretical calculations predict the formation of bicontinuous emulsions, the so-called bijels (bicontinuous interfacially jammed emulsion gels).^[31]

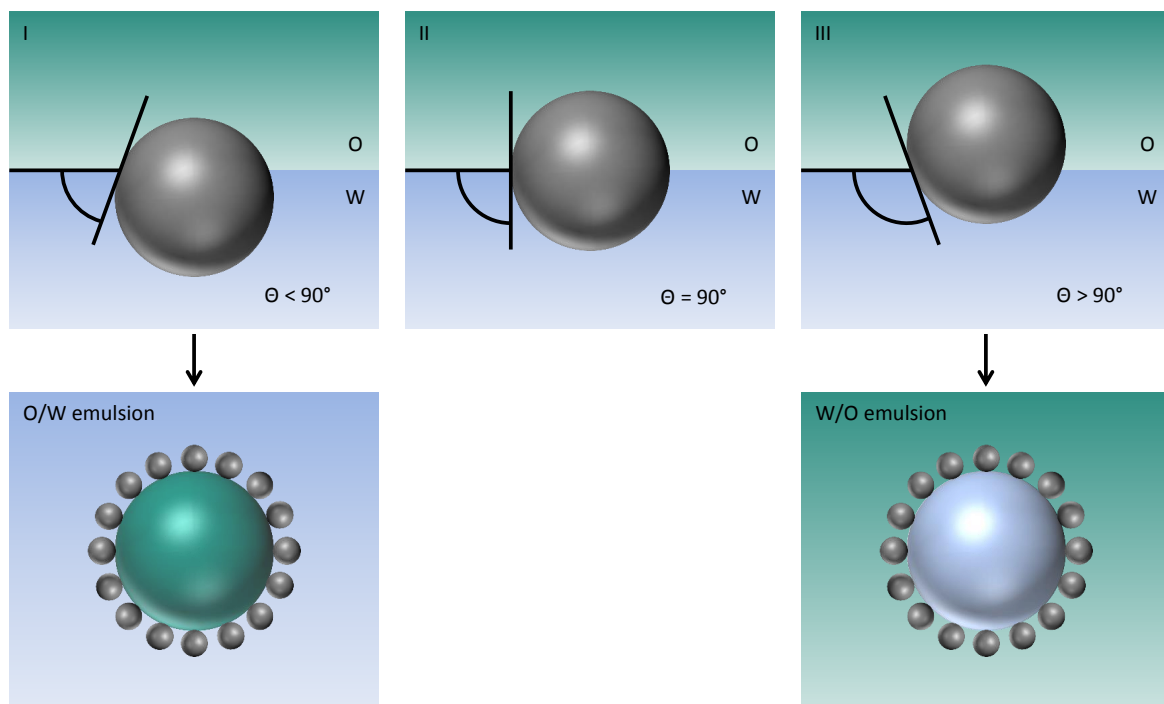


Figure 2.4: The contact angle of particles at the oil/water interface is crucial for their ability to stabilize oil-in-water (O/W) or water-in-oil (W/O) emulsions.^[29]

2.2. Nanocapsule Formation in Miniemulsion

Nanocapsules consist of a solid shell and a liquid core. There are plenty of possible materials for both of these phases. The liquid core can consist either of water, aqueous solutions, or other hydrophilic and hydrophobic liquids. The shell can be formed by polymers as well as inorganic materials such as silica. The synthetic strategy for nanocapsules depends on the desired combination of materials. Hydrophobic liquids can be encapsulated in direct miniemulsions, while hydrophilic liquids require the use of inverse miniemulsions. These systems also affect the possible synthetic routes. In direct systems, core and shell material are usually present simultaneously inside the droplet before phase separation forms the capsule morphology. In inverse systems, capsule formation is mainly initiated by two-component reactions at the liquid/liquid interface.

2.2.1. Capsule Formation via Phase Separation

According to a model described by Torza and Mason,^[32] the morphology of a system consisting of three immiscible liquid phases, where two of them are combined in the dispersed phase, can be described using the spreading coefficient s_i . This coefficient depends on the interfacial

tensions between the different phases and can be calculated by:

$$s_i = \gamma_{jk} - (\gamma_{ij} + \gamma_{ik}) \quad (2.4)$$

γ describes the interfacial tensions between the different components i, j and k , while s_i represents the spreading coefficient of compound i . For a three-phase system, three general situations can be described. The following examples describe a system, where phase 1 and 3 are immiscible, hydrophobic oils, while phase 2 is an aqueous surfactant solution. The morphologies of the systems are shown in Figure 2.5:

- I)
 - Oil 3 is much more hydrophobic than oil 1 ($\gamma_{12} > \gamma_{23}$).
 - The surface tension between the oil phases is low ($\gamma_{31} < (\gamma_{12} + \gamma_{23})$).
 - $\Rightarrow s_1 < 0, s_2 < 0, s_3 > 0$
 - \Rightarrow Core-shell morphology
- II)
 - The hydrophobicity of oil 1 and oil 3 is similar ($\gamma_{12} \approx \gamma_{23}$).
 - The surface tension between the oil phases is low ($\gamma_{31} < (\gamma_{12} + \gamma_{23})$).
 - $\Rightarrow s_1 < 0, s_2 < 0, s_3 < 0$
 - \Rightarrow Partial engulfment of oil 1
- III)
 - The hydrophobicity of oil 1 and oil 3 is similar ($\gamma_{12} \approx \gamma_{23}$).
 - The surface tension between the oil phases is high ($\gamma_{31} > (\gamma_{12} + \gamma_{23})$).
 - $\Rightarrow s_1 < 0, s_2 > 0, s_3 < 0$
 - \Rightarrow Two separated droplets

In consequence, the value of the spreading coefficient s_i and, therefore, the interfacial tensions between the different phases helps to predict the morphology of the resulting system.

The model described above can also be applied to systems, where one of the oils is replaced by a solid.^[33] To determine the structure of this system, the Gibbs free enthalpy G has to be calculated:

$$G = \sum_{ij}^n \gamma_{ij} A_{ij} \quad (2.5)$$

Here, γ_{ij} describes the interfacial tension between the phases i and j . A_{ij} is the area of this interface. For a thermodynamically stable system, G has to reach a minimum. The morphology of the system is determined by the minimization of the overall interfacial energy. The most favorable structure of the material is, therefore, the assembly, in which the interfacial tensions and interfacial areas between the three phases result in the lowest interfacial energy G .

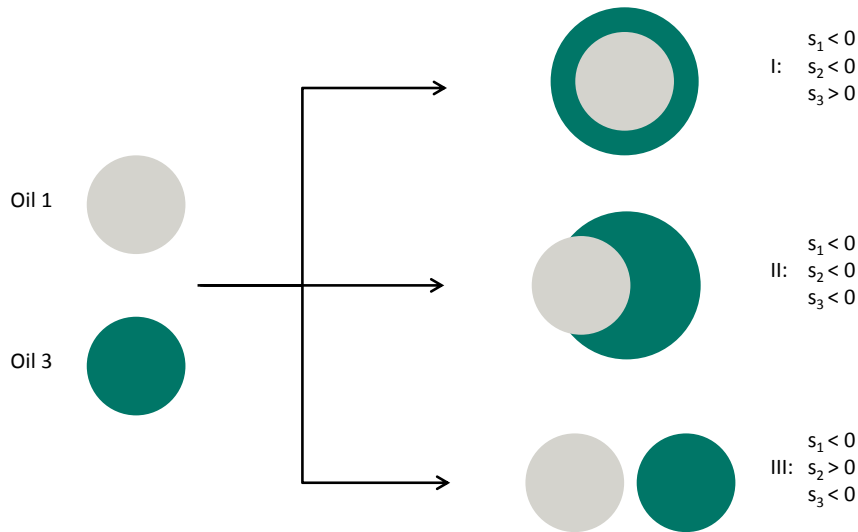


Figure 2.5: Resulting morphologies for different combinations of spreading coefficients s_i . The schemes show capsule formation (I), partial engulfment (II) and complete separation (III).^[32]

In miniemulsion, the phase separation process can occur either during a polymerization reaction^[34] or during evaporation of a solvent.^[35] Both techniques will be discussed in detail in section 2.4.2. Possible payloads that can be encapsulated using this strategy are for instance fragrances^[34] or vegetable oil.^[36]

2.2.2. Capsule Formation via Interfacial Reactions

Inverse miniemulsions with a hydrophilic dispersed phase and a hydrophobic continuous phase offer the possibility to encapsulate hydrophilic, water-soluble substances. These substances can be for example drugs, biological materials such as DNA or RNA, or contrast agents.^[37] The capsule shells are in these cases formed by an interfacial reaction of two chemicals. Usually, one reactant is dissolved inside the droplets and the other one is added via the continuous phase. When both reagents meet at the liquid/liquid interface, they react and form a solid capsule shell.

The most important example for interfacial polymerizations in miniemulsion is polyaddition with diisocyanates. The diisocyanates are added to the continuous phase, while the dispersed, aqueous phase contains compounds with hydroxyl or amine groups. When the reagents meet at the liquids/liquid interface they react and form polyurethane and polyurea shells.^[38] Besides low-molecular reagents such as diamines and diols, biopolymers like hydroxy ethyl starch or chitosan can be the water-soluble compounds. In these cases, biocompatible or biodegradable capsule shells can be synthesized.^[39] Alternative polymerization techniques

for inverse systems are radical polymerization^[40] and ionic polymerization.^[41]

Instead of polymers, shells can also be formed by inorganic materials. One example is the precipitation of silica at the interface.^[42] Tetraethyl orthosilicate is added to the continuous phase and precipitates at the interface due to a high pH value of the aqueous phase. Transition metal oxides have also been precipitated successfully at the water/oil interface to form capsule morphologies.^[43,44]

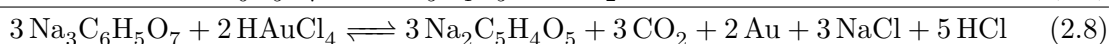
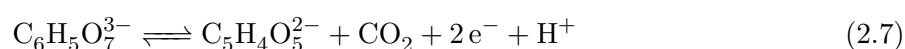
2.3. Synthetic Strategies for the Formation of Inorganic Nanoparticles

Inorganic particles are of overall importance as functional materials and are widely used in plenty of applications. One of the most famous examples is the use of the UV active materials like titania (TiO₂) and zinc oxide (ZnO) as UV absorbing ingredients for coatings or as photocatalysts. Also iron oxide nanoparticles or metal nanoparticles are often used because of their unique magnetic and electrochemical properties. Another field of application is the use as filler material to improve the chemical and mechanical resistance of a material without negative effects on the homogeneity or optical clarity. In this field, silica (SiO₂) is a common material because of its low price and good processability.

The production of inorganic nanoparticles can be divided into two main strategies: the *top down* and the *bottom up* approaches.^[45] In the top down approach, the material is produced in macroscopic dimensions and afterwards crushed to reach the desired particle size. A common method is ball milling, where the inorganic material is put into a cylinder together with balls made of a hard material (e.g., tungsten carbide). The balls grind the inorganic material and break it down to nanoscopic particle sizes. This technique is cheap and allows to process large amounts of material. Unfortunately, the obtained particles are very heterogeneous regarding size and shape, which has a negative influence on their electrical, optical, and mechanical properties.^[46] For a higher homogeneity and a better control over the particles' properties, bottom up methods have to be used. Here, the particles are synthesized directly in a nanoscopic size and the properties can be tuned precisely.

2.3.1. General Overview of Different Bottom-Up Strategies

2.3.1.1. Redox Reactions Redox reactions are used for the synthesis of many metallic nanoparticles such as gold or cobalt. Metal salts are reduced to the pure metal using reduction agents like sodium borohydride. An example is the synthesis of gold nanoparticles using chloroauric acid and sodium citrate:^[47]



2.3.1.2. Metathesis Reactions The second class of synthesis strategies are the metathesis reactions. Here, two salts react with each other and exchange their counterions or ligands. A famous example is the synthesis of cadmium sulfide (CdS) nanoparticles:^[48]



2.3.1.3. Acid/Base Reactions Most metal oxides are produced via acid/base reactions. Two examples are the oxides of zinc and titanium:^[6]



Another nanomaterial which is produced in industrial scale is silica. This synthesis usually follows the Stöber process,^[10] which is described in detail in the following section 2.3.2.

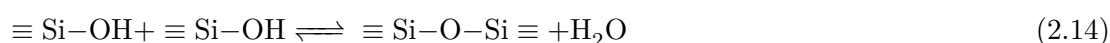
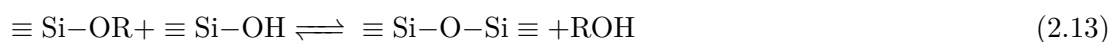
2.3.2. Synthesis of Silica Nanoparticles – The Stöber Process

Silica nanoparticles are accessible via sol–gel chemistry. They are synthesized from tetraalkoxy silanes via a condensation reaction. The alkoxides (Si–OR) are hydrolyzed to silanols (Si–OH). These species can then condensate to siloxanes (Si–O–Si):^[49]

Hydrolysis:



Condensation:



Overall:



As most alkoxides are not soluble in pure water, alcohols or alcohol/water mixtures have to be used as solvents for the reaction. Additionally, catalysis with acids or bases is necessary. The resulting mixture is a highly complex system of coupled equilibria which depend on many different parameters:^[49]

- type of precursors

- ratio of alkoxy groups to water
- type of catalyst (acid or base)
- solvent
- temperature
- pH value

Due to different mechanisms, the reactions can be divided into acidic and basic systems. With acidic catalysts, the growth of long chains is preferred. Under basic condition, branched networks are favored. To obtain particles, the number of siloxane bonds has to be maximized. This is reached by the use of basic catalysts, while acidic catalysts promote the formation of gels.

The Stöber process was first described by Stöber et al. in 1968.^[10] They described the synthesis of monodisperse silica particles from tetraalkyl silanes such as tetraethyl orthosilicate (TEOS). The tetraalkyl silanes are dissolved in an alcohol and, after addition of ammonia, react to silica particles. The pH in these systems is typically in the range of 9 to 10. Under these conditions, condensation reactions are much faster than hydrolysis.^[49] In consequence, hydrolyzed species are consumed immediately, which favors the formation of clusters. Another important effect is that hydrolytic cleavage of terminal siloxane bonds is quite fast in the applied pH range. This leads to a constant source of available monomers and inhibits the growth of long chains. In general, Ostwald ripening is a prominent mechanism and supports the formation of particles while hindering gelation.^[49]

With the Stöber process, silica particles in the size range of 5–5000 nm can be obtained. Precise size control is possible by adjusting the concentrations of the different reactants in solution. For this, the initial concentrations of alkoxy silanes, solvents and catalysts as well as temperature and pH have to be regulated accurately.^[10] For the experiments in this dissertation, a commercial silica dispersion with a particle diameter of 22 nm is used.

2.3.3. Synthesis of Superparamagnetic Magnetite Nanoparticles

Superparamagnetic particles are paramagnetic particles in the size range of Weiss domains. In these particles, a strong magnetic field is induced upon application of an external magnetic field without retentivity. As all spins in a particle are aligned, the particles are highly magnetic already at small external fields. Superparamagnetic particles typically consist of transition metal oxides with a spinel structure (M_3O_4). The size range is usually in the range of 4–25 nm.^[4] The most prominent examples are magnetite particles (Fe_3O_4).

For the synthesis of superparamagnetic nanoparticles, two major routes are used: thermal decomposition or a change of pH. In the thermal decomposition route, high temperatures

lead to the the decomposition of precursor molecules followed by nucleation and crystal growth. This technique usually gives a very narrow size distribution, but the experimental requirements regarding temperature control are quite high.^[50] In the second strategy, an increase in pH leads to deprotonation of the precursors and, therefore, to the formation of particles.^[51,52] Compared to thermal decomposition, this technique gives a much broader size distribution, especially under basic conditions.^[53] However, the magnetite nanoparticles used in this dissertation were synthesized following the second route. The obtained particles were about 5 nm in diameter and the size distribution was sufficiently narrow for encapsulation experiments.

2.3.4. Surface Functionalization of Inorganic Nanoparticles

After synthesis, most inorganic nanoparticles show a homogeneous composition with the same material in the inner regions and on the surface. The surface is usually hydrophilic, as it often carries charged groups. This structure of inorganic particles might not be useful for many types of applications as there can be a lack of reactive groups on the surface, no sufficient stability in dispersions or no biocompatibility. For the systems dealt with in this dissertation, the most important drawback of pure inorganic particles is their incompatibility with hydrophobic substances. In the following sections, several strategies for the surface functionalization of inorganic nanoparticles will be presented. The categories are divided by the type of binding between particle surface and functionalization agent.

2.3.4.1. Surface Functionalization with Surfactants Surfactants offer a very intuitive way to change the surface properties of nanoparticles, as they easily adsorb to it. Especially surfactants with positively-charged headgroups such as ammonium salts are suitable, as they can be attracted electrostatically by the often negatively charged particle surface.^[54,55] Surfactants are useful to change the hydrophobicity of the particles and to stabilize aqueous or non-aqueous dispersions. However, the adsorption of surfactants on the surface is reversible and they adsorb and desorb in a dynamic equilibrium.^[55] Therefore, the surfactants can be removed easily. The system is very sensitive to changes in outer parameters (which often happens during reactions) and hard to control.

2.3.4.2. Surface Functionalization with Substrate-Specific Groups Some functional groups show an exceptionally high affinity towards certain materials. This effect can be used to easily functionalize these materials. A famous example is the use of carboxylic acids like oleic acid for the functionalization of magnetite. The acid groups act as chelating ligands and form stable connections to the magnetite.^[51] Another example is the functionalization of gold nanoparticles with thiols. In both examples, the functionalization agents form a quite stable bond to the substrates and are much harder to remove than the surfactants described in

the previous section.^[47] This technique also offers the possibility to introduce reactive groups that can act for example as catalysts or comonomers. Unfortunately, this type of surface functionalization is limited to a few pairs of substrate and functionalization agent. Another disadvantage can be that the specific group itself can disturb reactions. Thiol-capped gold nanoparticles, for example, can be hard to encapsulate via radical polymerization, as the thiol groups might act as scavengers for the radicals.^[56]

2.3.4.3. Core-Shell Particles Especially for more sophisticated inorganic materials, it might be hard to find a suitable functionalization agent. In many of these cases, it can be helpful to coat the particle with a layer of another material. Depending on the material and desired application, this shell can have a thickness of up to several nanometers without negative effects on the performance of the particles (e.g., magnetism or optical properties). The most common coating materials for this strategy are polymers^[57,58] and silica.^[59] After coating, the properties of the shell material can be used directly (e.g., a hydrophobic polymer layer) or the new shell material is much easier to functionalize than the initial core material (e.g., silica).

2.3.4.4. Silanization as Versatile Functionalization Technique The main technique used for the experiments in this dissertation is the silanization with trimethoxy silanes. Regarding the categories described before, this technique can be seen as specific strategy for silica particles (as in section 4.1, 4.3, 4.4 and 4.6) or as functional silica shell for magnetite nanoparticles (as in section 4.2). The silane chemistry offers a broad spectrum of accessible functional groups.^[60] It is easy to use and very versatile regarding the substrate material, which can be inorganic materials (like silica and magnetite) or several polymers.^[61–63] The reaction mechanism of the silanization is very similar to the Stöber process described in section 2.3.2 and is explained in detail in Figure 2.6.

In a basic environment, the trialkoxy silanes are hydrolyzed to silanols. In the next step, these silanols condensate and form oligomers, which adsorb to the particle surface. These steps together form a coupled equilibrium that is extremely sensitive towards changes in the parameters of the system. It is important to properly control the reaction conditions, such as concentrations, temperature and especially pH, to achieve a reproducible functionalization. The equilibration time of the system can take from a few hours up to several days. Heating of the mixture leads to condensation of the adsorbed oligomers on the silica surface. The functionalization agent is then attached covalently to the particle. Afterwards, the particles have to be dried to remove excess water and, therefore, make the connection between particle and functionalization agent irreversible.^[64]

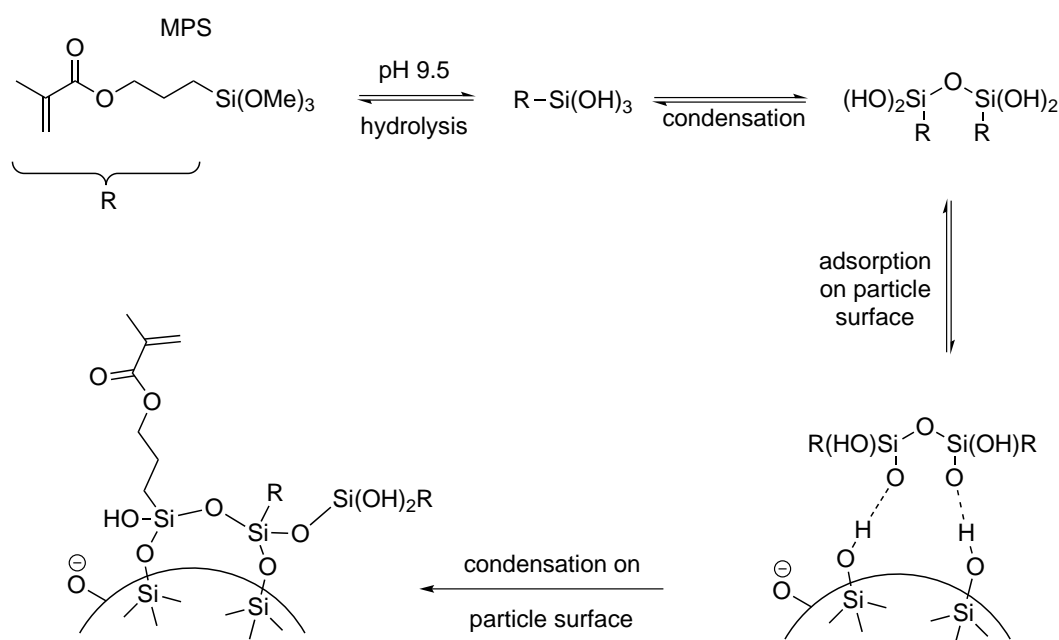


Figure 2.6: Functionalization of silica nanoparticles with trimethoxysilanes. The functionalization agent 3-methacryloxypropyl trimethoxysilane (MPS) has been used for several experiments presented in this thesis.^[64]

2.4. Synthetic Routes Towards Polymer/Inorganic Hybrid Nanomaterials

2.4.1. General overview¹

Polymer/inorganic hybrid nanoparticles are highly attractive in both academic and industrial research. They are able not only to combine the properties of both components, polymers and inorganic matter, but also to provide unique and tunable properties. Industrially important features of polymers such as poly(methyl methacrylate) (PMMA) are, for example, flexibility, optical clarity, and excellent dimensional stability, whereas inorganic materials show mechanical strength, thermal stability, and a high modulus. Even more important for many industrial applications are the optical, magnetic, and electronic properties of many inorganic materials, such as titania,^[65] cadmium selenide,^[66,67] or magnetite.^[68,69] To benefit from these properties and to make them accessible for particular applications, the combination with polymer materials is often necessary.^[70,71] As an example, the use of polymers as supporting materials can help to avoid agglomeration of the inorganic material in coating applications.^[72–74] They can also either protect reactive materials for catalytic applications or, vice versa, provide a better contact to the surrounding reaction medium.^[75] In other fields,

¹This section is based on the publication “Structure Control in PMMA/Silica Hybrid Nanoparticles by Surface Functionalization” by Alexander Schoth, Caroline Wagner, Lena L. Hecht, Svenja Winzen, Rafael Muñoz-Espí, Heike P. Schuchmann and Katharina Landfester, published 2014 in *Colloid and Polymer Science*, volume 292 on the pages 2427 to 2437. © 2014, with kind permission from Springer Science and Business Media.

like biomedicine, the use of hybrid materials can minimize the risk of a toxic shock by making inorganic materials biocompatible^[68,76] and protecting drugs from metabolization.^[13,77]

Heterophase polymerization methods like dispersion,^[9,78] suspension,^[79,80] or seeded emulsion polymerization^[9,81,82] are reported in literature for the synthesis of polymer/inorganic hybrid nanoparticles. A big challenge in these systems, however, is the control of morphology. The attainable morphologies of these systems are limited to hybrids with the inorganic particles at the surface^[83] or to single inorganic particles covered by a polymer shell.^[84] The miniemulsion technique is a suitable way to overcome these problems.^[85] Here, the monomer droplets are kinetically stabilized and diffusion between the droplets, and therefore Ostwald ripening, is effectively suppressed by the addition of an osmotic reagent. As a consequence, the droplets loaded with inorganic particles ideally stay constant in size and shape. They can be transformed into hybrid particles and their morphology is directly connected to the morphology of the loaded miniemulsion.^[86]

2.4.2. Hybrid Nanomaterials in Miniemulsion

For the encapsulation of inorganic particles in miniemulsions, the particles are dispersed inside the emulsion droplet during polymerization. A schematic description of the process is given in Figure 2.7. As already described in section 2.3.4, surface functionalization of the hydrophilic, inorganic particles is absolutely crucial in order to make them compatible with the hydrophobic monomer phase. After functionalization, they can be dispersed in the organic phase and the miniemulsion can be prepared by homogenization under high shear forces, e.g. using ultrasound. In a next step, the miniemulsion is polymerized and the loaded monomer droplets become hybrid particles.

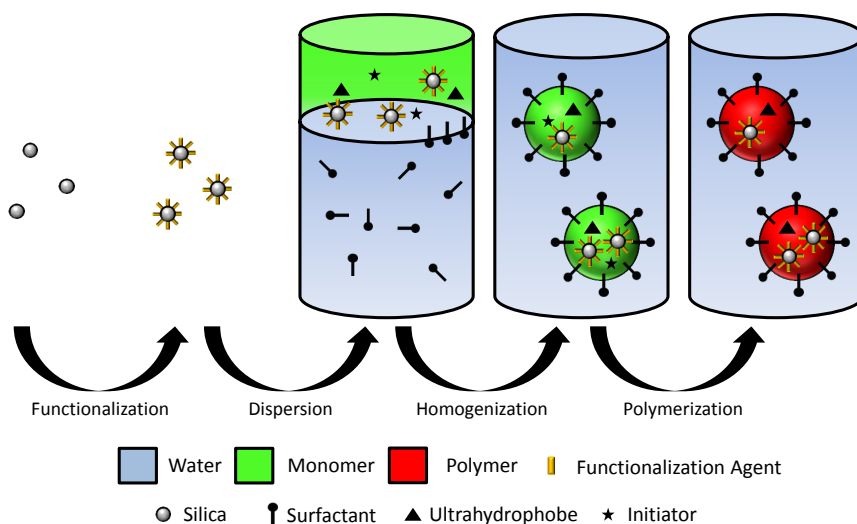


Figure 2.7: Scheme for the preparation of polymer/silica hybrid particles by the miniemulsion polymerization technique.^[87]

Hybrid nanoparticles prepared in miniemulsion can be helpful in many fields of application, for example as adhesives,^[88] anticorrosives,^[89] responsive materials^[90] or for energy storage.^[91] Miniemulsion polymerization is a very versatile technique that offers the possibility to combine a broad variety of materials. As inorganic particles, for example silica,^[54,61,87] magnetite,^[51,69] titania,^[92] zinc oxide,^[93] gold,^[47] and nickel^[94] have been encapsulated successfully. Additionally, the technique is not limited to inorganic materials. Also the encapsulation of other solid particles, such as organic pigments, has been reported.^[73] As polymers, most hydrophobic materials such as poly (methyl methacrylate) (PMMA),^[54,87] polystyrene^[93,95] or polylactide^[96] can be used.

Encapsulation in miniemulsions also works in inverse systems. Here, the inorganic particles stay hydrophilic and are dispersed in water droplets, while the continuous phase consists of an organic solvent such as cyclohexane. The inorganic particles are in principle the same as in direct systems, for example magnetite,^[97,98] zinc oxide,^[99] clay^[100] or nickel.^[101] The polymers have to be water-soluble, as polymerization occurs inside the water droplets. Possible candidates are polyacrylamide,^[97,100] poly(acrylic acid)^[99] or poly(hydroxyethyl methacrylate).^[98] As the inorganic material and the polymer are compatible with the water droplets, it is also possible to synthesize hybrid particles in a one-pot system. The inorganic material can be precipitated from precursors inside the water droplets, followed by subsequent encapsulation with a polymer.^[102]

A different strategy is the synthesis of particles via the solvent evaporation technique, as it is described in Figure 2.8. Instead of a monomer as in the polymerization route, a pre-formed polymer is used. This polymer is dissolved in an organic solvent such as chloroform or toluene. The miniemulsion droplets are then formed by this polymer solution. In the next step, the organic solvent is evaporated. During evaporation, the polymer precipitates inside the droplets and forms particles.^[103]

Hybrid particles are obtained in the same way as in miniemulsion polymerization. The surface-functionalized particles are dispersed in the organic polymer solution and, after homogenization, in the droplets. During evaporation of the solvent and precipitation of the polymer, the particles stay inside the droplet and become part of the developing hybrid particle. In general, this technique offers the possibility to encapsulate the same materials as the polymerization route while avoiding chemical reactions inside the droplet.^[96,104–106] Therefore, the chemical composition of the hybrid particles and the properties of the pre-formed polymer can be controlled very precisely.

However, the presence of inorganic particles in the preparation process of a miniemulsion leads to some complications. Solid particles inside a droplet increase the overall viscosity of the droplet by hindering its deformation. Therefore, a higher shear force is necessary for droplet break-up.^[107] In the beginning of the homogenization process, some droplets contain more inorganic particles than others. Due to the higher viscosity of the filled droplets, this

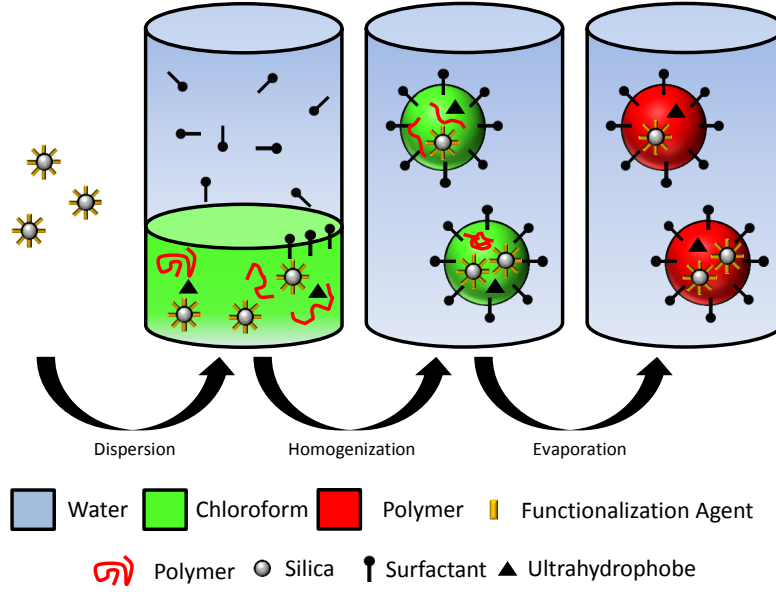


Figure 2.8: Scheme for the preparation of polymer/silica hybrid particles by the miniemulsion solvent evaporation technique.

inhomogeneity increases during homogenization. The highly-loaded droplets are not broken up and stay large, while the empty droplets become smaller. The result is a high number of small, empty droplets and a low number of larger droplets with high solid content.^[107,108] To overcome this problem, a stronger and more homogeneous shear field is necessary. This can be achieved by using high pressure homogenizers instead of ultrasound. This process requires a more detailed optimization of the parameters but leads to a more homogeneous distribution of the inorganic material and to a lower polydispersity of the resulting hybrid particles.^[108]

2.4.3. The Structure of Hybrid Materials in Miniemulsion

The control of the inner structure of hybrid particles synthesized in miniemulsion is still a challenge. In most publications, the inorganic particles are either homogeneously distributed inside the polymer, or a Janus morphology is reported with the inorganic particles aggregated on one side of the hybrid. A possible explanation for this observation is a mathematical model proposed by Gonzalez-Ortiz and Asua.^[109] In equilibrium, the morphology with the lowest interfacial energy E should develop, which is a similar principle as the explanation for capsule formation in equation (2.5):^[85]

$$E = A_{PW}\gamma_{PW} + A_{IW}\gamma_{IW} + A_{IP}\gamma_{IP} + A_{II}\gamma_{II} \quad (2.16)$$

E is expressed as the sum of the interfacial areas A_{ij} and the interfacial tensions γ_{ij} between polymer (P), inorganic material (I) and aqueous phase (W). As the surface material of all

inorganic particles is the same, γ_{II} should be very low and, therefore, this term can be neglected for the following considerations. The interfacial energy E and, as a consequence, the preferred morphology of the system can be described by the interfacial tensions γ_{PW} , γ_{IP} and γ_{IW} .

Gonzalez-Ortiz and Asua proposed a scheme to illustrate the correlations between the interfacial tensions and the different morphologies (Figure 2.9).^[109] The predictions of these considerations can be evaluated by comparison of results published by different groups.^[85]

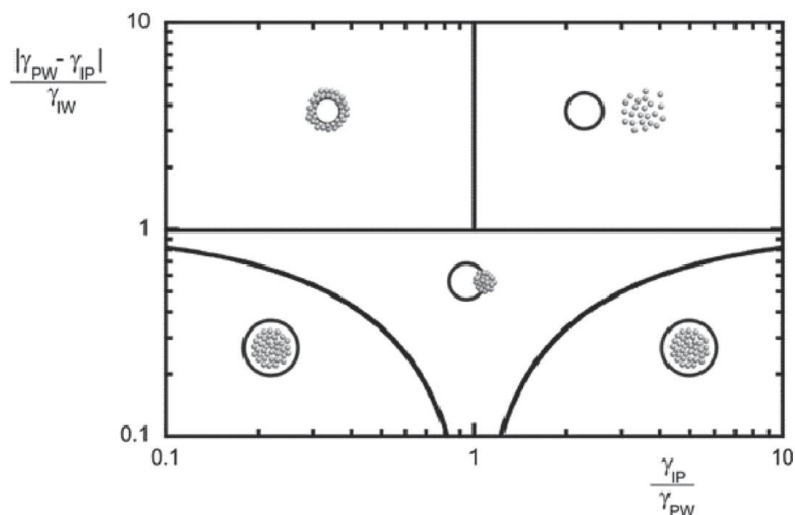


Figure 2.9: Influence of the interfacial tensions on the morphology of polymer/inorganic hybrid nanoparticles synthesized in miniemulsion. Reprinted from^[85] with permission. © 2014 John Wiley & Sons.

Asua described three main parameters that determine the inner structure of a hybrid particle. The first one is the choice of the initiator. Different groups showed that encapsulation of inorganic particles with a water-soluble initiator such as potassium peroxydisulfate (KPS) leads to a homogeneous distribution of the particles inside the polymer. In the same experiments, the use of an oil-soluble initiator like AIBN^[69] or V59^[94] leads to the formation of Janus particles. This effect can be explained by the influence of the initiators on the interfacial tension between polymer and water phase, γ_{PW} . Water-soluble initiators are usually charged in order to make them compatible with water. Therefore, when the radicals enter the hydrophobic monomer droplet, they stay close to the interface. The higher concentration of charges at the interface lowers γ_{PW} , so it is favorable to increase the interfacial area between polymer and water by keeping the inorganic particles inside the hybrid. With oil-soluble initiators, this effect does not exist, so the contact of inorganic material and the water phase is more likely and Janus structures form.^[85]

The second parameter is the concentration of the surfactant. While low concentrations lead to a homogeneous distribution of the inorganic particles inside the hybrid, high concen-

trations can promote the formation of Janus structures.^[110] At low surfactant concentrations, the material with the lower interfacial tension to water will be preferably at the interface. In most cases, this is the polymer. A high surfactant concentration lowers the interfacial tensions of water with the two other phases, γ_{IW} and γ_{PW} . In consequence, it is irrelevant, which material is in contact with the aqueous phase and Janus structures can form.^[85] The driving force for the structure is the interfacial tension between inorganic material and polymer, γ_{IP} . This observation is in accordance with the considerations concerning capsule formation described in section 2.2.1.

The interfacial tensions of the system depend mainly on the polarity of the polymer and the inorganic material. As an example, Staudt et al. showed that the encapsulation of inorganic particles in the polar MMA is possible, while the same reaction was not successful in the much less polar styrene.^[94] The polarity of the polymer determines the interfacial tensions γ_{PW} and γ_{IP} . The polarity of the inorganic material can be finely tuned by surface functionalization and influences the interfacial tensions γ_{IP} and γ_{IW} .

The theoretical model of Gonzalez-Ortiz and Asua gives a good overview of the parameters responsible for the development of differently structured hybrid particles. However, it is only valid for systems in equilibrium. The influence of the surface functionalization, especially, is limited to its effect on the interfacial tension. The introduction of reactive groups can help to form kinetically controlled morphologies, which will be discussed in detail in the sections 4.1, 4.2 and 4.3. As a result, the inorganic material as well as the polymer can be chosen independently from specific requirements concerning the interfacial tensions.

2.4.4. Hybrid Materials via Pickering Emulsions²

In the previous sections, the synthesis of hybrid materials with inorganic material inside the polymer or with a Janus structure was presented. Another type of structure is accessible via Pickering-stabilized emulsions, as they were explained in section 2.1.3. Pickering stabilization offers the possibility to prepare hybrid particles, in which the polymer particle is surrounded by a shell of inorganic particles.^[23] Pickering stabilization is a well-established technique in emulsion and miniemulsion polymerization.^[24]

The most frequently used, Pickering-stabilized polymerization technique is emulsion polymerization. The advantage of this method is that no high energy input is necessary and, therefore, the scale-up of the experiments is relatively easy. Particle sizes of the hybrid particles are usually in the micrometer range. Typical stabilizers are inorganic nanoparticles like silica,^[111,112] clay,^[113] magnetite,^[114] zinc oxide^[115,116] or titania.^[117,118] The polymers are usually formed by hydrophobic vinyl monomers like styrene,^[114,117] MMA,^[113,119]

²This section is based on the publication “Surfactant-Free Polyurethane Nanocapsules via Inverse Pickering Miniemulsion” by Alexander Schoth, Katharina Landfester and Rafael Muñoz-Espí, published in 2015 in *Langmuir*, volume 31 on pages 3784 to 3788. © 2015, with kind permission from American Chemical Society.

4-vinylpyridine^[111] or acrylonitrile.^[119] Stabilization is also possible in inverse emulsions^[120] as well as by using in situ synthesized nanoparticles as stabilizers.^[121] A very elegant method is the use of polymeric Janus particles.^[122,123] The combination of two polymers with different wettability simplifies their assembly at the liquid/liquid interface and helps to form the stabilizing particle film. As diffusion between the droplets plays a major role in emulsion polymerization, side reactions are relatively likely.^[24] Size control is possible by varying the size of the stabilizing particles^[124] or by changing the composition and polarity of the continuous phase.^[125]

Similar materials as in emulsion polymerization are also known in miniemulsion. Nanoparticles have been synthesized with a large number of differently functionalized inorganic stabilizers, such as clay,^[126–128] silica,^[54,129–132] or ceria.^[133] The synthesis of nanocapsule morphologies in direct miniemulsion has also been achieved successfully.^[129,132,134,135] In general, capsules surrounded by smaller particles are often referred to as colloidosomes. Among the inorganic nanoparticles used in the stabilization of such systems, silica is by far the most common one. Especially in direct systems, the chemical environment (e.g., pH value and salt concentration) plays an important role, as it influences the surface properties and, therefore, the stabilizing ability of the inorganic particles.^[136–138] However, the synthesis of Pickering-stabilized nanomaterials in water-in-oil systems is still a challenge. Up to now, only a few synthetic routes for nanoparticles have been successful.^[100,126,139] Pickering-stabilized capsule morphologies with a liquid hydrophilic core are only known with diameters above 10 μm .^[140,141] Smaller capsules with a size in the sub-micron range are presented in section 4.6.

3. Characterization Techniques

3.1. Electron Microscopy

Microscopic measurements in the nanometer range require the use of electron microscopes. For investigating the inner structure of nanoparticles and capsules, transmission electron microscopy (TEM) is used, while scanning electron microscopy (SEM) gives information about the surface structure of the observed material. Due to the shorter wavelength of electron beams compared to visible light, the angular resolution δ of electron microscopes is much higher than in light microscopes. The angular resolution is defined as the smallest distance between two image points that can be resolved and is described by the Abbe equation:^[142,143]

$$\delta = \frac{\lambda}{2 \cdot \eta \cdot \sin(\alpha)} \quad (3.1)$$

In this equation, λ is the wavelength of the electromagnetic wave, η is the refractive index of the medium and α is the angular aperture of the objective lense. The term $\eta \cdot \sin(\alpha)$ is often referred to as numerical aperture and describes the quality of the lense system.

3.1.1. Transmission Electron Microscopy (TEM)

TEM is a direct imaging technique, similar to standard optical microscopy. An electron beam is generated via thermal emission at a thermionic cathode at an acceleration voltage of 50–200 kV. The beam is then focused on the specimen by electromagnetic lenses. Interaction with the sample leads to scattering of the beam. Depending on the properties and the thickness of the observed material, the ratio of scattered to transmitted light varies. For example, heavy elements and thick samples lead to more scattering compared to light elements and thin samples. Due to this effect, it is possible to distinguish between inorganic material with a high scattering intensity, and polymeric material with a low scattering intensity. The transmitted electrons are detected under the sample by a CCD chip, which shows the direct image of the sample.

3.1.2. Scanning Electron Microscopy (SEM)

The generation of the electron beam in SEM is comparable to the system used in TEM. The acceleration voltage is usually smaller and in the range of 0.1–30 kV. In contrast to TEM, the sample is not observed in total, but is scanned line by line. When the electron beam hits the sample, secondary electrons are emitted from the surface and are observed by a detector sideways above the sample. The detected signal intensity and, therefore, brightness at the observed matrix spot is proportional to the number of emitted electrons and depends on the material properties. As the number of detected electrons and, therefore, the signal intensity also depends on the position of the observed spot relative to the detector, a three-dimensional

image of the sample surface is generated. This is also the reason, why the spatial resolution of SEM is not determined by the wavelength of the applied electron beam, but by the size of the different matrix points.

3.2. Dynamic Light Scattering (DLS)

Size and size distribution of nanoparticles can be measured by dynamic light scattering (DLS). A laser beam is scattered by interaction with the particles in dispersion. The scattered light can be detected in a 90° angle relative to the laser beam. Due to Brownian motion of the particles, fluctuations in density and concentration occur in the sample. These fluctuations can be observed in the intensity of the scattered light. As the speed of particle movement depends on the hydrodynamic radius R_h , the particle size can be determined by mathematical treatment of the scattering signal. Statistical fluctuations can be described by autocorrelation functions. These functions determine the average of the temporal evolution at the time τ after different starting times t . The movement of particles in the sample can be described with the van Hove autocorrelation function $G_s(\vec{r}, \tau)$:^[144]

$$G_s(\vec{r}, \tau) = \left\langle n(\vec{0}, t) \cdot n(\vec{r}, t + \tau) \right\rangle \quad (3.2)$$

As Brownian motion follows the random walk model, the van Hove function for this systems corresponds to a Gaussian function:

$$G_s(\vec{r}, \tau) = \left[\frac{2}{3} \cdot \pi \cdot \langle \Delta R(\tau)^2 \rangle \right]^{3/2} \cdot \exp \left(-\frac{3 \cdot \vec{r}(t)^2}{2 \cdot \langle \Delta R(\tau)^2 \rangle} \right) \quad (3.3)$$

The average squared displacement $\langle \Delta R(\tau)^2 \rangle$ of the particles at the time τ describes the speed of Brownian motion and gives the diffusion coefficient D :

$$\langle \Delta R(\tau)^2 \rangle = 6 \cdot D \cdot \tau \quad (3.4)$$

After elimination of the particle form factors and the influence of the scattering angle, the hydrodynamic radius R_h of the particles can be calculated via the Stokes-Einstein equation for hard spheres:

$$R_h = \frac{k_B \cdot T}{6 \cdot \pi \cdot \eta \cdot D} \quad (3.5)$$

In this context, k_B is the Boltzmann constant, T is the temperature and η is the viscosity of the solvent.

3.3. Thermal Analysis

3.3.1. Thermogravimetric Analysis (TGA)

The composition of hybrid materials were determined by thermogravimetric analysis (TGA). The main components of the device are a balance and a heater. By heating the sample constantly under detection of the weight, the organic parts of the sample evaporate, while the inorganic material remains unchanged. The result is the present weight of the sample as a function of the temperature, which tells us the ratio between organic and inorganic materials.

3.3.2. Differential Scanning Calorimetry (DSC)

Differential scanning calorimetry (DSC) is a method to determine the thermal properties of a compound. The sample is placed in a calorimeter with a reference cell. Temperature changes induce processes in the sample like e.g. phase transitions. The enthalpies of these processes can be determined by detecting the heat flow between sample and reference cell.

3.4. Infrared Spectroscopy

Fourier transform infrared spectroscopy (FTIR) shows the absorption of electromagnetic radiation in the infrared region. The absorbed radiation excites vibrational states inside the molecules and is characteristic for different types of chemical bonds. The energy difference E_{ϑ} between the ground state and the excited state depends on the force constant k of the bond and on the reduced mass μ of the involved atoms:

$$E_{\vartheta} \propto \sqrt{\frac{k}{\mu}} \quad (3.6)$$

Generally, FTIR spectroscopy is a useful tool for the determination of characteristic functional groups.

3.5. Calorimetric Methods

3.5.1. Reaction Calorimetry

The central part of a reaction calorimeter consists of two vessels, the reaction cell and the reference cell. These cells are enclosed by thermocouples, which measure the heat flow between the cells and the surrounding adiabatic jacket. This basic setup is also part of the isothermal titration calorimeter described in Figure 3.1. While the observed reaction takes place in the reaction cell, the reference cell is filled with the pure reaction medium (in our experiments pure water), which has the same temperature and heat capacity as the sample. If the reaction in the reaction cell is exothermal or endothermal, a temperature gradient will arise between reaction cell and reference cell. Due to the Seebeck effect, this temperature

difference generates a voltage in the thermocouples, which is proportional to the temperature difference. The signal observed is the power of the thermocouples which is necessary to keep the cells in equilibrium. Integration over time gives the heat ΔH of the reaction.

3.5.2. Isothermal Titration Calorimetry (ITC)

The basic setting of an isothermal titration calorimeter (ITC) is similar to the standard reaction calorimeter described in section 3.5.1 and is presented in Figure 3.1. In addition to a standard reaction calorimeter, ITC enables us to titrate a solution into the reaction cell and observe dynamic processes, such as the adsorption of surfactants on particle surfaces.

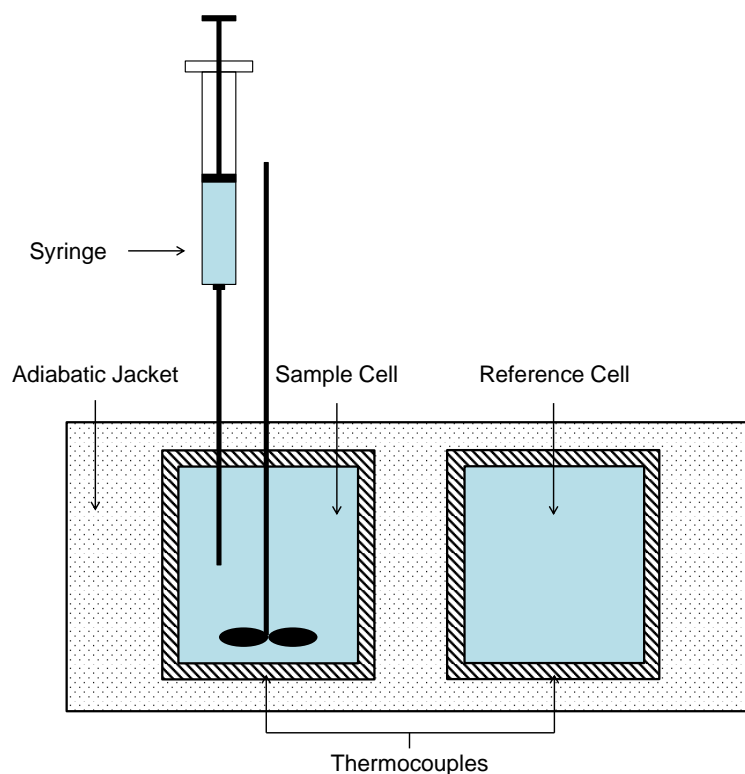


Figure 3.1: Schematic description of an isothermal titration calorimeter.^[145]

4. Results and Discussion

The focus of this dissertation is on the structure control of polymer/inorganic hybrid nanomaterials in miniemulsion. In the following part, several techniques for the synthesis of hybrid nanomaterials are presented. These examples represent systems in direct as well as in inverse miniemulsions. Nanoparticles and nanocapsules are prepared, using different polymers and inorganic materials. The sections of this chapter give a broad overview of the achievable morphologies of hybrid nanomaterials in miniemulsion.

The first part, section 4.1, describes the encapsulation of functionalized silica nanoparticles in PMMA. This combination is a suitable model system for investigations of the structure, as these materials are easily accessible. Silica nanoparticles with a narrow size distribution are commercially available in large scales. Furthermore, the silane chemistry offers a versatile and easy way for the surface functionalization of the inorganic particles. The effect of different functionalization agents on the structure of hybrid particles is explained for two different synthetic strategies. The first one, miniemulsion polymerization, is the traditional way to encapsulate nanoparticles in polymer droplets. The second approach is the solvent evaporation strategy. By using pre-formed polymers, this method offers the possibility to prepare hybrid particles with the same chemical composition, but without a polymerization reaction in the droplet. The effect of these two preparation techniques on the structure of the hybrid materials is described in detail.

In the next section 4.2, the findings of section 4.1 are transferred to magnetite as an example for other material systems. Magnetite is suitable as a model for functional materials, as magnetic nanoparticles are already widely used for a large number of applications. The encapsulation of functionalized magnetite nanoparticles in different polymers is presented. The experiments show that the strategy developed in section 4.1 can be applied to different inorganic materials and polymers.

Section 4.3 describes a possible application for the materials prepared in the previous sections. Hybrid nanoparticles consisting of poly(MMA-*co*-BMA) copolymers and differently functionalized silica particles are used as starting material for film formation. The structure of the hybrid particles determines the structure of the resulting hybrid films. Therefore, the exact control of the particle structure in miniemulsion can help to tune the morphology of hybrid films with different compositions.

Direct miniemulsions offer the possibility to encapsulate hydrophobic liquids in a polymer shell, which is shown in section 4.4. Especially in the presence of inorganic particles, the structure control is a big challenge, as the system consists of four phases. As an example, the synthesis of PMMA nanocapsules with hexadecane as liquid core is presented. As inorganic materials, differently functionalized silica particles are present in the system. Capsules are synthesized using the polymerization as well as the solvent evaporation technique.

A different strategy compared to the previous chapters is the synthesis of hybrid nanomaterials using Pickering stabilization, as it is described in section 4.5 and 4.6. In Pickering-stabilized emulsions, the inorganic particles form a layer around the stabilized droplets. Therefore, the structure of the resulting hybrid material is determined during emulsification. In section 4.5, the synthesis of PMMA particles stabilized by silica nanoparticles in direct miniemulsion is described. Section 4.6 shows the synthesis of nanocapsules with an aqueous core in inverse miniemulsion. Here, functionalized silica particles act as stabilizers during the formation of a polyurethane shell via interfacial polymerization.

4.1. Structure Control in PMMA/Silica Hybrid Nanoparticles³

In this section, different techniques for the synthesis of PMMA/silica hybrid nanoparticles in miniemulsion polymerization are discussed with regard to the structures of the resulting hybrids. The first part describes possible strategies for the surface functionalization of silica nanoparticles. Cetyl trimethylammonium chloride (CTMA-Cl) is presented as an example for surface functionalization using surfactants. In comparison, 3-methacryloyloxypropyl trimethoxysilane (MPS) and octadecyl trimethoxysilane (ODTMS) are examples for the surface functionalization with covalently bound reagents. Hybrid particles with differently functionalized silica particles are synthesized, evaluating the behavior of the functionalization agent during emulsification and polymerization. As second synthesis technique, the solvent evaporation strategy is introduced. By using a pre-formed polymer instead of a monomer, chemical reactions inside the miniemulsion droplets are avoided and further structures for the hybrid particles are accessible.

4.1.1. Hydrophobization of Silica Particles

In a first series of experiments, silica particles were modified with CTMA-Cl. In the aqueous phase, CTMA⁺ cations adsorbed due to the opposite charges of silica and CTMA⁺ on the silica particle surface, forming a double layer of CTMA⁺ around the silica particle. The hydrophobic tails of the CTMA⁺ cations change the wettability of the silica particles, when placed in a hydrophobic environment.^[54]

The interaction between negatively charged silica particles and positively charged CTMA⁺ was analyzed by isothermal titration calorimetry (ITC), see Figure 4.1a. The concentration of the silica nanoparticles was set to 5 g L⁻¹ and the concentration of the CTMA-Cl solution to 0.15 g L⁻¹.

³This section is based on the publication “Structure Control in PMMA/Silica Hybrid Nanoparticles by Surface Functionalization” by Alexander Schoth, Caroline Wagner, Lena L. Hecht, Svenja Winzen, Rafael Muñoz-Espí, Heike P. Schuchmann and Katharina Landfester, published 2014 in *Colloid and Polymer Science*, volume 292 on the pages 2427 to 2437. © 2014, with kind permission from Springer Science and Business Media.

The titration of CTMA-Cl into pure water is shown as a reference. The titration curve indicates that the adsorption of CTMA^+ on the silica particles is an exothermic reaction. Although the CTMA^+ builds a double layer around the silica particle, the adsorption is only a single step mechanism.^[146] A two-step mechanism, in which a monolayer of CTMA^+ is adsorbed first, is not favored because this process would lead to a hydrophobization of the surface. Thus, the continuous formation of a double layer via hemimicelles^[147] or admicelles^[148] is more likely, in order to keep the silica surface polar and to avoid destabilization of the dispersion. Total coverage of the surface is reached after about 310 min (45 injections), which corresponds to an added volume of surfactant solution of 225 μL . This leads to the conclusion that each silica particle is covered by a double layer consisting of about 1200 CTMA^+ cations (see Figure 4.1b). In the synthesis experiments, CTMA-Cl was added in excess to ensure complete coverage of the silica surface. The unreacted surfactant was removed by centrifugation.

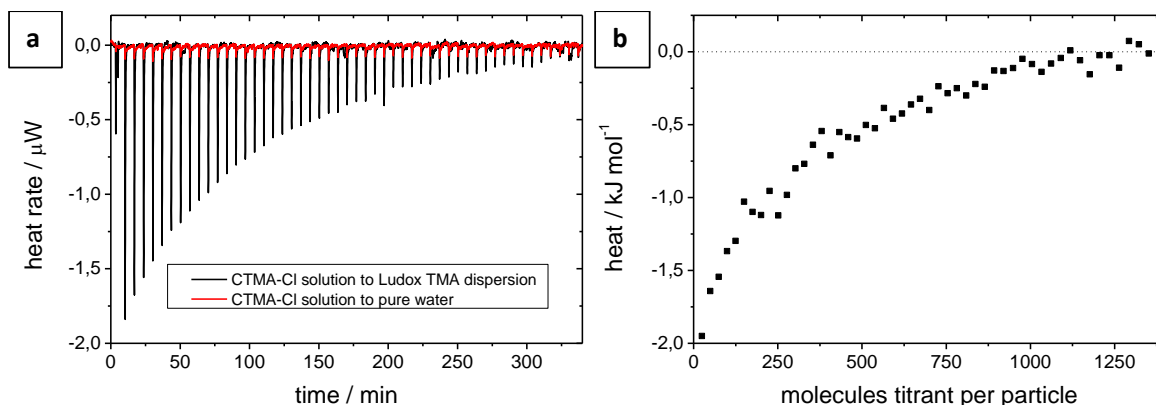


Figure 4.1: Isothermal titration curve of added CTMA-Cl solution to a Ludox TMA silica particles dispersion.^[87]

In a second series of experiments, silica particles modified with MPS were prepared for the encapsulation into PMMA particles. The trimethoxysilyl groups of MPS react to silanols in a hydrolysis reaction. The silanols form oligomers, which adsorb on the surface of the silica particles and are then covalently attached by condensation.^[64] The alkyl chains lead to a hydrophobization of the particle surface. Furthermore, MPS carries a vinyl group that allows for a copolymerization with MMA.^[9] We assume that the mechanism for the functionalization with ODTMS is analogous to MPS, including the hydrolysis, formation of oligomers, adsorption, and condensation onto the silica surface. The hydrophobic part of ODTMS consists of a long alkyl chain. The only effect of ODTMS is the change of wettability of the silica surface. There are no reactive groups attached and, therefore, the ODTMS-functionalized silica particles cannot copolymerize with the MMA, as it is the case in the MPS-functionalized ones.

The amount of hydrophobization agent attached to the silica surface was determined by thermogravimetric analysis (TGA) of the dried particles. Figure 4.2 shows that the total amount of organic material is about 10 wt.% for MPS and CTMA-Cl and about 20 wt.% for ODTMS. Regarding only the organic part of the molecules of MPS and ODTMS (without the silanol), which is vaporized during the TGA, the molar amounts of both functionalization agents attached to the surface are equivalent. As the applied molar amount was the same, the yield is also identical for both reactants. The TGA curves also give an indication on whether the functionalization agent forms a stable bond to the silica surface or can be simply removed by a washing process. To evaluate this effect of washing, the thermal degradation of functionalized particles was observed before and after purification. Therefore, all modified silica particles were washed once with water/ethanol. The amount of CTMA⁺ on the particle surface is decreased by 58 % due to this washing process, as can be seen in Figure 4.3a. For MPS-functionalized silica, no significant change in the MPS amount is observed (Figure 4.3b). The result of grafting MPS on the Ludox TMA particles is also supported by FTIR spectroscopy, as shown in Figure 4.4 for unmodified silica and MPS-grafted silica. The peak at $1000\text{--}1200\text{ cm}^{-1}$ shows the asymmetric stretching vibration of Si–O–Si,^[149] the broad peak at 1626 cm^{-1} results from the bend vibration of water,^[150] while the signal at $3100\text{--}3700\text{ cm}^{-1}$ shows the O–H stretching vibrations of water and silica.^[149,150] Typical bands indicating MPS grafted onto the silica surface are at 1720 cm^{-1} for C=O of the methacrylate group and at 2962 cm^{-1} for the C–H stretching vibration. This observation confirms that the MPS is bound covalently to the silica surface, while CTMA⁺ binds only via ionic interaction.

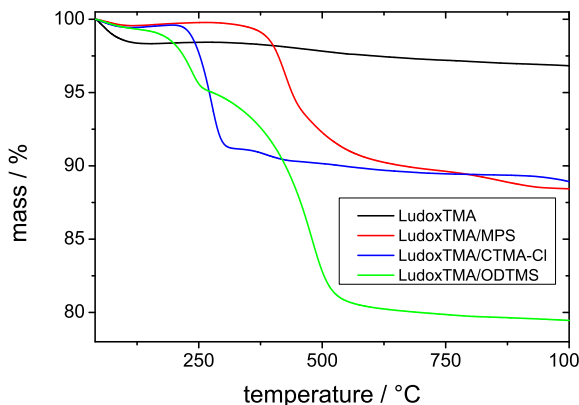


Figure 4.2: Thermogravimetric analyses of differently modified Ludox TMA particles.^[87]

4.1.2. Encapsulation of Hydrophobized Silica Particles

In the following experiments, miniemulsions with CTMA-Cl-modified silica dispersed in the monomer phase were synthesized. High amounts up to 40 wt.% of the hydrophobized silica

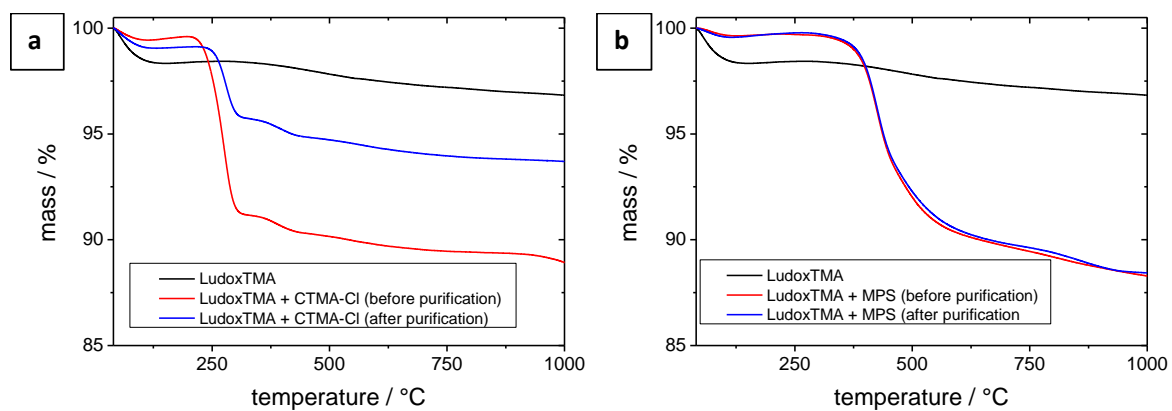


Figure 4.3: Thermogravimetric analyses of a) CTMA-Cl- and b) MPS-modified Ludox TMA particles before and after purification.^[87]

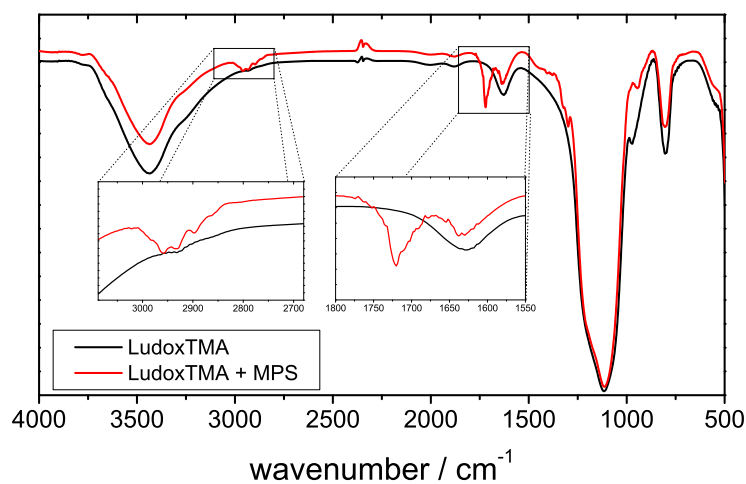


Figure 4.4: FTIR spectra of Ludox TMA particles before and after functionalization with MPS.^[87]

were dispersed in the monomer phase, subsequently this dispersion phase was miniemulsified in an aqueous surfactant solution. The amounts of disperse and continuous phase were kept constant and only the amount of silica added to the monomer was varied. In this case, the non-ionic surfactant Lutensol AT50 was used, because the counterion of anionic surfactants – such as sodium in SDS – could lead to desorption of CTMA⁺ from the silica surface.

Table 4.1: Compositions of polymer/silica hybrid nanoparticles via the miniemulsion polymerization process.

Sample	Silica		Monomers					Surfactant	
	Funct.	Amount [g]	MMA [g]	4VP [g]	HD [mg]	V59 [mg]	H ₂ O [g]	Type	Amount [mg]
C1	CTMA-Cl	1.2	6	-	240	100	24	Lut. AT50	200
C2	CTMA-Cl	1.2	5	1	240	100	24	Lut. AT50	200
M1	MPS	1.2	6	-	240	100	24	SDS	27
M2	MPS	2.4	6	-	240	100	24	SDS	27
O1	ODTMS	1.2	6	-	240	100	24	SDS	27

When MMA is used as sole monomer, the encapsulation of CTMA-Cl-modified silica particles is not possible, as reflected by the TEM image in Figure 4.5a. The silica particles are located outside the polymer particles, which is in agreement with the results reported by Armes et al.^[111] The interaction between PMMA and the silica components does not seem to be sufficient to favor the formation of composite particles.^[151]

To enhance the interaction between CTMA-Cl-modified silica and the organic phase, 4VP was used as a co-monomer forming strong acid-base interactions to the silica.^[54] These strong interactions are necessary for a successful encapsulation of the hydrophobized silica particles in the polymer particle, as seen in the micrograph of Figure 4.5b. The CTMA-Cl-modified silica particles have a tendency to aggregate inside the monomer droplets and the aggregates are forced to one side of the droplet during polymerization.

Another obvious difference between samples prepared with and without 4-VP is the size of the polymer particles. If the CTMA-Cl-modified silica particles are not dispersed inside the organic phase, the CTMA⁺ cations can desorb from the silica surface and act as additional surfactant for the miniemulsion droplets in the aqueous phase.^[152] Therefore a larger interface can be stabilized in the emulsification process and smaller droplets are formed. Additionally, secondary particle nucleation might occur if the energy input is not sufficient to gain small droplets, so that the whole amount of surfactant is needed to cover their surface.^[153] Both effects lead to a decrease in size of the resulting hybrid particles. Also for encapsulated CTMA-Cl-modified silica particles, an increase of the amount of silica leads to a diminution of the particle diameter, as shown in Figure 4.6. These results indicate that a certain amount of CTMA⁺ cations leaves the silica surface even if the particles are located in the monomer

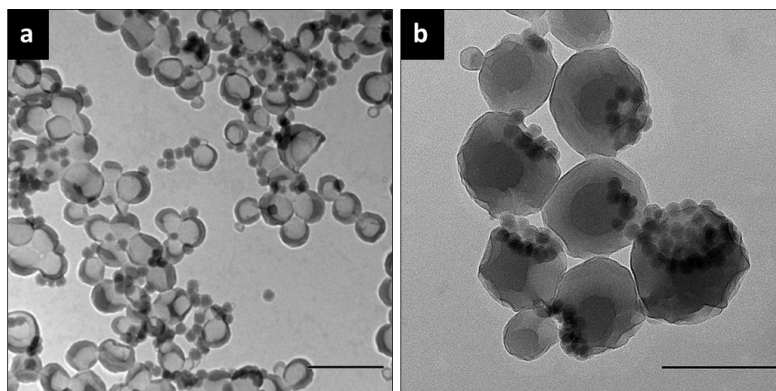


Figure 4.5: TEM images of miniemulsion dispersions containing CTMA-Cl-modified Ludox TMA particles in a) PMMA (C1) and b) PMMA-*co*-4VP (C2). Scale bar is 200 nm.^[87]

phase. In previous work the desorption of CTMA^+ cations and their transfer to the water phase was shown by interfacial tension measurements.^[153] The desorption of the modification agent from the particle surface could be an explanation for the observed separation between silica and polymer due to insufficient hydrophobization.

In a different set of experiments, MPS- and ODTMS-functionalized silica was used to prepare hybrid particles. The amount of silica dispersed in the MMA phase was varied from 1 wt.% to 40 wt.% with respect to the dispersed phase and the amounts of the oil phase and the continuous phase were kept constant.

The average particle size is in the range of 120 nm for amounts until 20 wt.% of silica and up to 150 nm for an amount of silica of 40 wt.% (Figure 4.6). Generally, a higher amount of dispersed silica results in larger hybrid particles, increasing also the standard particle size deviation. The increase in size and the higher polydispersity can be attributed to an insufficient droplet break-up by sonication. For pure liquids, the droplet break-up is depending on the viscosity ratio λ between dispersed phase and continuous phase. In laminar shear flow, λ is ideal between 0.1 and 1.^[154] The addition of nanoparticles leads to an increased viscosity of the droplets and, therefore, to a higher viscosity ratio and larger resulting droplet sizes.^[108] In addition, the presence of particles also influences the droplet deformation and induces counter-acting stresses.

All particles exhibit homogeneous structures with silica particles inside the polymer phase. Figure 4.7 shows TEM and SEM images of samples prepared with 20 and 40 wt.% of MPS-functionalized silica dispersed in the monomer phase. Because of the thermal instability of the PMMA under TEM observation conditions, the samples are coated by carbon, so that the particles appear lighter in the core. The more silica was added in the disperse phase of the miniemulsion, the more silica particles are present in the composite particles. For up to 20 wt.% of MPS-functionalized silica, the composite particles have only a small number

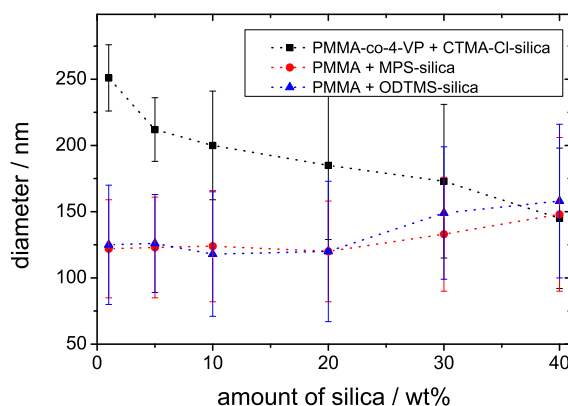


Figure 4.6: DLS measurements of hybrid nanoparticles (C2, M1, O1) with differently functionalized Ludox TMA particles.^[87]

of silica nanoparticles close to the surface and they are well distributed. However, small empty particles resulting from secondary nucleation can be observed in all samples, which is consistent with previous results.^[107]

With more than 20 wt.% of silica particles, aggregates inside the monomer droplets start to form, resulting in a heterogeneous distribution of the inorganic particles in the monomer phase. The composite particles are filled inhomogeneously due to insufficient droplet breakup of highly filled monomer droplets.^[108] SEM images show clearly that the silica nanoparticles are mostly inside the polymer phase and not located at the interface. Only for the large, overfull hybrid particles, silica can also be observed on the surface. The amount of single silica particles with a thin polymer shell outside the large hybrid particles is quite low, but increases with the total amount of silica.

The structure of PMMA/ODTMS-silica particles is similar to the PMMA/CTMA⁺-silica particles. Figure 4.8 shows hybrid particles with an amount of ODTMS-functionalized silica of 20 wt.% with regard to the polymer phase. The silica particles are located together in a bulk at the polymer/water interface, forming a Janus-like structure (i.e., the silica particle are placed on one side of the polymer hybrid particle). Like in case of the PMMA/4VP/CTMA⁺-silica particles, segregation occurs, whereupon the silica particles agglomerate inside the polymer phase.

The difference between the silica particles functionalized with MPS, on the one hand, and with CTMA-Cl or ODTMS, on the other hand, can be explained by a suppression of the agglomeration/separation process of silica particles and the polymer phase. This is due to copolymerization of the silica-bound acrylate with the surrounding monomer MMA. During copolymerization, the MPS-functionalized silica particles are immobilized inside the composite particles. Agglomeration and separation is suppressed, although it might be energetically preferred for all systems studied in this work, taking into account the polarity differences

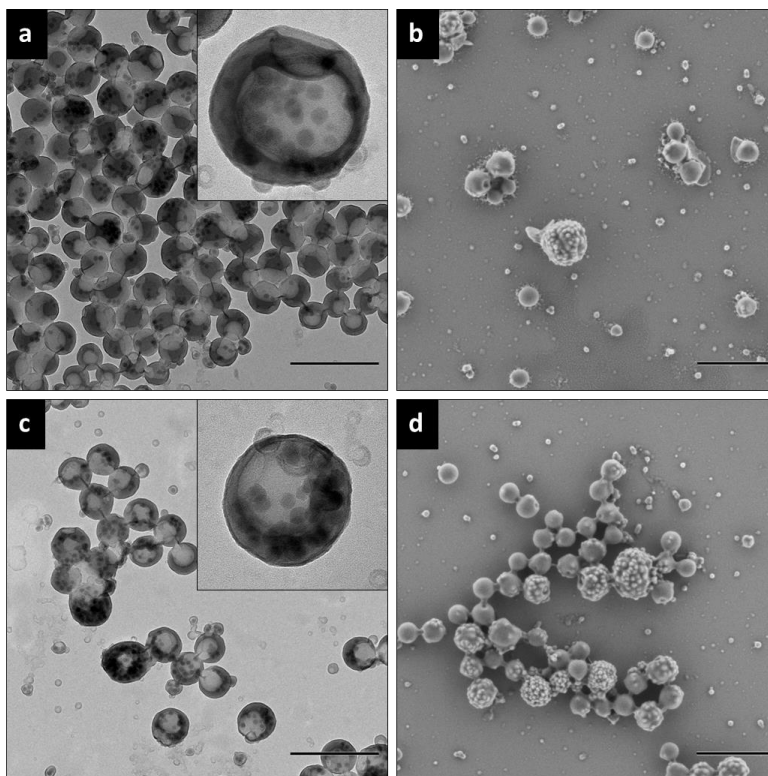


Figure 4.7: TEM (a, c) and SEM (b, d) images of PMMA/MPS-silica composite particles, synthesized with a silica content of a/b) 20 wt.% (M1) and c/d) 40 wt.% (M2). Scale bars are 500 nm.^[87]

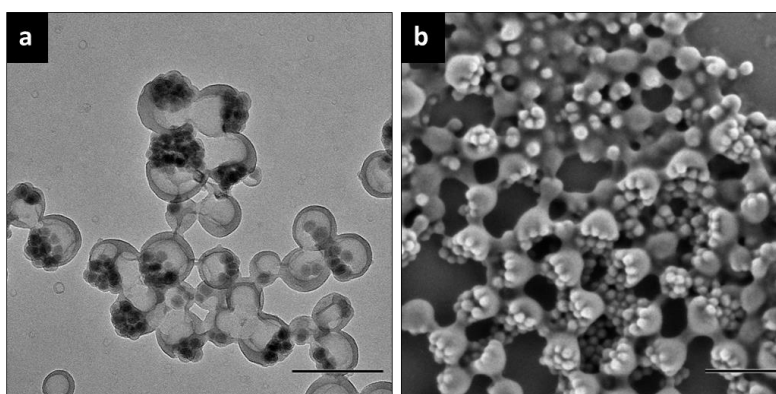


Figure 4.8: TEM (a) and SEM (b) images of PMMA/ODTMS-silica composite particles (O1), synthesized with a silica content of 20 wt.%. Scale bars are 200 nm.^[87]

between polymer and functionalized silica particles. The comparison between CTMA-Cl and ODTMS also shows that the agglomeration/separation process is not caused by desorption of the functionalization agent and the resulting agglomeration of too hydrophilic silica particles inside the organic phase. Because of the covalent bond of ODTMS to silica, desorption is not possible (as it is for CTMA-Cl) and sufficient hydrophobicity is ensured in this case.

4.1.3. Measurement of the Polymerization Kinetics

The influence of varying amounts of silica dispersed in the monomer phase on the reaction time and the kinetic behavior was studied by calorimetry. The reaction rates of miniemulsion polymerizations can be influenced by different parameters, such as droplet size, water solubility of the monomers and co-monomers, and the nucleation mechanisms. Droplet nucleation, homogenous nucleation, and micellar nucleation are generally the three different nucleation mechanisms in heterophase polymerization.^[16,155,156] In an ideal miniemulsion polymerization, the droplet nucleation mechanism is predominant. The polymerization is initiated by an oil-soluble initiator, forming a radical inside the monomer droplet where it reacts with the monomer. This nucleation takes place in every single droplet.^[157] The second nucleation mechanism, which might occur in heterophase, is the homogenous nucleation. This mechanism is sensitive to the initiator concentration and its solubility in the aqueous phase. In general, micellar nucleation can be suppressed by working at surfactant concentrations below the cmc of the respective miniemulsion system. For MMA polymerization it is supposed that the mechanism of droplet nucleation and the mechanism of homogeneous nucleation overlap because of the high water solubility of the monomer.^[108,158]

The calorimetric data of the polymerization of a MMA miniemulsion loaded with different amounts of MPS- and ODTMS-functionalized silica is shown in Figure 4.9. The three typical intervals for miniemulsion polymerization described by Harkins^[159] (interval I: particle nucleation; interval III: depletion of monomer in the droplets; interval IV: Trommsdorff–Norrish effect; interval II: monomer diffusion; does not exist in a typical miniemulsion) can only be partially observed for the pure and loaded MMA miniemulsions.^[152,158] Interval I is only weakly pronounced within the first 200 s, when the polymerization starts with low heat flows. Interval III results in a slow rise and lasts from 300 s–500 s. The gel peak is obtained approximately after 1000 s. The reason for the deviation from expected reaction kinetics might be due to the high water solubility of MMA and the two different nucleation mechanisms (micellar and homogeneous nucleation) taking place.

Bechthold et al.^[160] described the influence of droplet size on polymerization rate: the smaller the droplets are, the faster the overall reaction. With higher amounts of MPS-functionalized silica, the particle size of the composite particles increased slightly and the reaction rate should have decelerated. In our experiments, this was not observed. The change in droplet size is not significant enough to cause a change in polymerization rate, at

least within the limit of error of our calorimetric measurements. Particularly, there is no difference between MPS- and ODTMS-functionalized silica. This is notable, because MPS copolymerizes with the MMA and, thus, it could be assumed to have a serious effect on polymerization kinetics.

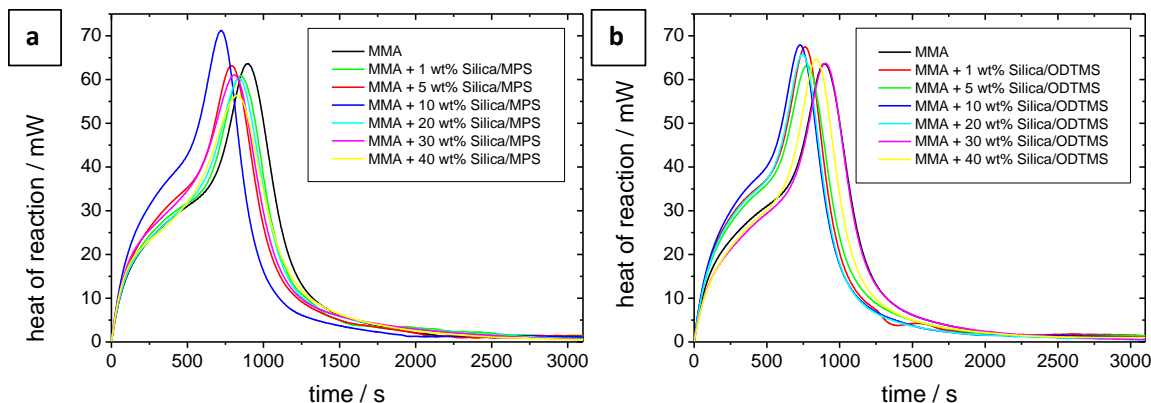


Figure 4.9: Calorimetric curves of the polymerization of PMMA miniemulsions containing different amounts of a) MPS- and b) ODTMS-functionalized Ludox TMA particles.^[87]

4.1.4. Hybrid Particles via the Solvent Evaporation Approach

To ensure the role of the covalent connection between particles and polymer for the structure control, hybrid particles with the same chemical composition, but without this bond would be desirable. Such samples were achieved with the solvent evaporation technique.^[35,161] Here, pre-formed PMMA was dissolved in chloroform together with the modified silica particles. This suspension acts as dispersed phase in the miniemulsion. The chloroform is evaporated after emulsification, what leads to a precipitation of the previously dissolved polymer inside the droplet. In this process, the silica particles are free to migrate to the position that is energetically preferred. The silica is located on the surface of the hybrid particles, as seen in the micrographs in Figure 4.10. This observation indicates that the homogeneous distribution after polymerization (Figure 4.7) has to be caused by a fixation of the silica particles by covalent bonds to the surrounding polymer matrix. This connection is mandatory and cannot be substituted by a higher hydrophobicity (e.g., with ODTMS).

4.1.5. Conclusions

This work shows which parameters are crucial for a controlled synthesis of polymer/silica nanocomposite particles in a variety of structures in miniemulsion. Silica particles are hydrophobized with three different modifications. The first one is CTMA-Cl as an example for functionalizations using ionic surfactants. The functionalization agent desorbs from the

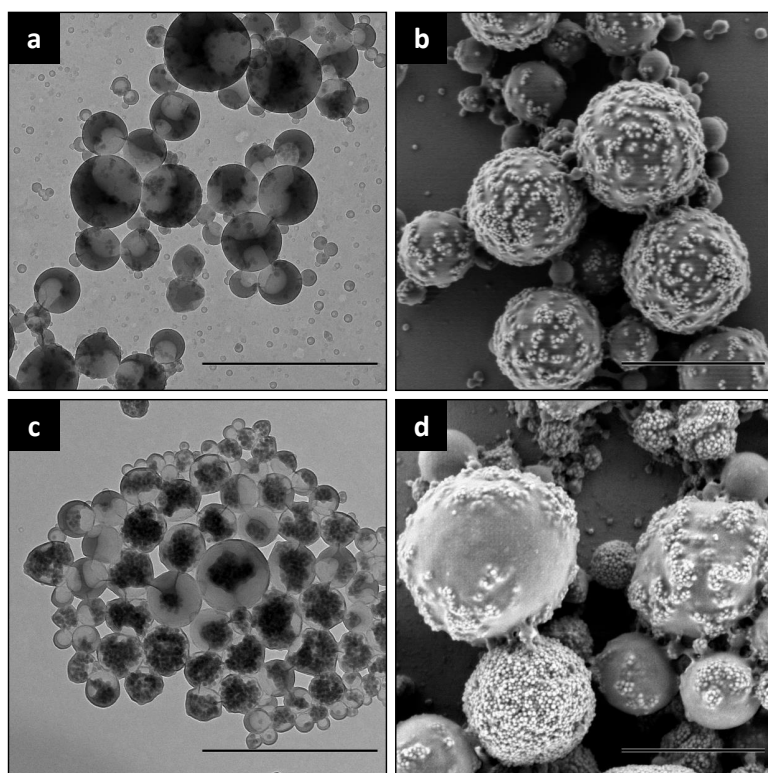


Figure 4.10: TEM (a, c) and SEM (b, d) images of PMMA/silica composite particles, synthesized via the solvent evaporation approach. The silica particles were functionalized with MPS (a, b) and ODTMS (c, d). Scale bars are 1 μm .^[87]

surface during emulsification and acts as additional surfactant in the system. In consequence, high amounts of CTMA-functionalized silica lead to a diminution of the droplet size. After desorption, the amount of surfactant on the particle surface is not sufficient to enable encapsulation of the silica. Addition of the comonomer 4VP is necessary to increase the interaction between silica surface and the surrounding polymer. The hybrids show a Janus-like distribution of the silica. Generally, surfactants used as functionalization agents give only a limited control over the structure of the hybrids.

The other strategy is the functionalization using the trimethoxysilanes MPS and ODTMS. Both reagents form a covalent connection to the silica surface and, therefore, do not desorb during emulsification. After polymerization, the MPS-functionalized particles are distributed homogeneously in the hybrid particles, while ODTMS-functionalized silica tends to form a Janus-like structure. By using the solvent evaporation technique, both silica types assemble on the surface of the hybrid particles. While the MPS-silica is distributed homogeneously on the surface, the ODTMS-silica shows a higher tendency for agglomeration. These findings can be partially explained by the theoretic model of Gonzalez-Ortiz and Asua.^[85,109] As MPS-functionalized silica has a very similar polarity as PMMA, nearly no interfacial energy is gained by a reduction of this interface. As ODTMS is much more hydrophobic than MPS, the interfacial tension to PMMA is also much higher, leading to a reduction of the polymer/silica interface and, therefore, more agglomeration of the silica. The difference to the hybrids synthesized via polymerization can be only partially explained by differences in the interfacial energies. The copolymerization of MPS leads to an additional fixation of the silica. This kinetic effect hinders segregation and keeps the particles distributed in the polymer.

These findings are the basis for the experiments described in the next chapters. The results for silica and PMMA are transferred to magnetite particles to show the versatility of the method regarding the inorganic material as well as the compatibility with different polymers (section 4.2). By the formation of hybrid films from particle dispersions, a possible field of application for the prepared hybrid particles is demonstrated (section 4.3). Finally, the system is extended to capsule morphologies by adding a liquid core to the hybrid particles (section 4.4). In all these systems, the basic principles for structure control described above, are valid and can be used to tune the properties of the synthesized product.

4.2. Encapsulation of Magnetic Nanoparticles⁴

This section describes the transfer of the findings presented in section 4.1 to a second material system. As example for functional materials, magnetite is encapsulated in different

⁴This section is based on the manuscript “Silanization as a Versatile Functionalization Method for the Synthesis of Polymer/Magnetite Hybrid Nanoparticles with Controlled Structure” by Alexander Schoth, Alasdair D. Keith, Katharina Landfester and Rafael Muñoz-Espí.

polymers. For magnetite nanoparticles, capping with oleic acid is one of the most common functionalization strategies.^[162] The carboxylic acid group has a high affinity to the iron atoms and acts as chelating agent. Although encapsulation of oleic acid-functionalized magnetite particles in miniemulsion is possible, the structure of these materials is in most cases a Janus-like morphology. As a variation of the surface functionality can be helpful to achieve a homogeneous distribution of the particles in the polymer, MPS and ODTMS are used as alternative functionalization agent for magnetite nanoparticles.

4.2.1. Surface Functionalization of Magnetite Nanoparticles

Superparamagnetic magnetite nanoparticles with a size of around 5 nm were synthesized according to the co-precipitation method described by Ramírez et al.^[51,52] Surface functionalization with oleic acid was successful, as proven by the thermogravimetric analysis (TGA) traces shown in Figure 4.12. As we already showed in a previous work for silica nanoparticles, the structure of hybrid particles depends on the surface functionalization. A polymerizable methacrylic acid ester leads to a homogeneous distribution of the inorganic particles in the polymer, while a long alkyl chain gives a Janus-like structure.^[87] To achieve a similar result with magnetite particles, oleic acid as functionalization agent was replaced by methacrylic acid (MA). As shown in Figure 4.12, this functionalization was not successful. We assume that the solubility of methacrylic acid in water is too high and the adsorption to the magnetite surface is not favorable. To prove that the reactive group of methacrylic acid and the double bond of oleic acid have no influence on the functionalization reaction, we repeated the same experiments with stearic acid and propionic acid. The thermal decomposition of magnetite particles functionalized with stearic acid and propionic acid (shown in Figure 4.13) is similar to the particles functionalized with oleic and methacrylic acid: functionalization with the very hydrophobic acids is successful (high amount of organic material), while functionalization with the more hydrophilic acids is not achievable (low amount of organic material).

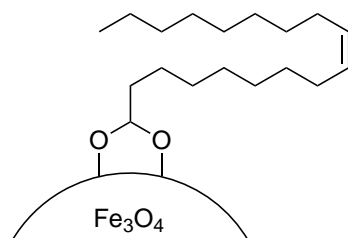


Figure 4.11: Schematic description of oleic acid-functionalized magnetite nanoparticles.

A possible alternative to carboxylic acids is the use of trimethoxysilane compounds as functionalization agents. Trimethoxysilanes offer a relatively easy way for surface functionalization. Furthermore, many different reactive groups and chain lengths are accessible and facilitate the tuning of the properties of the functionalized particles.^[60] For the functionalization of

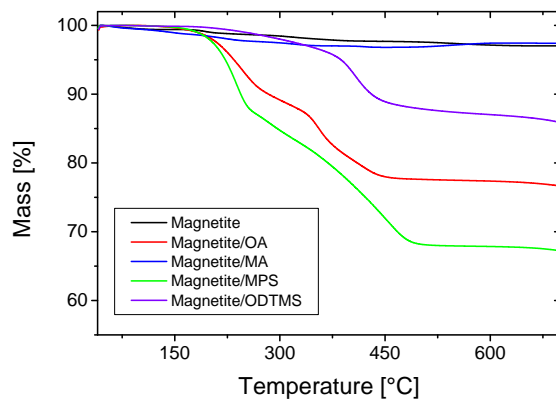


Figure 4.12: Thermogravimetric analysis of magnetite nanoparticles with different surface functionalizations.

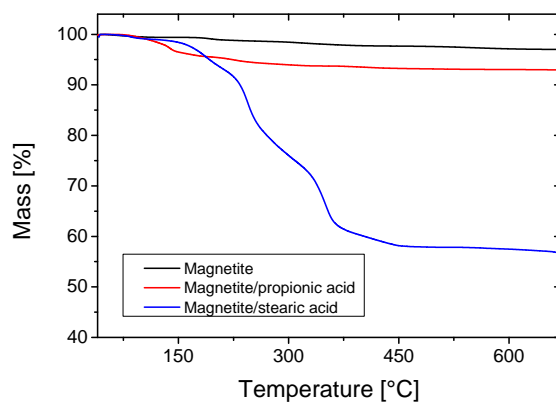


Figure 4.13: Thermogravimetric analysis of magnetite nanoparticles functionalized by different carboxylic acids.

the superparamagnetic magnetite particles, a method reported by Bourgéat-Lami et al.^[61] for the surface functionalization of silica nanoparticles was transferred to magnetite. Condensation of the precursors leads to the formation of a covalent attachment of the functionalization agent around the particles,^[163] so that removal during purification or polymerization is effectively avoided. As functionalization agents, 3-methacryloxypropyl trimethoxysilane (MPS), and octadecyl trimethoxysilane (ODTMS) were used. Both reagents have already been used successfully for structure control of encapsulated silica particles in different polymers.^[163] The MPS content of the functionalized particles is 30 wt.%, while the amount of organic materials on the ODTMS-functionalized particles is only 10 wt.% (Figure 4.12). This difference can be explained by a higher solubility of MPS in the reaction mixture. Before adsorption on the particles, the trimethoxysilanes hydrolyze and form oligomers.^[64] As ODTMS is much more hydrophobic than MPS, the oligomers should precipitate at much shorter chain lengths and, therefore, not be any more available for surface functionalization. This behavior can be macroscopically observed during the reaction by an increase of turbidity in the reaction mixture. The precipitated functionalization agents were removed after functionalization by magnetic purification.

4.2.2. Composition of Hybrid Materials

The differently functionalized magnetite particles were encapsulated by miniemulsion polymerization. Since the polarity of the polymer plays a major role for the structure of the resulting hybrid material,^[85,94] we chose methyl methacrylate (MMA) and styrene as representative cases for polar and non-polar polymers. Additionally, we used 4-vinylpyridine (4VP) as a co-monomer. The latter is widely used for the encapsulation of inorganic materials, as it provides acid-base interactions with the particle surface and helps to increase the affinity between polymer and inorganic material.^[111] Miniemulsions containing a mixture of MMA and 4VP were not stable. For all further experiments, only the samples with pure MMA (M), pure styrene (S) or a mixture of styrene and 4VP (SV) are discussed.

After polymerization, the samples were filtered to remove coagulates. Purification was done by putting the samples on a magnet to collect the hybrid particles containing magnetite. The supernatant, non-magnetic dispersions were removed and replaced by water. To evaluate the efficiency of the purification process, the solid content (SC) of the dispersions (determined by lyophilization) and the magnetite content of the lyophilized particles (measured by thermogravimetric analysis (TGA)) were determined before and after the purification step. Furthermore, the samples were analyzed by dynamic light scattering (DLS) before and after purification. The results of these measurements are shown in Table 4.2 and Figure 4.14. Since TGA measurements were conducted under nitrogen atmosphere, the organic material did not oxidize completely, remaining a carbon residue. Therefore, also the pure polymer samples (M4, S4, SV4) show a residual mass of 3 wt.%.

Table 4.2: Solid contents of the dispersions (SC), magnetite contents of the hybrid particles (MC) and particle diameters (d) of differently synthesized hybrid particles before and after magnetic purification.

Sample	Monomer	Magnetite	Before Purification			After Purification		
			SC [wt.%]	MC [wt.%]	d [nm]	SC [wt.%]	MC [wt.%]	d [nm]
M1	MMA	MPS	9.0	7 ^a	150 ± 60	1.2	46 ^a	200 ± 50
M2	MMA	ODTMS	8.5	5 ^a	130 ± 50	0.4	41 ^a	240 ± 30
M3	MMA	OA	8.3	3 ^a	140 ± 60	1.2	24 ^a	370 ± 170
M4	MMA	—	9.4	3	140 ± 30	—	—	—
S1	Sty	MPS	8.8	7 ^a	110 ± 40	1.2	57 ^a	190 ± 40
S2	Sty	ODTMS	8.8	5 ^a	110 ± 40	0.7	50 ^a	190 ± 60
S3	Sty	OA	9.7	7 ^a	120 ± 30	1.4	57 ^a	220 ± 120
S4	Sty	—	6.9	3	130 ± 20	—	—	—
SV1	Sty/4VP	MPS	8.2	9 ^a	1040 ± 740	1.7	33 ^a	240 ± 90
SV2	Sty/4VP	ODTMS	8.6	7 ^a	1790 ± 1020	0.4	48 ^a	220 ± 70
SV3	Sty/4VP	OA	9.4	5 ^a	620 ± 400	1.4	44 ^a	270 ± 90
SV4	Sty/4VP	—	8.1	3	100 ± 40	—	—	—

^aThe residual amount of polymer (3 wt.%) has already been subtracted from this value.

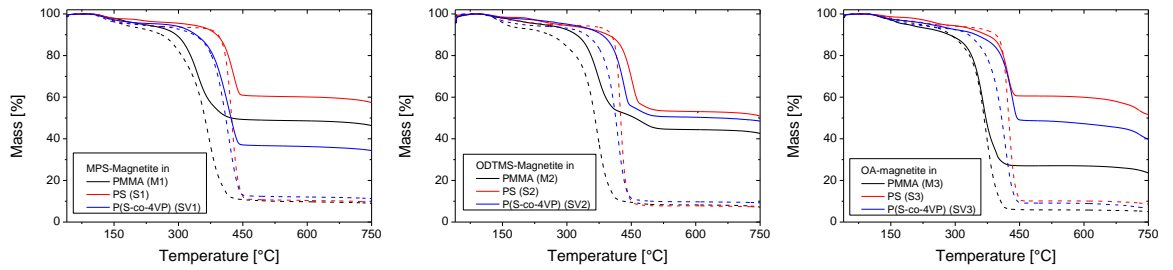


Figure 4.14: Thermogravimetric analyses of hybrid nanoparticles containing differently functionalized magnetite nanoparticles and different polymers. The dashed lines are the samples before magnetic purification.

Directly after polymerization and filtration, the solid content of the samples is around 9 wt.%. This value is close to the theoretical one of 10 wt.%, which proves that the miniemulsions were stable and showed only a small amount of coagulate. After purification, the solid content is roughly around 1.5 wt.% for the samples containing MPS- and OA-magnetite and around 0.5 wt.% for the samples with ODTMS-magnetite. This means that only about 12 % of the particles were sufficiently magnetic to be collected by the magnet. The rest of the particles were either pure polymer particles or contained only a low amount of magnetite. This observation is also in accordance with the electron micrographs of the samples before purification, as they are shown in Figure 4.15, Figure 4.16 and Figure 4.17. Most of the particles consist only of polymer, while the magnetite is concentrated in higher amounts only in a few particles.

In theory, the samples should contain 10 wt.% of magnetite. With the residual polymer in TGA measurements taken into account, the expected result for the magnetite content (MC) in the TGA measurements should be 13 wt.%. In most of the samples, between 40 % and 55 % of the magnetite was encapsulated and is still present in the sample after filtration, while the rest has been removed before as coagulate. The best result gave the combination of MPS-functionalized magnetite in poly(styrene-*co*-4VP) with an encapsulation efficiency of 70 % (SV1), while the lowest amount is found for OA-magnetite in MMA with 23 % (M3). In general, no clear trend regarding the encapsulation efficiency and the influence of different polymers or surface functionalizations can be observed.

After magnetic purification, the compositions of the dispersions change dramatically. Due to removal of the pure polymer particles, the samples contain only the highly magnetic particles. This leads, of course, to a decrease of the solid content, as already stated before. Contrarily, the magnetite content of the particles is much higher after purification. Most samples show magnetite contents of 40 up to 60 wt.%.

The huge difference of solid content and magnetite content before and after magnetic purification proves the heterogeneous distribution of the magnetite in the particles. Besides some particles with high magnetite content, a big part of the particles consist of pure polymer. This effect can be explained by regarding the emulsification process. The preparation of the miniemulsion was done by applying ultrasound to a macroemulsion. A high content of solid particles in a droplet leads to an increased viscosity, which hinders deformation and droplet breakup.^[108] As a consequence, empty particles are much more likely to be broken up than particles containing magnetite. After emulsification, the samples consist of a large number of small, empty particles besides some larger particles filled with magnetite. The DLS data in Table 4.2 before and after purification support this finding. The same effect has also been observed for the encapsulation of silica particles.^[87,108,163] The big advantage of magnetite is that purification with a magnet is easy and the concentration of magnetic hybrid particles in dispersion can be increased dramatically.

4.2.3. Structure of the Hybrid Nanoparticles

Electron micrographs of the hybrid nanoparticles are shown in Figure 4.15, Figure 4.16 and Figure 4.17. Figure 4.15 shows magnetite particles encapsulated in PMMA. The particles in Figure 4.16 are encapsulated in polystyrene, while Figure 4.17 shows particles in poly(styrene-*co*-4VP). As already shown by TGA, the magnetite content of the hybrids increases significantly after magnetic purification. Before purification, all samples show a high amount of empty polymer particles, as can be seen in the first rows of the electron micrographs. After purification (second row), all particles contain a high amount of magnetite. The structure of the particles, however, differs significantly depending on the applied surface functionalization. The first columns of each Figure (M1, S1, SV1) show hybrids containing MPS-functionalized magnetite. The magnetite particles are distributed homogeneously inside the polymer. Especially in PMMA (M1), the particles are fully loaded and lost their anisotropic shape due to the high amount of encapsulated magnetite.

The structures of the particles containing ODTMS-functionalized magnetite (second columns, M2, S2, SV2) show a Janus-like structure. The magnetite particles are agglomerated only at one side of the hybrids, while the other side consists of pure polymer. Sample SV2 shows an “open shell” structure, where the magnetite seems to be trapped in a pocket formed by the polymer. This shows a very low affinity between polymer and ODTMS-functionalized magnetite. With OA-functionalized magnetite, the structures are quite similar (M3, S3, SV3). All samples show a Janus morphology. Especially in PMMA (M3), a high amount of free magnetite besides open polymer pockets can be found, which also indicates a low affinity between polymer and functionalized magnetite in this case.

In general, the structure of hybrid particles is controlled by a minimization of the interfacial energies in the system.^[85,109] As all other parameters are kept constant in our experiments, the difference in structure should be controlled by the varying polarity of the different functionalization agents and polymers. ODTMS and OA possess a long alkyl chain and are much more hydrophobic than MPS. This results in a higher affinity to hydrophobic monomers like styrene, while MPS should be more compatible with the polar MMA. In consequence, the more hydrophobic particles with ODTMS and OA should be expected to be preferably inside the monomer to reduce the magnetite/water interface as much as possible, which is not the case. As the structures of the hybrids with differently functionalized magnetite are basically the same for all polymers, this theory does not explain our observations. The description given by Gonzalez-Ortiz and Asua is limited to systems in thermal equilibrium.^[85,109] In our system, MPS is able to copolymerize with the surrounding monomer.^[163] This leads to a kinetic fixation of the MPS-functionalized particles inside the hybrids and avoids formation of the thermodynamically preferred Janus structure.

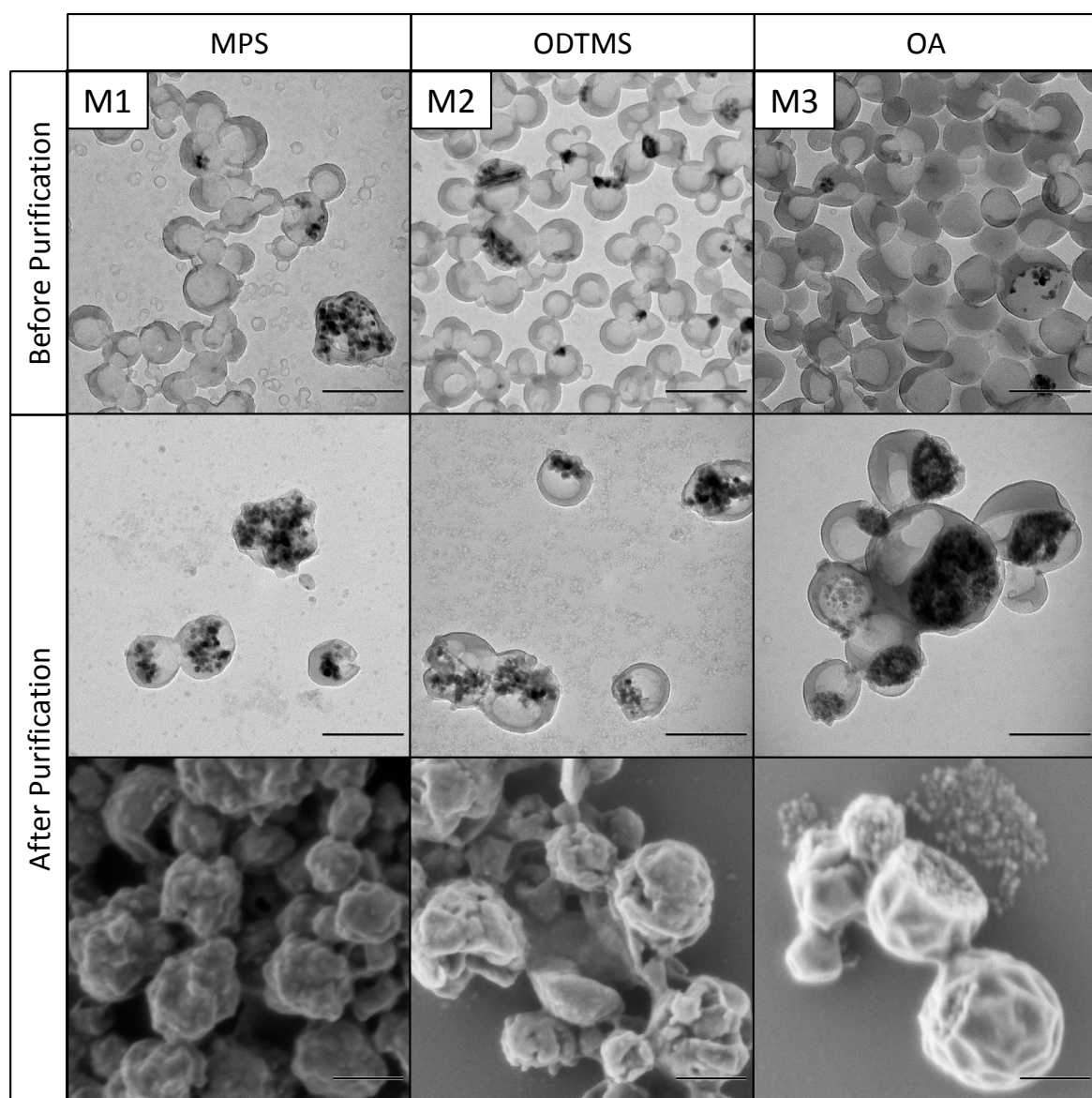


Figure 4.15: Transmission and scanning electron micrographs of differently functionalized magnetite nanoparticles in PMMA before and after magnetic purification. Scale bars are 200 nm.

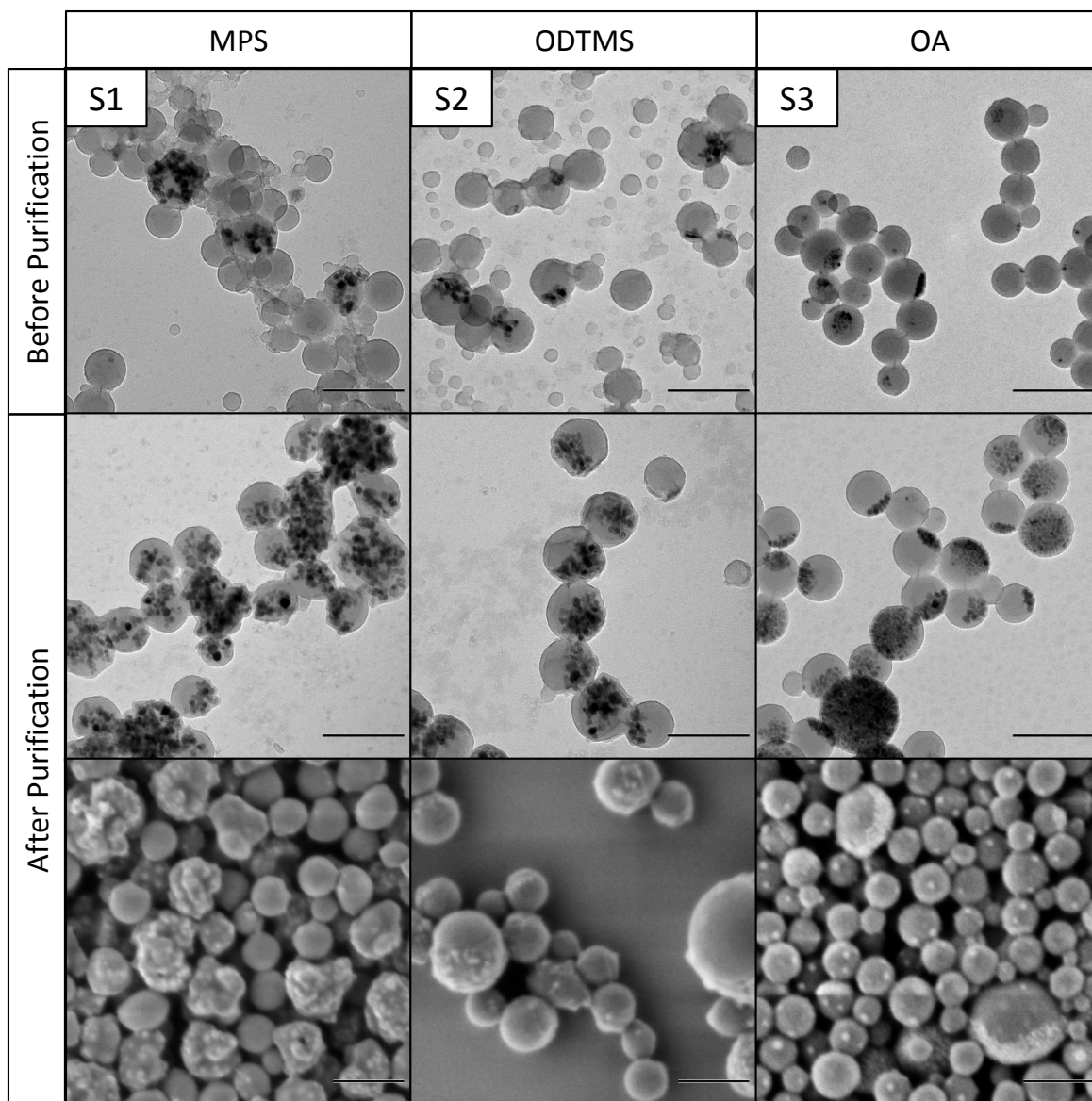


Figure 4.16: Transmission and scanning electron micrographs of differently functionalized magnetite nanoparticles in polystyrene before and after magnetic purification. Scale bars are 200 nm.

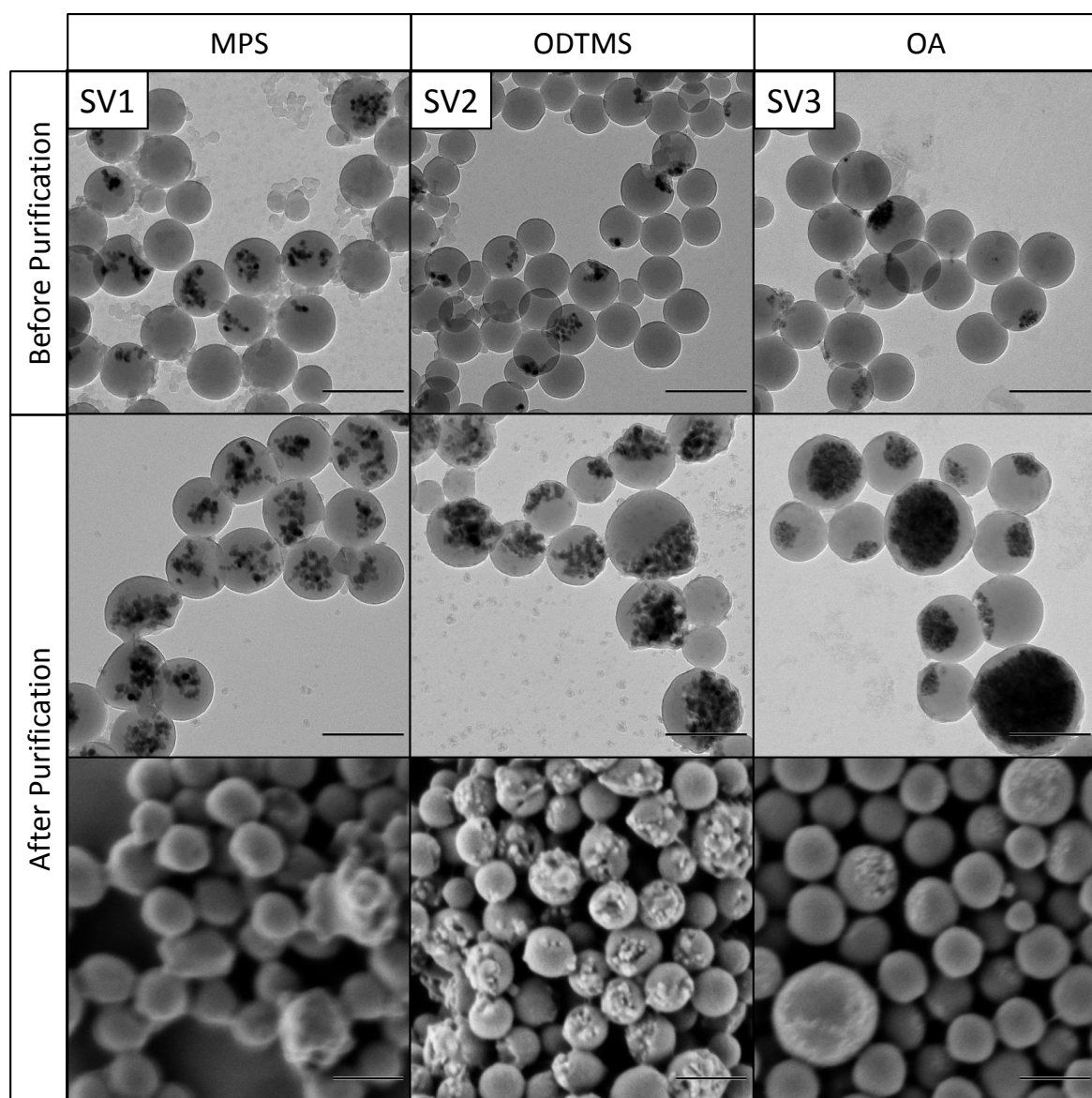


Figure 4.17: Transmission and scanning electron micrographs of differently functionalized magnetite nanoparticles in poly(styrene-*co*-4VP) before and after magnetic purification. Scale bars are 200 nm.

4.2.4. Conclusions

We demonstrate that the functionalization of magnetite nanoparticles with trialkoxy silanes is a good alternative to the classical method using oleic acid. The versatility of the functionalization agents gives various possibilities to tune the surface properties of magnetite particles and, therefore, control the structure of hybrid particles in encapsulation experiments. While MPS-functionalized magnetite is homogeneously distributed in the polymer, ODTMS- and OA-functionalized magnetite forms Janus structures. Magnetic purification of the dispersions can help to increase the magnetite content up to 60 wt.% in polymers with different polarities. Our work shows that silanization offers a tailorable surface functionalization that can help to tune the properties of hybrid particles according to the desired structure and material combination.

4.3. Polymer/Silica Hybrid Nanoparticles and their Structure in Coatings⁵

As an example for possible applications of hybrid nanoparticles synthesized in miniemulsion, their behavior during film formation is investigated. Films are prepared by drop-casting of particle dispersions on glass plates and silicon wafers. The dispersions contain particles consisting of differently functionalized silica nanoparticles and copolymers of methyl methacrylate and butyl methacrylate. The influence of the silica particles on the glass transition temperature T_g is investigated by differential scanning calorimetry (DSC). Furthermore, the preservation of the different structures during the transition from hybrid particles to hybrid films is observed by transmission and scanning electron microscopy.

4.3.1. Synthesis of Hybrid Particles

Silica nanoparticles (Ludox TMA) were hydrophobized by a condensation reaction with two different trimethoxysilane compounds to compatibilize them with the hydrophobic monomers. One batch was functionalized with 3-methacryloxypropyl trimethoxysilane (MPS) and a second one with octadecyl trimethoxysilane (ODTMS). Both functionalization agents are attached covalently to the silica surface and, therefore, cannot desorb during the following processes.

For the preparation of hybrid nanoparticles, free radical miniemulsion polymerization was used, as shown in Figure 4.18. Poly(methyl methacrylate-*co*-butyl methacrylate) (poly(MMA-*co*-BMA)) particles with different compositions were prepared. The applied polymer ratios ranged from pure MMA to a MMA:BMA ratio of 1.

⁵This section is based on the publication “Waterborne Polymer/Silica Hybrid Nanoparticles and their Structure in Coatings” by Alexander Schoth, Emad S. Adurahim, Mohammed A. Bahattab, Katharina Landfester and Rafael Muñoz-Espí, published in 2015 in *Macromol. React. Eng.*, DOI: 10.1002/mren.201500029. © 2015, with kind permission from John Wiley & Sons.

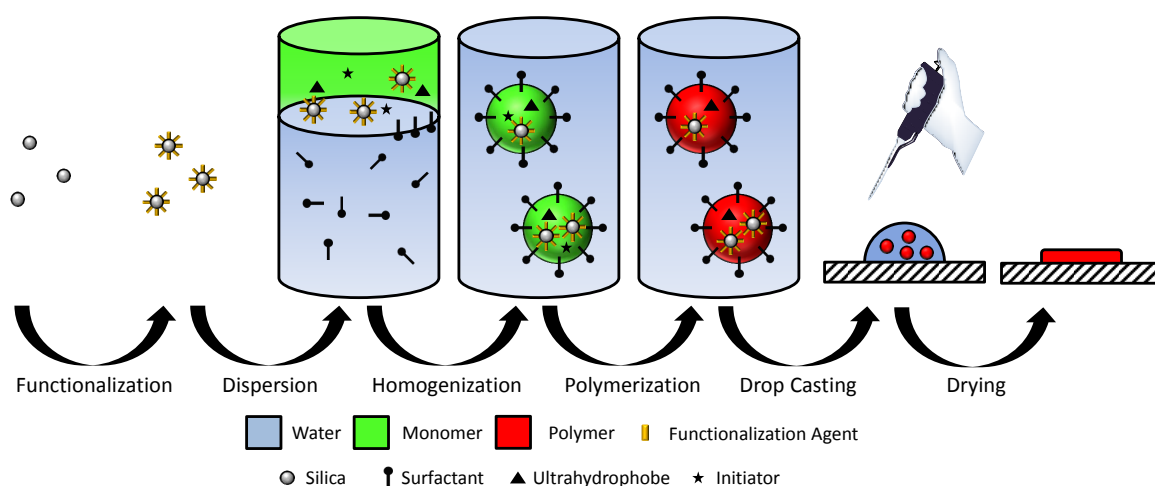


Figure 4.18: Schematic description of the preparation of hybrid films by miniemulsion polymerization.^[163]

The amount of silica in the final product was determined by TGA. The corresponding curves are shown in Figure 4.19. Theoretically, the pure polymer particles should decompose completely during the heating process. The residue of about 5 wt.%, is an artefact of the measurement technique. As the experiments were conducted under nitrogen atmosphere, the organic material has not been oxidized and a certain amount remained as carbon. Taking this into account, the samples containing MPS-functionalized silica have roughly the same amount of silica before and after polymerization, which shows that the amount of aggregated and precipitated silica particles is quite low. For samples prepared with ODTMS-functionalized silica, the silica amount in the final particles is only around 10 wt.%, which means that a significant amount of the silica has been removed in the filtration step after polymerization. This effect can be connected to the high tendency of the silica particles to form aggregates during polymerization, which can also be seen in the final hybrid particles. The structure of these hybrid particles differs depending on the silica functionalization applied. As shown in Figure 4.20, the MPS-silica particles are homogeneously dispersed inside the polymer, while the ODTMS-silica particles show a higher tendency to form aggregates in the polymer phase. This behavior can be explained by the chemical differences between the two functionalization agents: while ODTMS carries an inert alkyl chain, MPS is a methacrylic acid ester. This functional group is able to copolymerize and, therefore, form covalent bonds to the surrounding monomers. This connection between silica and polymer leads to a fixation and helps to suppress aggregation, as shown for pure PMMA particles in section 4.1. The change of the polymer composition has no influence on the amount of encapsulated silica. The deviations shown in Figure 4.19 are statistical and no clear trend can be observed. The change in hydrophobicity due to the presence of longer butyl chains (compared to methyl groups in pure PMMA) has also no influence on the encapsulation efficiency.

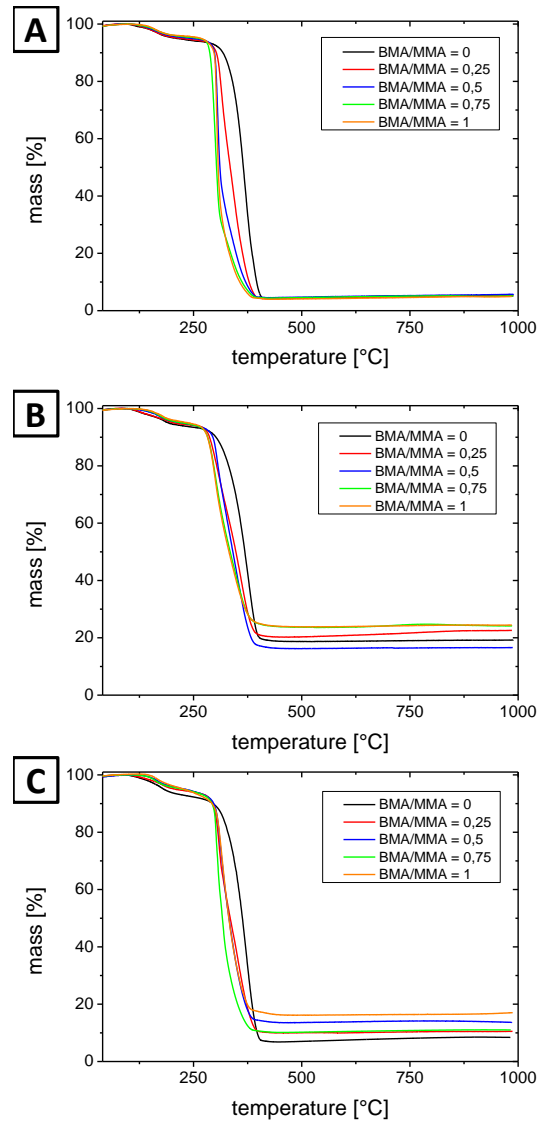


Figure 4.19: Thermogravimetric analyses of hybrid particles with different polymer compositions. The samples contain (A) no silica, (B) 20 wt.% MPS-silica and (C) 20 wt.% ODTMS-silica.^[163]

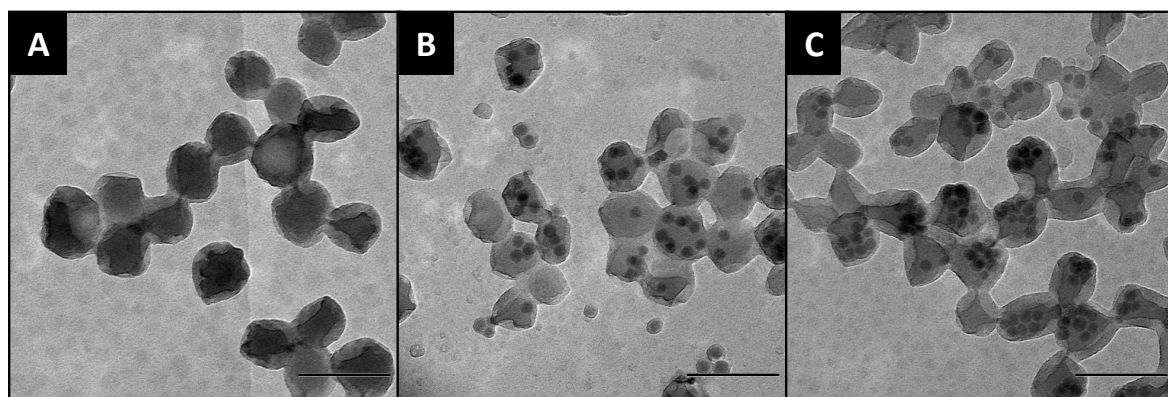


Figure 4.20: Transmission electron micrographs of hybrid nanoparticles with a BMA/MMA ratio of 1:2. The particles contain (A) no silica, (B) 20 wt.% MPS-silica and (C) 20 wt.% ODTMS-silica. Scale bars are 200 nm.^[163]

4.3.2. Physical Properties of Hybrid Particles

Particle sizes of the hybrid particles, determined by DLS, are shown in Figure 4.21 and Table 4.3. Within the accuracy of the method, no size dependence on the polymer composition or on the presence of functionalized silica particles could be observed. This result is plausible because the particle size in miniemulsion is predominantly determined by the surfactant concentration.^[86]

Table 4.3: Physical properties of hybrid particles with different compositions.

Functionalization	SiO ₂ [wt.%]	$\frac{m(\text{BMA})}{m(\text{MMA})}$	M_W [g mol ⁻¹]	T_g [°C]	diameter [nm]
—	—	0	348 000	79	160 ± 40
—	—	0.25	375 000	73	160 ± 10
—	—	0.5	384 000	50	140 ± 30
—	—	0.75	400 000	53	150 ± 10
—	—	1	403 000	45	140 ± 10
MPS	20	0	371 000	83	150 ± 50
MPS	20	0.25	282 000	67	160 ± 50
MPS	20	0.5	203 000	47	140 ± 20
MPS	20	0.75	295 000	45	140 ± 30
MPS	20	1	288 000	52	150 ± 40
ODTMS	20	0	140 000	78	150 ± 30
ODTMS	20	0.25	213 000	66	140 ± 40
ODTMS	20	0.5	311 000	46	130 ± 30
ODTMS	20	0.75	293 000	40	110 ± 40
ODTMS	20	1	232 000	35	130 ± 30

The thermal properties of the hybrid particles are largely important for application as

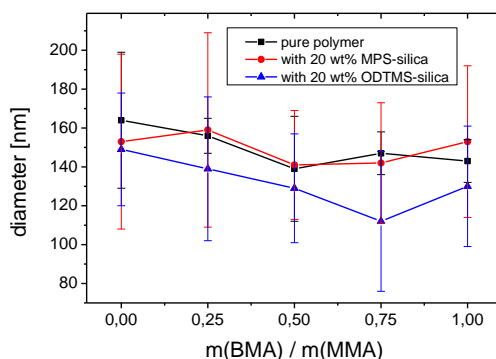


Figure 4.21: Particle size of hybrid particles with different compositions as determined by DLS.^[163]

coating materials. The glass transition temperatures, T_g , of the different particles were determined by differential scanning calorimetry (DSC, Table 4.3). The T_g of the pure PMMA sample is at 79 °C, which is much lower than the literature value expected for PMMA (105 °C). This huge difference is caused by the high amount of impurities in our samples (hexadecane, surfactant, remains of the initiator, etc.), which provide up to 10 wt.% of the dispersed phase. These impurities can act as plasticizers and lower T_g significantly. A higher amount of BMA leads to a decrease of the T_g , as it reduces the crystallinity of the polymer. In the presence of silica particles, the T_g does not change significantly. DSC data show no significant difference between MPS-silica and ODTMS-silica, so the surface properties of the silica do not affect the T_g . Particularly, the copolymerization of MPS, compared to the inert ODTMS, has no influence on the thermal properties. To further investigate the polymer properties, we determined the molar weight distribution of the polymers by gel permeation chromatography (GPC). For this purpose, we dissolved the lyophilized hybrid particles in THF. Pure polymer particles and those prepared with ODTMS-silica gave a clear solution, while the samples with MPS-silica were turbid. The solutions were centrifuged to separate the silica particles, and only the supernatant solution was used for GPC measurements. Integration of the signals shows that for pure polymer and for the sample with ODTMS-silica the whole polymer stays dissolved in the supernatant solution, which means that only silica particles are removed by centrifugation. In the case of MPS-silica, only 45 % of the polymer could be found in the supernatant solution. A significant amount of it copolymerized via the functional groups with the silica particles and, therefore, was removed from the solution during centrifugation. Table 4.3 shows the molar mass distributions of the samples with varying BMA:MMA ratios and different types of silica. It can be seen that the addition of silica particles results in a reduction of the average chain length, which can be explained by two main reasons. On one hand, the surface of the silica particles contains reactive groups that can possibly terminate chain growth and, therefore, lead to a shorter chain length. On the other hand, the free

volume in the droplets is smaller. While the droplet size is comparable for all samples, as seen in Figure 4.21 and Table 4.3, the amount of monomer per droplet is smaller in the presence of silica. The higher surface-to-volume ratio leads to an increased rate of termination reactions (e.g., due to oxygen dissolved in the aqueous phase) and, therefore, shorter chains. For MPS, this effect is even larger, because the polymerizable groups on the particle surface are less reactive than the free monomer, which results in a retardation of the reaction.

4.3.3. Film Formation

As a proof of concept, we drop-casted the diluted dispersions on silicon wafers and observed the formed films under SEM before and after tempering above the T_g , as it is shown in Figure 4.22. Before tempering, the particle structure can be clearly observed and the particles show no tendency for film formation.

After annealing at 100 °C for 24 h, the particles formed a homogeneous film, as seen in the SEM images. The pure polymer particles lead to a smooth surface, while the silica can clearly be seen on the surface of the films. Similar to the structure of the hybrid particles, the films containing ODTMS-silica show a higher amount of large silica aggregates than in the case of MPS-silica. This structure is not limited to the surface, but can be observed throughout the whole film, as proven by cross section SEM. The differences in the film thickness in the range of about 1–5 μm are caused by the applied drop-casting method, which is not suitable to produce homogeneous films. However, for a structure analysis, the accuracy of the method is absolutely sufficient. Another requirement for possible applications is that the inorganic particles have no negative effect on the optical properties of the films. To test this influence, we applied the same process as described before to prepare hybrid films on glass wafers. Figure 4.23 shows that the particles form translucent films. The presence of silica in general and especially the larger number of aggregates for ODTMS-silica has no negative effect on the optical clarity.

4.3.4. Conclusions

In conclusion, we showed that the structure differences in polymer/silica hybrid nanoparticles can also be observed in hybrid films formed by these particles. The structure of the hybrid material, in particular the amount of silica aggregates, can be preserved during the film formation process. Surface functionalization of the silica particles gives us the possibility to tune the degree of aggregation in the hybrid particles as well as in the final films. While polymerizable groups on the silica surface cause a fixation of the silica in the surrounding polymer matrix, leading to a homogeneous distribution of the silica in the polymer, the presence of inert alkyl chains leads to a segregation of silica and polymer. This structure difference could be observed by TEM in the particles and by SEM in case of the films.

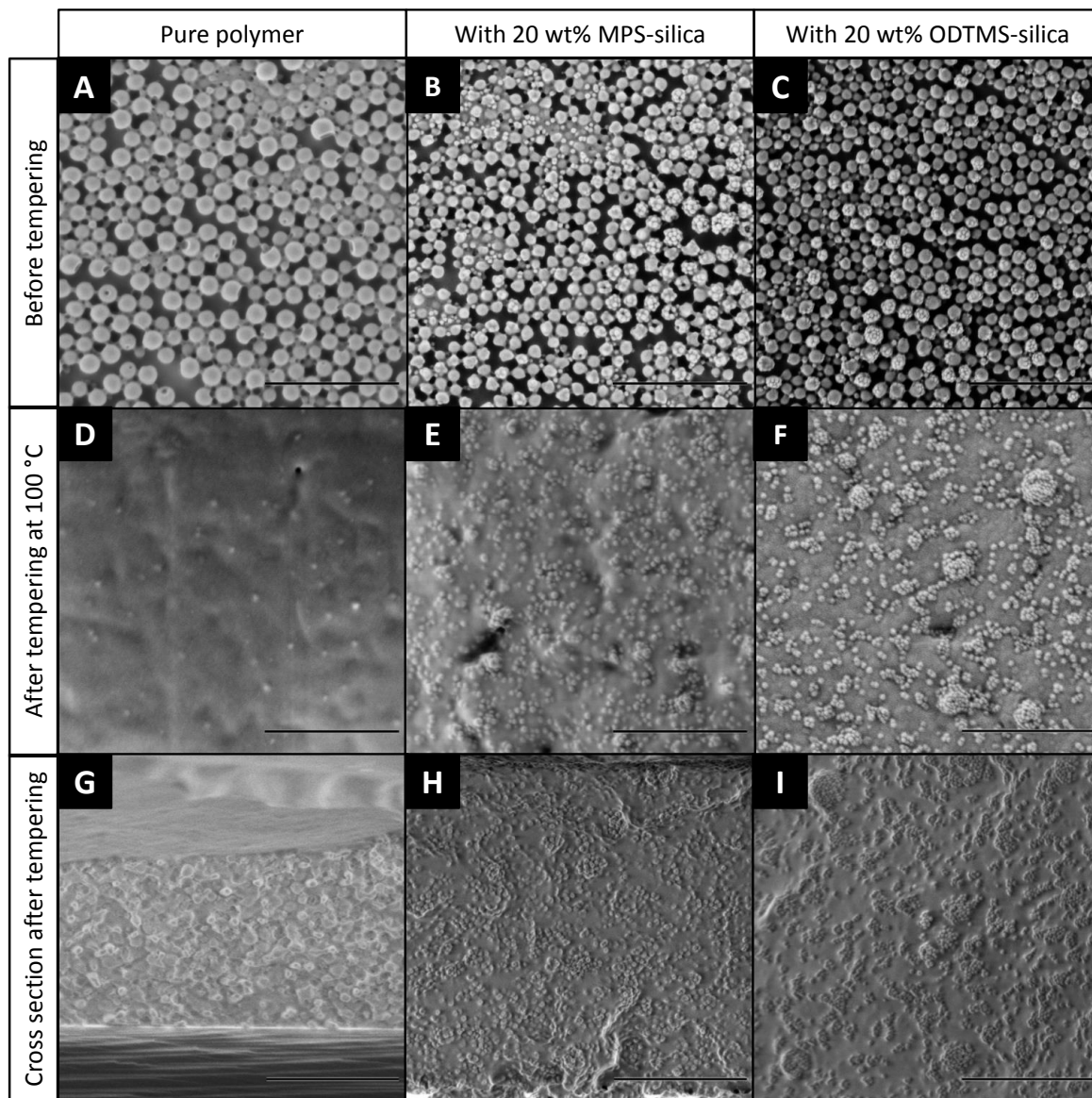


Figure 4.22: Scanning electron micrographs of hybrid particles with a BMA:MMA ratio of 1:2, containing (A, D, G) no silica, (B, E, H) 20 wt.% MPS-silica and (C, F, I) 20 wt.% ODTMS-silica. The images were taken (A, B, C) directly after drop-casting and drying, (D, E, F) after tempering at 100 °C for 24 h, and (G, H, I) as cross-sections images after tempering. Scale bars are 1 μm .^[163]

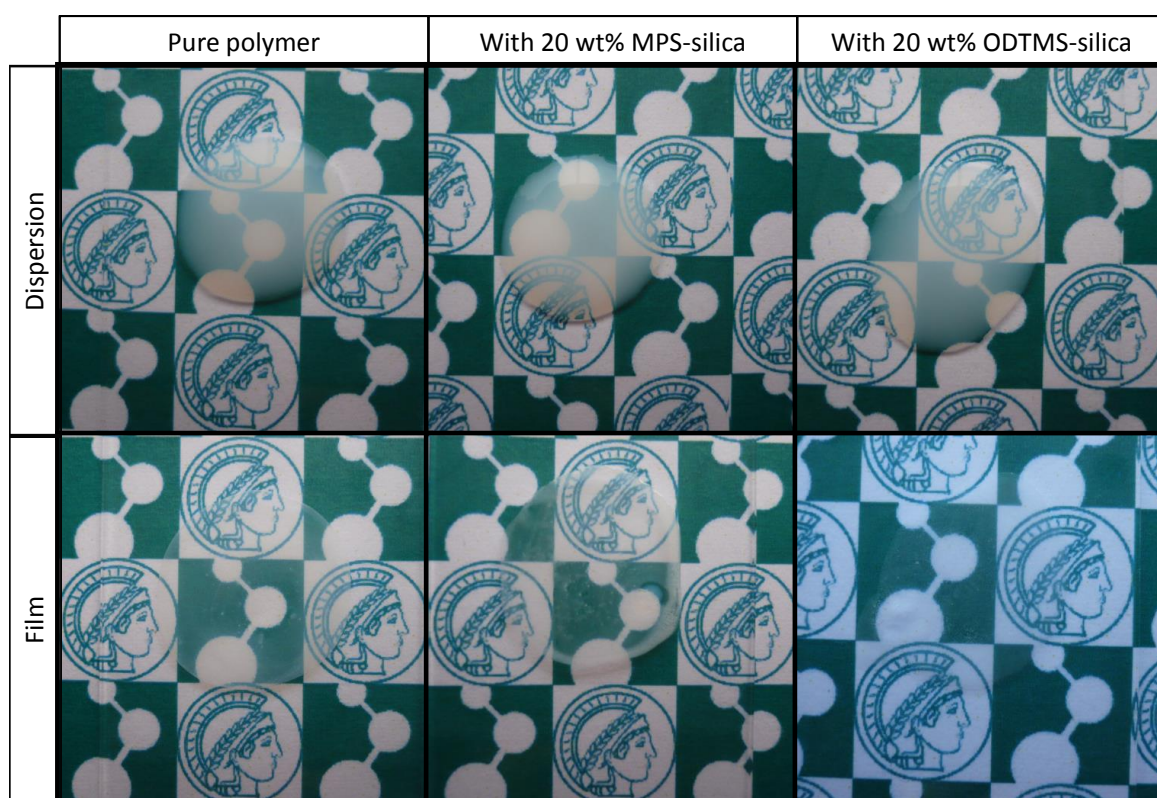


Figure 4.23: Photographs of hybrid particles with a BMA:MMA ratio of 1:2 as dispersions and as dry films after tempering at 100 °C for 24 h.^[163]

4.4. Encapsulation of Hydrophobic Liquids in the Presence of Silica Nanoparticles

The formation of nanocapsules in miniemulsion follows a process similar to the particle synthesis described in chapter 4.1. To obtain a second liquid phase, the amount of hexadecane is increased. As the polymer PMMA is not soluble in hexadecane, phase separation occurs, and the system assembles according to the physical principles described in section 2.2.1, which results in the formation of a core-shell morphology. In the following experiments, we demonstrate the synthesis of PMMA/hexadecane hybrid nanocapsules via miniemulsion polymerization as well as solvent evaporation. Furthermore, the assembly of functionalized silica nanoparticles in the presence of two organic phases inside the nanodroplets is presented.

4.4.1. Nanocapsules via Polymerization in Miniemulsion

In a first series of experiments, we synthesized nanocapsules using miniemulsion polymerization. MMA and hexadecane were combined in the dispersed phase of the miniemulsion. During polymerization, the solubility of the oligomers in the hexadecane decreases, until phase separation occurs. Due to the combination of interfacial tensions, as capsule morphology with hexadecane surrounded by PMMA develops. The structure of these capsules with in the size range of 200 nm is shown in the micrographs in Figures 4.24a and b. DLS shows that the size distribution of the capsules (Table 4.4) is broader than the distribution of the corresponding particles. Especially in the SEM image, open capsules can be seen, which is mostly caused by a decomposition of the polymer shell under the electron beam.

Table 4.4: Compositions and sizes of nanocapsules synthesized via miniemulsion polymerization.

MMA [wt.%]	Hexadecane [wt.%]	V59 [wt.%]	Silica [wt.%]	Funct.	diameter [nm]
47.5	50	2.5	0	—	210 ± 67
45	47.5	2.5	5	MPS	200 ± 71
45	47.5	2.5	5	ODTMS	221 ± 57

Figures 4.24c and d show capsules containing 5 wt.% MPS-silica. A significant amount of the silica is not encapsulated, but can be found as aggregates. Therefore, encapsulation is much less efficient compared to the particle system described in chapter 4.1. Addition of ODTMS-silica leads to more homogeneous capsules. The silica particles seem to assemble preferably in the hexadecane core, which can be explained by the much higher hydrophobicity of the particles compared to the ones with MPS.

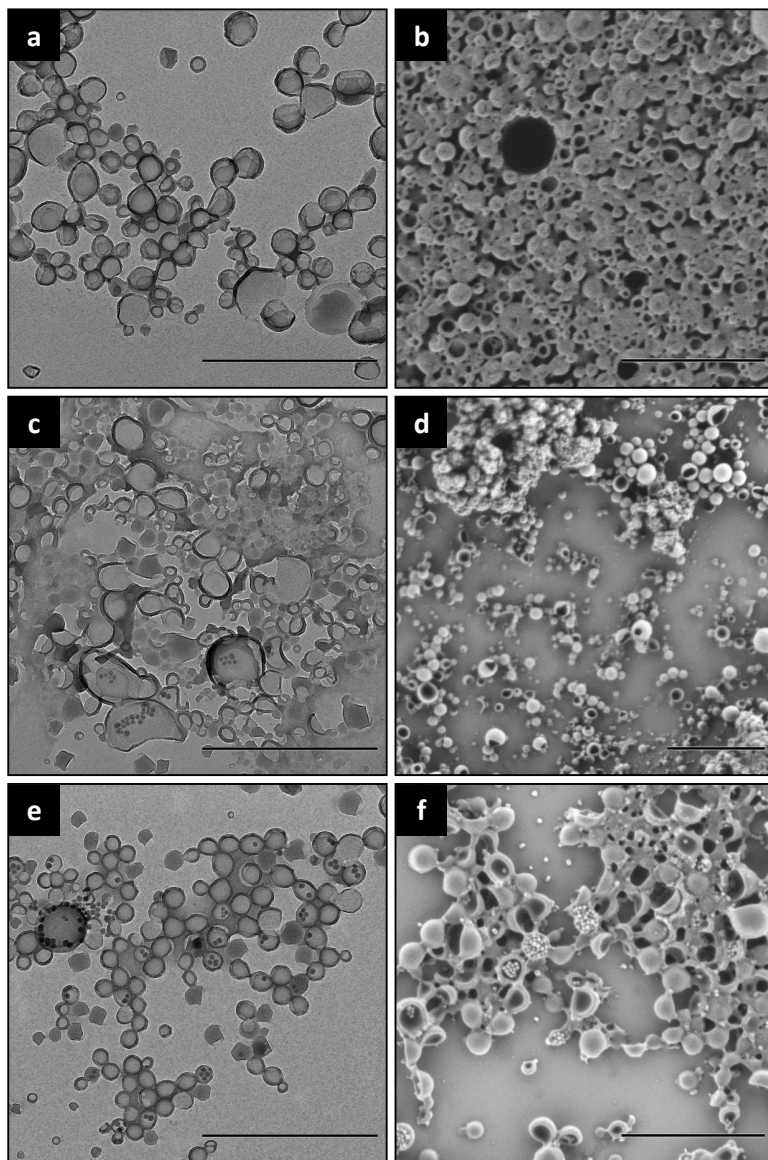


Figure 4.24: TEM (a, c, e) and SEM (b, d, f) images of PMMA nanocapsules containing hexadecane as liquid core, synthesized via miniemulsion polymerization. The capsules contain (a, b) no silica, (b, c) 10 wt.% MPS-silica and (e, f) 10 wt.% ODTMS-silica. Scale bars are 1 μm .

4.4.2. Nanocapsules via Solvent Evaporation in Miniemulsion

The synthesis of nanocapsules is also possible via the solvent evaporation approach. At the beginning, PMMA and hexadecane are dissolved in chloroform and form the droplets of the dispersed phase. During evaporation of the chloroform, PMMA precipitates and separates from the hexadecane. Nanocapsules form analogous to the mechanism described in the previous section. According to DLS data (Table 4.5), the size distribution of the capsules is comparable to the ones obtained by polymerization (Table 4.4).

Table 4.5: Compositions and sizes of nanocapsules synthesized via solvent evaporation.

PMMA [wt.%]	Hexadecane [wt.%]	SiO ₂ [wt.%]	Funct.	diameter [nm]
50	50	0	—	189 ± 63
45	45	10	MPS	256 ± 139
45	45	10	ODTMS	189 ± 62

However, regarding the electron micrographs in Figure 4.25, the capsules obtained via solvent evaporation show a much more homogeneous structure. The high amount of hexadecane seems to hinder polymerization of MMA, leading to a labile capsule shell. Using already pre-formed polymer for solvent evaporation helps to overcome this problem and gives nanocapsules with a homogeneous structure that can also be observed in the electron microscopes.

MPS-silica added to the capsules can be found attached to the capsule shell (Figures 4.25c and d). The TEM image reveals that the particles show a higher tendency to assemble at the capsule shell, while the SEM image shows a large amount of particles on top of the shell. Contrarily, the surface of capsules containing ODTMS-silica (Figures 4.25e and f) are smooth. The particles assemble preferably in the liquid hexadecane core.

4.4.3. Conclusions

We were able to achieve the structure control by changing the surface functionalization of inorganic particles, even in a system containing four different phases. The silica particles do not hinder phase separation between polymer and liquid core and stable nanocapsules are formed. The particles assemble according to their polarity. While the very hydrophobic ODTMS-functionalized particles go to the hydrophobic liquid core, the more polar MPS-functionalized particles can be found as part of the polymer shell. With this finding, a precise tuning of the structure of hybrid nanocapsules carrying functionalized inorganic particles is possible.

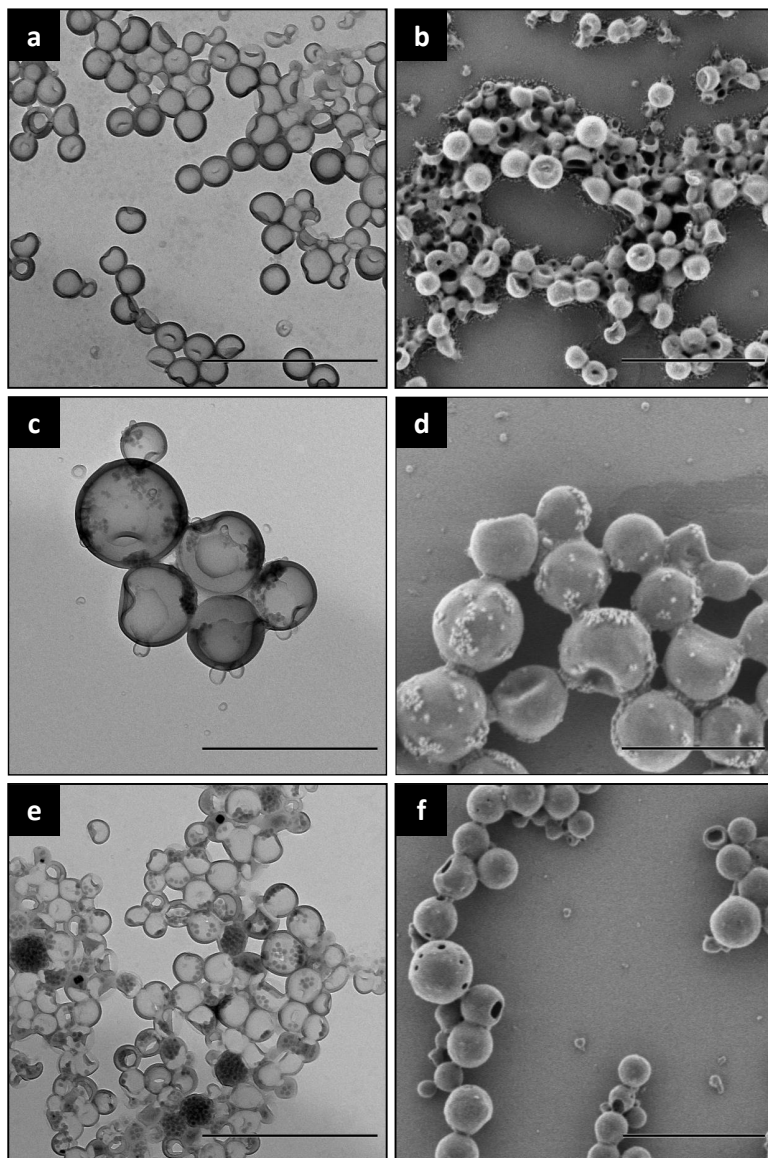


Figure 4.25: TEM (a, c, e) and SEM (b, d, f) images of PMMA nanocapsules containing hexadecane as liquid core, synthesized via solvent evaporation. The capsules contain (a, b) no silica, (b, c) 10 wt.% MPS-silica and (e, f) 10 wt.% ODTMS-silica. Scale bars are 1 μm .

4.5. Pickering-Stabilized Nanoparticles in Direct Miniemulsion

A further possibility to control the structure of hybrid particles is the use of Pickering emulsions. In Pickering emulsions, the droplets are stabilized by a mechanically stable film of nanoparticles at the liquid/liquid interface.^[22] The geometry of such a system leads to hybrid particles with a polymeric core and a shell formed by the adsorbed inorganic nanoparticles. This strategy offers a convenient way to synthesize hybrid particles with a defined morphology, without the necessity to functionalize the surface of the inorganic material in advance.

4.5.1. Stabilization Using Laponite Clay

In miniemulsion, the stabilization with clay nanoplatelets is oftentimes used.^[126,128] In the following experiments, Laponite RD clay particles are used to stabilize polystyrene droplets in miniemulsion, as already shown by Bon and Colver.^[127] Laponite RD clay particles are synthetic layered silicate particles with a lateral diameter of around 30 nm and a thickness of 1 nm. The chemical composition of the particles is $[\text{Si}_8(\text{Mg}_{5.45}\text{Li}_{0.4})\text{O}_{20}(\text{OH})_4]\text{Na}_{0.7}$.

Laponite RD clay particles can be dispersed in water by applying ultrasound. The resulting dispersion is completely transparent, which shows that the clay particles are perfectly dispersed. Addition of sodium chloride leads to a destabilization of the particles.^[164] Due to the increased ionic strength of the salt solution compared to pure water, the ionic double layer around the dispersed particles is compressed.^[165] Electrostatic repulsion is lowered and the particles flocculate. As a result, the dispersion gets turbid and the viscosity increases dramatically.

Addition of an organic monomer phase leads to an assembly of the agglomerates at the liquid/liquid interface, as the clay is not well dispersed in the salt solution. Application of ultrasound to the system breaks the clay agglomerates and the monomer droplets. As a result, the system is able to rearrange and form a Pickering emulsion, in which the single clay platelets adsorb at the droplet surface and induce Pickering stabilization.^[127] The composition of the sample DP1 is described in Table 4.6. Polymerization of the Pickering-stabilized droplets leads to nanoparticles with a diameter of about 200 nm, as shown in Figure 4.26. It can also be seen that the dispersion is not stable and big aggregates in the size range of several microns are formed. Although these results show the limits of this system, the overall strategy seems promising for the stabilization of emulsions. In the next step, silica particles are tried as alternative to Laponite clay.

4.5.2. Stabilization Using Silica

Silica is by far the most frequently used stabilizer for Pickering emulsions. It is available in a wide size range and with plenty of different surface functionalizations and, therefore, offers a large variety of strategies.^[54,140] For example, the adjustment of pH can be used to tune

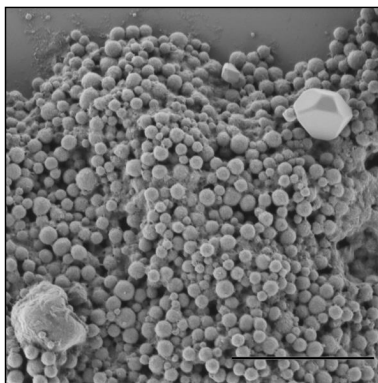


Figure 4.26: Scanning electron micrograph of clay-stabilized polystyrene nanoparticles (DP1). Scale bar is 2 μm .

the stabilizing properties of dispersed Ludox TMA silica particles.^[130]

In our experiments, we use the same strategy as described in chapter 4.5.1 for Laponite clay as stabilizer.^[127] Addition of sodium chloride leads to a destabilization of well-dispersed Ludox TMA particles and enhances their adsorption at the water/oil interface. As the silica particles are round-shaped with a diameter of 22 nm and have a higher surface charge, much higher amounts of salt are necessary in order to destabilize the dispersion. As shown in Table 4.6, the salt amount is increased by the factor 10 to 30 compared to the clay-stabilized systems.

Table 4.6: Compositions of Pickering-stabilized nanoparticles. The dispersed phase content is 10 wt.% for all samples and the composition of the dispersed phases is the same in every sample as described in chapter 5.5. All values are given in wt.% with respect to the continuous phase.

Sample	H ₂ O	Laponite RD	Ludox TMA	NaCl
DP1	98.5	1	—	0.5
DP2	94	—	1	5
DP3	89	—	1	10
DP4	84	—	1	15

The higher stability of the dispersed Ludox TMA particles can also be seen with the bare eye. Even after addition of 15 wt.% of sodium chloride, the dispersions stay transparent and the silica particles do not flocculate. However, the particles are able to stabilize emulsions, as can be seen in Figure 4.27. The ideal amount of salt for this system is 10 wt.% with respect to the continuous phase, as it is shown in Figure 4.27B. The hybrid particles show the narrowest size distribution compared to the other samples. However, the particles are in the size range of around 5 μm and, therefore, much larger than it would be desirable for a miniemulsion. A lower salt amount, as shown in Figure 4.27A, leads to a very broad size

distribution. If the amount of salt is too high, big crystals of sodium chloride can be found all over the sample and a huge part of the silica particles forms free aggregates, as can be seen in Figure 4.27C.

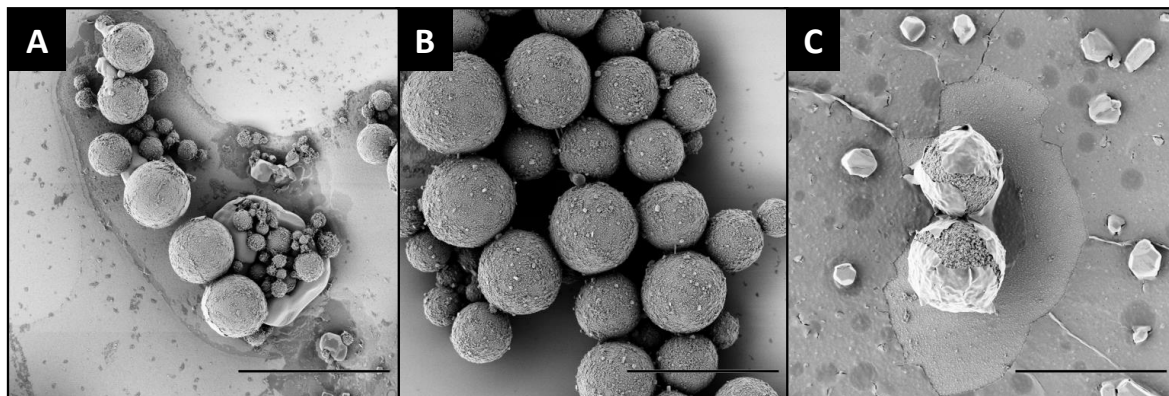


Figure 4.27: Scanning electron micrographs of particles stabilized with Ludox TMA. The samples contain 5 wt.% (DP2, A), 10 wt.% (DP3, B) and 15 wt.% (DP4, C) of NaCl in the continuous phase. Scale bars are 10 μm .

4.5.3. Conclusions

The stabilization of miniemulsions with inorganic particles is an alternative to the classical method using surfactants. It is not only possible to avoid the disadvantages of surfactants, but the Pickering stabilization offers a direct possibility to control the structure of hybrid particles. It was shown that the stabilization of emulsions using silica particles is possible by using sodium chloride as destabilizer for the aqueous silica dispersion in the continuous phase. Although the resulting particles are much larger than desired, this method offers promising possibilities for structure control, as the polymer is surrounded by and clearly separated from the inorganic nanoparticles.

4.6. Pickering-Stabilized Nanocapsules in Inverse Miniemulsion⁶

Silica particles with differently functionalized surfaces and, therefore, different wettability, are tested as candidates to stabilize inverse miniemulsions. In the next step, the emulsions are used as templates for the formation of polyurethane capsules. Different fields of application for the system are introduced by the encapsulation of water-soluble materials. As examples, the organic dye sulforhodamine 101 (SR101) as well as high amounts of sodium sulfate are used as payloads.

4.6.1. Stabilization of the Emulsions

The stabilization of emulsions with particles via the Pickering mechanism depends on the contact angles between the continuous phase, the dispersed phase, and the stabilizing particles. As a general rule, hydrophilic particles stabilize direct emulsions, while hydrophobic particles stabilize inverse emulsion.^[28] Therefore, the surface functionalization of the particles is crucial for this system, as it determines the hydrophobicity of the particle surface. As stabilizers, we used three different types of silica: Ludox TMA particles without modification, functionalized with propyl trimethoxysilane (PTMS), and with octadecyl trimethoxysilane (ODTMS) (see Figure 4.28).

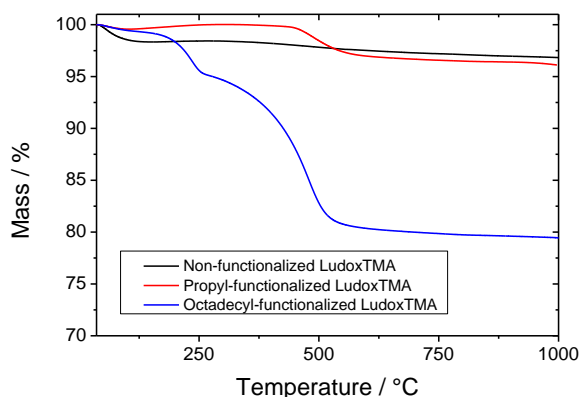


Figure 4.28: Thermogravimetric analyses of differently functionalized Ludox TMA silica nanoparticles.^[166]

Figure 4.29 shows the preparation of a miniemulsion according to the recipe IP2 shown in Table 4.7 with the three types of silica as stabilizers. The left vial (marked in blue) contains unfunctionalized Ludox TMA, the silica in the central vial (marked in red) is functionalized with PTMS while the right one (marked in green) contains ODTMS-functionalized silica. The

⁶This section is based on the publication “Surfactant-Free Polyurethane Nanocapsules via Inverse Pickering Miniemulsion” by Alexander Schoth, Katharina Landfester and Rafael Muñoz-Espí, published in 2015 in *Langmuir*, volume 31 on pages 3784 to 3788. © 2015, with kind permission from American Chemical Society.

first picture shows the silica particles in cyclohexane. While the non-functionalized particles are too hydrophilic and, therefore, precipitate immediately, the functionalized particles can be dispersed in cyclohexane to a certain extent. ODTMS-silica in the green vial gives an opaque suspension, whereas the dispersion of PTMS-silica is turbid, indicating a larger amount of aggregates. After addition of the aqueous phase consisting of water and 2.5 wt.% NaCl and stirring for 10 min, the hydrophilic, unfunctionalized particles do clearly not stabilize the emulsion. As the further steps do not lead to significant changes, this sample is neglected in the upcoming considerations. ODTMS-silica is able to stabilize the pre-emulsion, as can be seen in the second picture. PTMS-silica shows an unexpected behavior. After stirring, the organic phase becomes completely clear, while the aqueous part is turbid. Presumably, the silica has assembled around the water droplets without stabilizing the emulsion sufficiently. After ultrasonication, PTMS- and ODTMS-silica give stable miniemulsions. However, after 30 min and, more clearly, after 24 h, the ODTMS-silica precipitates and the emulsion is no longer stable. PTMS-silica gives a stable miniemulsion, which does not separate even after 24 h. The clear oil phase that evolves on top of the red vial can be explained by the high density difference between cyclohexane and the silica-loaded water droplets. In this case, shaking for a few seconds is already sufficient to regain a homogeneous emulsion.

4.6.2. Capsule Formation

With a stable miniemulsion system, the synthesis of a capsule shell via the interfacial polymerization reaction of 1,6-hexanediol and toluene diisocyanate (TDI) is possible. The capsule morphology of sample IP1 with a shell thickness of around 35 nm is shown in Figure 4.30A. The size distribution of the capsules, determined by statistical treatment of electron micrographs, with a diameter of (760 ± 430) nm can be seen in Figure 4.31. This is, to the best of our knowledge, the first Pickering-stabilized capsule synthesis in inverse miniemulsion. The broad size distribution of the particles can be improved by the addition of an ultralipophobe. In this case, sodium chloride (2.5 wt.%) was added, which led to a more homogeneous size distribution and an average size of (960 ± 320) nm for sample IP2, as shown in Figure 4.30B/C and Figure 4.31 (for the exact composition of the capsules, see also Figure 4.32).

4.6.3. Encapsulation of Organic Compounds

The permeability of the polyurethane shell is of great importance for potential applications. As a control compound, the water soluble dye SR101 was encapsulated as sample IP3, and its release in an aqueous surfactant solution was studied by fluorescence spectroscopy. Therefore, the capsule dispersion was dispersed in a 0.1 wt.% solution of SDS in water and stirred for 24 h to enable the release of the dye. These aqueous dispersions were sufficiently stable to perform the following spectroscopical analyses. The fluorescence intensity of the supernatant solution after centrifugation is close to zero, as shown in Figure 4.33. This observation indicates that

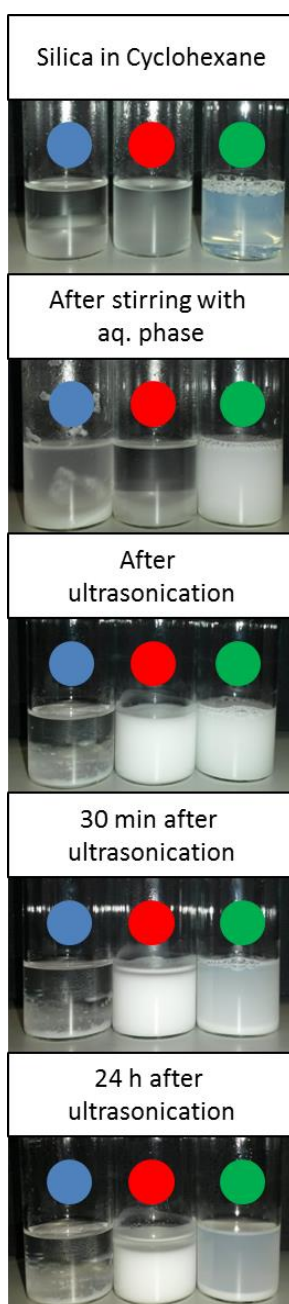


Figure 4.29: Preparation of Pickering miniemulsions consisting of water, NaCl, silica particles and cyclohexane according to composition IP2. The silica particles are non-functionalized (left vial), propyl-functionalized (central vial) and octadecyl-functionalized (right vial) Ludox TMA.^[166]

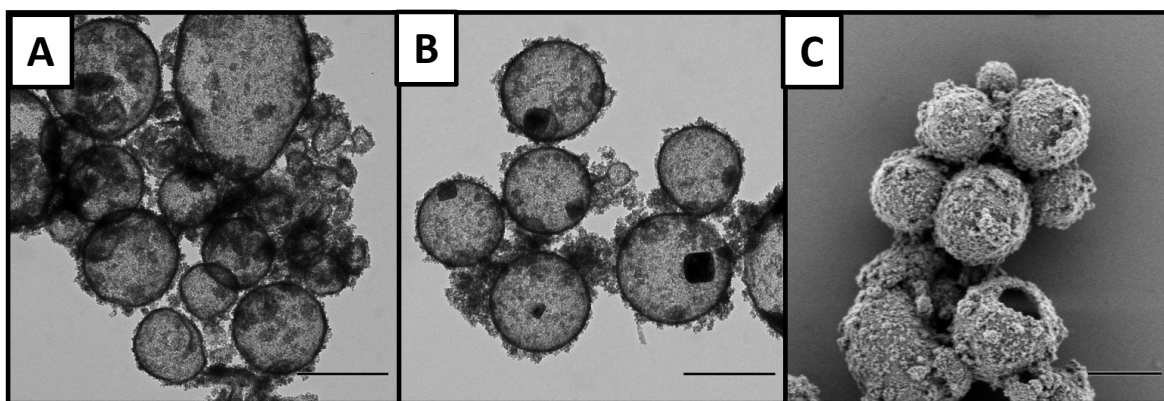


Figure 4.30: Transmission (A, B) and scanning (C) electron micrographs of PU nanocapsules containing water A) without (IP1) and B, C) with 2.5 wt.% sodium chloride (IP2). Scale bars are 1 μm .^[166]

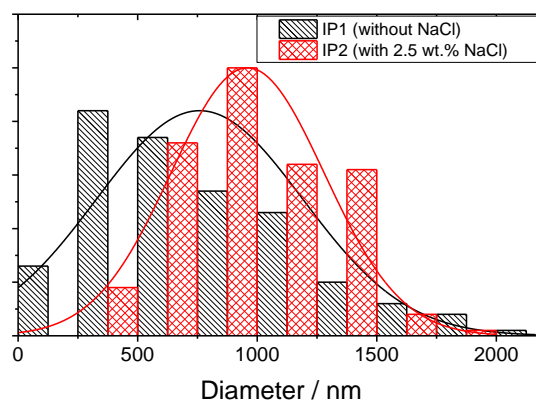


Figure 4.31: Size distribution of salt-free PU capsules (IP1) compared to capsules containing 2.5 wt.% NaCl (IP2).^[166]

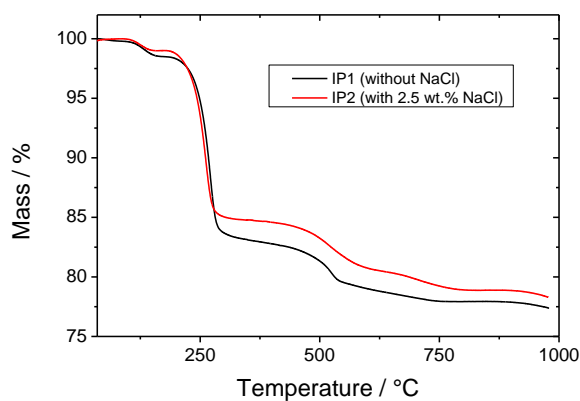


Figure 4.32: Thermogravimetric analyses of PU/silica nanocapsules without (IP1) and with 2.5 wt.% of sodium chloride (IP2).^[166]

the nanocapsules were impermeable for the dye and did not release it within the regarded time frame. Consequently, our system is a possible candidate for the safe encapsulation of water-soluble compounds, such as dyes or drugs.

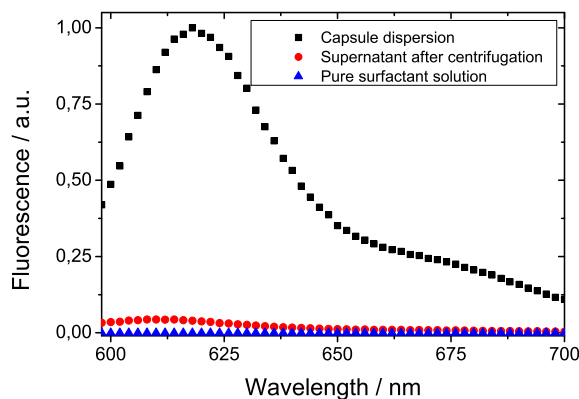


Figure 4.33: Fluorescence intensities of the fluorescent dye SR101 in the redispersed nanocapsule dispersion IP3 and the supernatant solution after centrifugation.^[166]

4.6.4. Encapsulation of Inorganic Salts

Besides organic compounds, the presented system also offers the possibility of encapsulating inorganic salts. As already shown in Figure 4.30, the salts act as ultralipophobes and lead to a stabilization of the miniemulsion. Furthermore, salts with special properties can add functions to the nanocapsules. An example for functional salts are the phase change materials (PCMs). This class of materials shows a high enthalpy of fusion, which makes them appropriate for heat storage. The two main groups of materials are paraffins and salt hydrates.^[87,167] The encapsulation of PCMs in sub-micron-sized capsules can offer advantages regarding the homogeneity of distribution and the mechanical stability of the capsules in the carrier material. In our experiments, we encapsulated sodium sulfate, whose decahydrate melts at 32 °C.^[168] Figure 4.34 shows electron micrographs of the nanocapsules with 5 wt.% sodium sulfate (IP4). The encapsulation was successful and the capsules show a homogeneous size distribution of (1050 ± 290) nm.

For applications as PCM storage material, a higher amount of salt is necessary. We were able to increase the salt content in sample IP5 up to 20 wt.%, as can be seen in Figure 4.35. The salt is inside the capsule and the capsule size stays in the same range with (860 ± 230) nm. Salt contents above 20 wt.% were not possible due to the limited solubility in water. Another reason is that with a higher salt concentration the viscosity of the aqueous phase increases. This increase hinders droplet breakup, which could lead to larger droplets and a much broader droplet size distribution. Differential scanning calorimetry (DSC) of the dried capsules is shown in Figure 4.36. In the first cycle, recrystallization to the decahydrate

occurs. The melting enthalpy of -58 J g^{-1} stays constant in the following measurement cycles and shows a stable condition of the dried capsules. Considering the salt content of 20 wt.%, this result fits perfectly the literature value^[168] of -254 J g^{-1} for the pure salt.

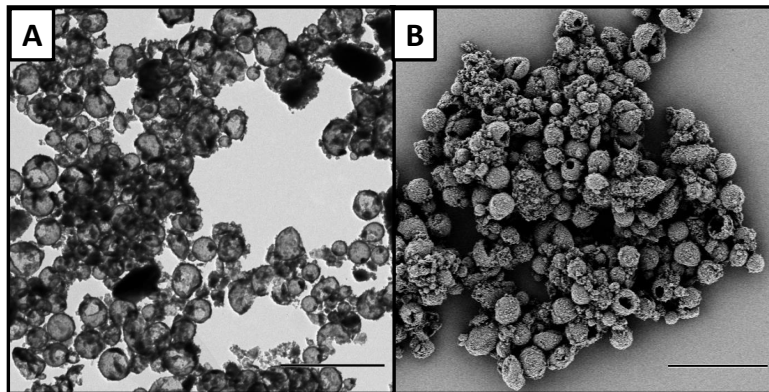


Figure 4.34: Transmission (A) and scanning (B) electron micrographs of PU nanocapsules IP4 containing 5 wt.% of sodium sulfate. Scale bars are $5 \mu\text{m}$.^[166]

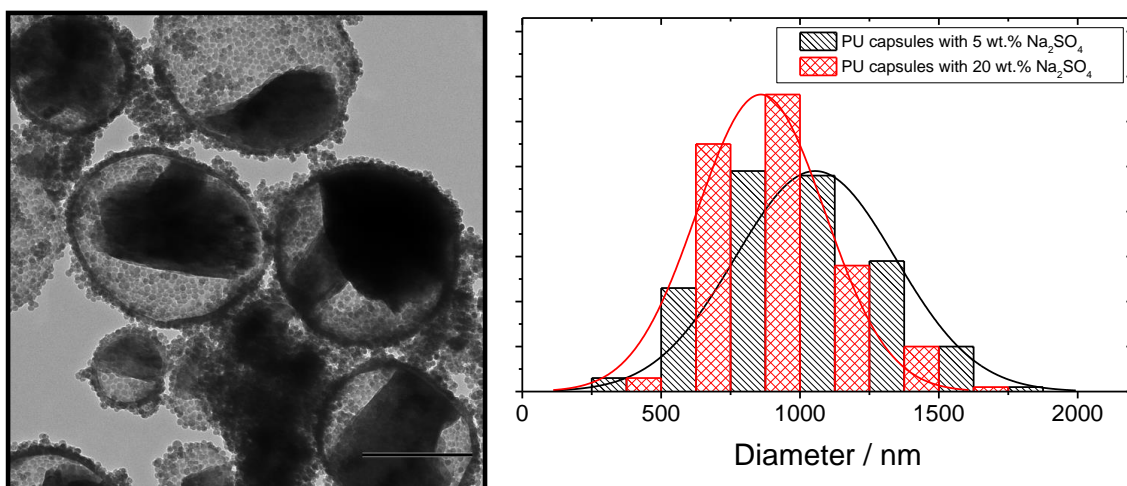


Figure 4.35: Transmission electron micrograph and size distribution of PU nanocapsules IP5 containing 20 wt.% of sodium sulfate. Scale bar is 500 nm .^[166]

4.6.5. Conclusions

In conclusion, we have demonstrated that the well-established Pickering stabilization mechanism can be extended to the synthesis of nanocapsules with a narrow size distribution in inverse miniemulsion. The wettability of inorganic particles can be tuned by changing the type of surface functionalization, making them capable to stabilize the emulsion. The synthesized capsules can be redispersed in aqueous surfactant solutions to make them suitable for a wide range of uses, from industrial to biomedical applications. The safe encapsulation of

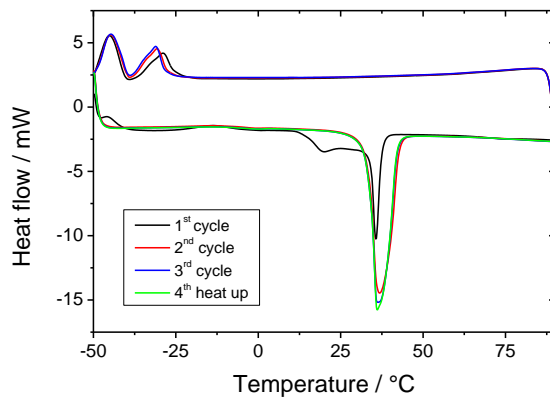


Figure 4.36: Thermal analyses of PU nanocapsules IP5 containing 20 wt.% of sodium sulfate.^[166]

Table 4.7: Compositions of Pickering-stabilized nanocapsules. All samples contain 5 wt. PTMS-functionalized silica nanoparticles with respect to the continuous phase. The dispersed phase content is 5 wt.% for all samples. All values are given in wt.% with respect to the dispersed phase.

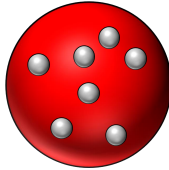
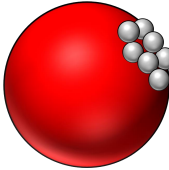
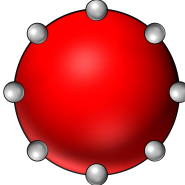
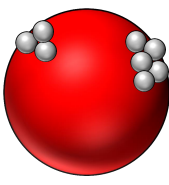
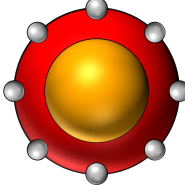
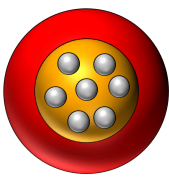
Sample	H ₂ O	hexanediol	TDI	NaCl	Na ₂ SO ₄	SR101
IP1	86.5	4.5	9.0	—	—	—
IP2	84.0	4.5	9.0	2.5	—	—
IP3	83.95	4.5	9	2.5	—	0.05
IP4	81.5	4.5	9.0	—	5.0	—
IP5	66.5	4.5	9.0	—	20.0	—

organic water-soluble compounds like the fluorescent dye sulforhodamine 101 is easily transferable to other dyes or drugs. With the encapsulation of inorganic salts, we demonstrated that also dissociated ions have no negative effect on the stability of the miniemulsion. As a consequence, our approach opens the door towards the surfactant-free encapsulation of any water-soluble substance in inverse miniemulsion.

4.7. General Discussion

In the different sections of this chapter, several parameters for the structure control of polymer/inorganic hybrid nanomaterials in miniemulsion have been presented. The materials have been prepared by using different techniques, which have been discussed in detail. An overview of the possible structures of the hybrids is given in Tables 4.8 and 4.9.

Table 4.8: Structures of hybrid nanomaterials achievable in miniemulsion systems by using different surface functionalization agents.

Procedure	MPS	ODTMS
Polymerization		
Solvent Evaporation		
Nanocapsules via Solvent Evaporation		

The main parameter that has been varied in our experiments to tune the structure of the hybrids is the surface functionalization of the inorganic nanoparticles, as it is shown in Table 4.8. In most experiments, MPS-functionalized particles have been compared to particles functionalized with ODTMS. Polymerization in miniemulsion leads to a homogeneous distribution of MPS-functionalized particles in the polymer, while ODTMS-functionalized particles assemble in a Janus-like structure. This result could be shown for silica particles in PMMA (section 4.1) and in different copolymers of MMA and BMA (section 4.3). By using

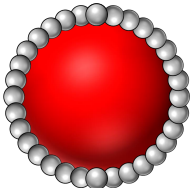
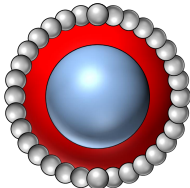
magnetite particles functionalized with MPS and ODTMS, the same results were obtained in PMMA, polystyrene, and a copolymer of styrene and 4VP (section 4.2). Both functionalization agents have also been used in the solvent evaporation approach. In these experiments, all silica particles assembled on the surface of PMMA particles. While the MPS-functionalized silica was well distributed over the whole surface, ODTMS-functionalized silica showed a high tendency to form aggregates. Addition of hexadecane lead to the formation of nanocapsules. In this case, the MPS-functionalized silica could be found in the PMMA shell, while the ODTMS-functionalized particles assembled inside the liquid core.

To explain these findings, two main differences between MPS and ODTMS have to be taken into account: polarity and reactivity. The effect of the polarity of inorganic particles has already been shortly discussed in section 2.4.3. In general, the interfacial energy of the system has to be minimized. This is reached by a suitable self-assembly of the different materials. A similar polarity between two phases (e.g. inorganic particles and polymer) leads to a low interfacial tension between these phases. In consequence, a large interfacial area between them is favorable to achieve a low interfacial energy. This effect can be clearly seen in the solvent evaporation experiments. The chemical structure and, therefore, the polarity of MPS is very similar to PMMA. In consequence, the interfacial area between these phases can be large and the MPS-functionalized particles are distributed homogeneously around the PMMA particle. ODTMS, on the contrary, is much more hydrophobic than PMMA. To reduce the interfacial area between particles and polymer, the ODTMS-functionalized silica forms aggregates. Addition of hexadecane leads to the formation of nanocapsules with a liquid core. This additional phase makes the energetic considerations apparently more complicated, but the result is plausible. As the surface of the MPS-silica particles is similar to PMMA, they assemble preferably in the polymer shell. The C₁₈-chain of ODTMS has a similar structure as hexadecane and, therefore, leads to a preferred assembly of the ODTMS-functionalized particles inside the liquid core.

The second main difference between MPS and ODTMS is their reactivity. While ODTMS carries an inert alkyl chain, MPS is a methacrylic acid ester. This reactive group is able to copolymerize with the surrounding monomer phase. Regarding all systems shown in Table 4.8, only the hybrids with MPS-functionalized silica prepared via a polymerization reaction show a structure, where the silica is distributed homogeneously inside the polymer. In comparison with the solvent evaporation experiments, this result cannot be explained by differences in the interfacial energies, as the composition of the systems is basically the same. Copolymerization of the MPS leads to a fixation of the inorganic particles inside the polymer particle. This is a kinetic effect, which is not considered in the model proposed by Gonzalez-Ortiz and Asua.^[85,109] By forming covalent bonds between functionalized particles and surrounding polymer, the system is forced out of thermodynamic equilibrium and the interfacial energy between particle and polymer is no longer decisive for the developing structure.

A different approach has been chosen for the experiments described in sections 4.5 and 4.6. Instead of stabilizing the miniemulsions with surfactants, nanoparticles have been used to stabilize the droplets, forming Pickering emulsions. The structures achieved by this approach are shown in Table 4.9. While the concept is different to the examples discussed above, the physical principles beyond these systems are quite similar. As already described in section 2.1.3, the contact angle of the stabilizing particles at the liquid/liquid interface should be close to 90° . In other words, the interfacial tension of the particles should be similar to both liquid phases. Compared to this, the interfacial tension between the two liquid phases is much higher. Assembly of the particles at the liquid/liquid interface leads to a reduction of the interfacial area between the two liquid phases and, therefore, to a reduction of the interfacial energy of the whole system.

Table 4.9: Structures of hybrid nanomaterials via Pickering-stabilized miniemulsions.

Direct Miniemulsion	Inverse Miniemulsion
	

To achieve an assembly of the particles at the liquid/liquid interface, the interfacial energies in the system have to be adjusted. In the direct miniemulsions in section 4.5, this is reached by the addition of salt. A high salt content increases the ionic strength of the continuous, aqueous phase. As the unfunctionalized silica particles are only stabilized by electrostatic repulsion, they become unstable. To reduce the interfacial area with the aqueous phase, they assemble at the liquid/liquid interface and form a film around the monomer droplets. In the inverse systems described in section 4.6, the polarity of the particles is tuned by choosing a suitable functionalization agent. Only particles functionalized with PTMS assemble at the liquid/liquid interface and form a film which is able to sufficiently stabilize the emulsion.

The different stabilization mechanisms between emulsions stabilized by surfactants or by particles can also explain the differences in the formation of capsule morphologies. Surfactants reduce the interfacial tension between continuous and dispersed phase. Therefore, it is possible to tune the interfacial tension in order to favor the formation of nanocapsules via phase separation, as it is described in section 2.2.1. In Pickering emulsions, the interfacial tension is not influenced, but the droplets are stabilized by a mechanically stable film of particles. Therefore, the interfacial tensions of four different phases (continuous phase, polymer,

liquid core, and inorganic particles) have to match in order to achieve a capsule morphology by phase separation. Only a few examples for this strategy are known in literature.^[129,134] For Pickering-stabilized systems, capsule formation via interfacial polymerization (as shown in section 4.6) is much more suitable, as the physical requirements are lower.

In conclusion, reactions in miniemulsion are an elegant way to produce polymer/inorganic hybrid nanomaterials in a huge variety of structures by using only a low number of different materials. The driving force that determines the structure of the hybrids is the overall interfacial energy of the system, which can be minimized by choosing the right combination of materials. To tune the polarity of the inorganic nanoparticles and, therefore, the interfacial tensions, surface functionalization is a versatile tool. Furthermore, addition of reactive groups on the surface can suppress the thermodynamic assembly of the materials by enabling kinetic control. The presented strategies can be easily transferred to a large variety of materials and guide the way to a toolbox for numerous structures.

5. Experimental Part

Chemical	Abbr.	CAS	Supplier	Purity
Ludox TMA		7631-86-9	Sigma-Aldrich	34 wt% ^a
3-(Methacryloyloxy)propyl trimethoxysilane	MPS	2530-85-0	Sigma-Aldrich	98%
Octadecyl trimethoxysilane	ODTMS	3069-42-9	Sigma-Aldrich	90%
Propyl trimethoxysilane	PTMS	1067-25-0	Sigma-Aldrich	98%
Oleic acid	OA	112-80-1	Sigma-Aldrich	95%
Methacrylic acid	MA	79-41-4	Sigma-Aldrich	99%
Methyl methacrylate	MMA	80-62-6	Merck	>99% ^b
Styrene		100-42-5	Sigma-Aldrich	>99% ^b
Butyl methacrylate	BMA	97-88-1	Sigma-Aldrich	99% ^b
4-Vinylpyridine	4VP	100-43-6	Sigma-Aldrich	95% ^c
Sodium dodecyl sulfate	SDS	151-21-3	Alfa Aesar	99%
Lutensol AT50	Lut. AT50	68439-49-6	BASF	^d
Cetyl trimethyl ammonium chloride	CTMA-Cl	112-02-7	Sigma-Aldrich	25 wt% ^a
2,2'-Azobis-(2-methyl butyro nitrile)	V59	13472-08-7	Wako	
Hexadecane	HD	544-76-3	Sigma-Aldrich	99%
Poly methyl methacrylate	PMMA	9011-14-7	Sigma-Aldrich	^e
1,6-Hexanediol	HDol	629-11-8	Sigma-Aldrich	99%
Toluene-2,4-diisocyanate	TDI	584-84-9	Sigma-Aldrich	95%
Sodium chloride	NaCl	7647-14-5	Sigma-Aldrich	>99.8%
Sodium sulfate	Na ₂ SO ₄	7757-82-6	Sigma-Aldrich	>99%
Sulforhodamine 101	SR 101	60311-02-6	Sigma-Aldrich	
Ferric chloride	FeCl ₃ · 6 H ₂ O	10025-77-1	Sigma-Aldrich	97%
Ferrous chloride	FeCl ₂ · 4 H ₂ O	13478-10-9	Sigma-Aldrich	98%
Ammonium hydroxide	NH ₃	1336-21-6	Sigma-Aldrich	28 % ^a
Laponite RD clay			Rockwood	
Ethanol		64-17-5	Fisher Scientific	99%
Chloroform		67-66-3	Fluka	>99%
Cyclohexane		110-82-7	VWR	>99%

^ain H₂O^bPurified chromatographically before use^cDistilled before use^dA poly(ethylene oxide)-hexadecyl ether with an EO block length of about 50 units^eM_W = 35 000 g mol⁻¹

5.1. Experimental Details for Section 4.1⁷

5.1.1. Modification of Silica Particles with CTMA-Cl

For the modification of the silica particles with CTMA-Cl, 6.4 g of the silica dispersion Ludox TMA were mixed with an aqueous solution of CTMA-Cl (0.33 g of CTMA-Cl in 5 g of water). The mixture was stirred for 3 d at room temperature. After filtration, the particles were dried under vacuum.^[153]

5.1.2. Functionalization of Silica Particles with Trimethoxysilane Compounds

For the functionalization of Ludox TMA silica particles, a modified method from that reported by Bourgéat-Lami et al.^[61] was applied. First, a mixture of the Ludox TMA suspension (50 mL), ethanol (50 mL), and SDS (50 mg) was prepared. The pH of this dispersion was set to 9.5, using concentrated ammonia solution. After adding 0.02 mol of the trimethoxysilane compound within 30 min, the dispersions were stirred for 24 h at room temperature to allow equilibration, and refluxed afterwards for 2 h. The modified particles were centrifuged at 4000 rpm for 30 min, washed several times with ethanol/water, and dried under vacuum.

5.1.3. Preparation of PMMA/Silica Hybrid Particles via Polymerization

The PMMA/CTMA⁺-silica nanocomposite particles were prepared by radical polymerization in miniemulsion. Therefore, the continuous hydrophilic phase (consisting of water and surfactant) and the lipophilic phase (consisting of monomer, hexadecane, initiator, and silica) were prepared separately and then combined. Different amounts (relative to the dispersed phase) of CTMA⁺-modified silica particles were dispersed in the oil phase of the miniemulsion, consisting of 6 g of monomer (either 6 g of MMA or 5 g of MMA and 1 g of 4-vinylpyridine), 240 mg of the osmotic reagent hexadecane, and 100 mg of the azo-initiator V59. The dispersion was added to a solution of the nonionic surfactant Lutensol AT50 (200 mg) in water (24 g). The mixture was stirred for 1 h for pre-emulsification and homogenized afterwards by ultrasonication for 120 s at 90 % intensity (Branson W 450 digital sonifier; ½" tip), while cooling in an ice-water bath. The polymerization was carried out for 18 h at 72 °C.

The preparation of PMMA/MPS-silica particles was performed similarly to the preparation of the PMMA/CTMA-silica particles. The dried MPS-functionalized silica particles were dispersed in the oil phase, which contained as monomer phase a mixture of MMA (6 g), hexadecane (240 mg), and V59 (100 mg). The mixture was combined with a continuous phase

⁷This section is based on the publication "Structure Control in PMMA/Silica Hybrid Nanoparticles by Surface Functionalization" by Alexander Schoth, Caroline Wagner, Lena L. Hecht, Svenja Winzen, Rafael Muñoz-Espí, Heike P. Schuchmann and Katharina Landfester, published 2014 in *Colloid and Polymer Science*, volume 292 on the pages 2427 to 2437. © 2014, with kind permission from Springer Science and Business Media.

consisting of water (24 g) and SDS (27 mg). The two-phase system was stirred 1 h for pre-emulsification and homogenized by ultrasonication for 120 s (Branson W 450 digital sonifier; ½" tip, 90 % intensity) under cooling with an ice-water bath. The polymerization took place for 18 h at 72 °C. The PMMA/ODTMS-silica hybrid particles were prepared in the same way.

5.1.4. ITC measurements

In an experiment, 250 µL of a CTMA-Cl solution (0.15 g L^{-1} , 0.5 mM in water) were titrated to a suspension of Ludox TMA nanoparticles (5 g L^{-1} in water). The temperature was kept constant at 25 °C. The same amount of CTMA-Cl solution was titrated into pure water to determine the heat of dilution for reference. The measurement consisted of 50 titration steps with an injected volume of 5 µL each. The interval between injections was set to 400 s. An initial injection of 1.5 µL was performed before the first titration step to avoid deviations due to diffusion. Accordingly, the area of this peak was not considered in the data evaluation. For the calculation of the final reaction heat, the integrated heats of dilution were subtracted from the integrated heats of the adsorption experiments.

5.1.5. Preparation of PMMA/Silica Hybrid Particles via Solvent Evaporation

PMMA (450 mg, $M_W = 35\,000 \text{ g mol}^{-1}$) and MPS-modified silica particles (50 mg) were dissolved/dispersed in chloroform (2.5 mL). This mixture was combined with a surfactant solution consisting of water (10 g) and SDS (10 mg). The system was stirred for 1 h and homogenized by ultrasonication for 180 s (Branson W 450 digital sonifier; ¼" tip, 70 % intensity, 30 s pulse/20 s pause) under cooling with an ice-water bath. The evaporation of chloroform was performed by stirring in an open flask at 40 °C and ambient pressure for 18 h.

5.2. Experimental Details for Section 4.2⁸

5.2.1. Synthesis of Acid-Functionalized Magnetite Nanoparticles

Acid-functionalized magnetite nanoparticles were synthesized according to a slightly varied procedure described by Ramírez^[51] and Bannwarth.^[52] Ferrous chloride (3.0 g, 15 mmol) and ferric chloride (6.1 g, 22.5 mmol) were dissolved in water (20 mL). The concentrated ammonia solution (10 mL) was diluted with water (5 mL) and added to the iron salt solution dropwise within 5 min under vigorous stirring. Oleic acid or methacrylic acid (3.5 mmol) was added and, afterwards, the reaction mixture was first heated to 70 °C for 1 h and then to 130 °C

⁸This section is based on the manuscript "Silanization as a Versatile Functionalization Method for the Synthesis of Polymer/Magnetite Hybrid Nanoparticles with Controlled Structure" by Alexander Schoth, Alasdair D. Keith, Katharina Landfester and Rafael Muñoz-Espí.

for 2 h. The magnetite particles were washed with water several times and then dried under vacuum.

5.2.2. Synthesis of Silanized Magnetite Nanoparticles

Ferrous Chloride (3.0 g, 15 mmol) and ferric chloride (6.1 g, 22.5 mmol) were dissolved in water (20 mL). The concentrated ammonia solution (10 mL) was diluted with water (5 mL) and added to the iron salt solution dropwise within 5 min under vigorous stirring. Afterwards, the reaction mixture was first heated to 70 °C for 1 h and then to 130 °C for 2 h. The supernatant solution was removed and the magnetite particles were redispersed in a mixture of water (100 mL), ethanol (50 mL) and SDS (30 mg). The pH of the mixture was set to 9.5 using concentrated ammonia solution. The silane compound (MPS or ODTMS, 20 mmol) was added dropwise within 30 min and the mixture was stirred at ambient temperature for another hour. After heating to reflux for 1.5 h, the particles were washed several times with a water/ethanol mixture (1:1) and then dried under vacuum.

5.2.3. Synthesis of Hybrid Nanoparticles

The organic phases were prepared by dissolving hexadecane (100 µL) and V59 (50 mg) in the different monomers. The samples contained MMA (1.8 mL), styrene (1.8 mL) or a mixture of styrene (1.4 mL) and 4VP (0.4 mL). Magnetite particles (200 mg) were added to the samples and dispersed in the ultrasound bath for 30 min. After addition of the aqueous phase consisting of water (18 mL) and SDS (36 mg), the emulsions were shaken for 30 min. Ultrasonication for 120 s at 70 % intensity with a pulse sequence of 300 s pulse and 10 s pause (Branson W 450 digital sonifier; ½" tip, ice cooling) was used to prepare the miniemulsions. Polymerization took place to 72 °C for 17 h at a thermoshaker. The polymerized samples were then filtered in order to remove coagulum.

Separation of the particles containing magnetite from the empty polymer particles was done by putting the dispersions on a magnet for 30 min. The supernatant dispersion was removed and the particles were redispersed in a 0.1 wt.% SDS solution (10 mL). The dispersion was again purified magnetically and then refilled with water. The solid content of the samples was determined by lyophilization.

5.3. Experimental Details for Section 4.3⁹

5.3.1. Silica Functionalization

The particles were functionalized according to the method described in section 5.1.2.

⁹This section is based on the publication “Waterborne Polymer/Silica Hybrid Nanoparticles and their Structure in Coatings” by Alexander Schoth, Emad S. Adurahim, Mohammed A. Bahattab, Katharina Landfester and Rafael Muñoz-Espí, published in 2015 in *Macromol. React. Eng.*, DOI: 10.1002/mren.201500029 © 2015, with kind permission from John Wiley & Sons.

5.3.2. Miniemulsion Polymerization

The hybrid particles were prepared by free radical miniemulsion polymerization.^[87] The continuous, hydrophilic phase (consisting of water and SDS) and the dispersed, hydrophobic phase (consisting of the monomers MMA and BMA, the initiator V59, the osmotic reagent hexadecane and the functionalized silica particles) were prepared separately and combined afterwards.

For the hydrophobic phase, 935 mg of the monomers (or 735 mg of the monomers and 200 mg of functionalized silica) in different mass ratios, ranging from pure MMA to a MMA to BMA ratio of 1:1, were mixed with V59 (15 mmol per mol of monomer) and hexadecane (50 μ L). To disperse the silica particles, the samples were placed in an ultrasonic bath for 10 min. Afterwards, the aqueous phase consisting of water (9 mL) and SDS (30 mg) was added, and the samples were stirred for 1 h for pre-emulsification. The emulsions were then homogenized by ultrasonication for 3 min (Branson W 450 digital sonifier; 1/4" tip, 70 % intensity, 30 s pulse/10 s pause) under cooling with an ice/water bath. Polymerization took place for 18 h at 72 °C. After polymerization, the samples were purified by filtration to remove coagulates.

5.4. Experimental Details for Section 4.4

5.4.1. Functionalization of Silica Particles

The particles were functionalized according to the method described in section 5.1.2.

5.4.2. Preparation of Nanocapsules via Polymerization

The continuous hydrophilic phases were prepared by dissolving SDS (16 mg) in water (8 mL). The lipophilic oil phases contained the initiator V59 (50 mg) and hexadecane as liquid core (1 g). MPS- and ODTMS-functionalized silica (100 mg) was added to some of the samples. As monomer for building the capsule shell, MMA was used (1 g for the pure polymer capsules and 900 mg for the capsules containing silica). The mixtures were stirred for 1 h for pre-emulsification and homogenized afterwards by ultrasonication for 180 s at 70 % intensity with a 30 s pulse/10 s pause sequence (Branson W 450 digital sonifier; 1/4" tip), while cooling in an ice-water bath. The polymerization was carried out for 18 h at 72 °C.

5.4.3. Preparation of Nanocapsules via Solvent Evaporation

The continuous hydrophilic phases were prepared by dissolving SDS (10 mg) in water (9.5 mL). PMMA ($M_W = 35\,000\text{ g mol}^{-1}$, 250 mg for the pure capsules and 225 mg for the capsules containing silica) and, for some of the samples, MPS- and ODTMS-modified silica particles (50 mg) were dissolved/dispersed in chloroform (5 mL). These mixtures were combined with

the surfactant solutions and stirred for 1 h. Homogenization was done by ultrasonication for 180 s (Branson W 450 digital sonifier; ¼" tip, 70 % intensity, 30 s pulse/20 s pause) under cooling with an ice-water bath. The evaporation of chloroform was performed by stirring in an open flask at 40 °C and ambient pressure for 18 h.

5.5. Experimental Details for Section 4.5

5.5.1. Particles Stabilized by Laponite Clay

The clay-stabilized nanoparticles have been synthesized according to the method described by Bon and Colver.^[127] Laponite RD clay (90 mg) was dispersed in water (8.9 mL) by using ultrasound (Branson W 450 digital sonifier; ¼" tip, 70 % intensity, 1 min, ice cooling), which resulted in a completely clear dispersion. Afterwards, sodium chloride (55 mg) was added and the dispersion was sonicated for another 2 min. The organic phase was prepared by dissolving hexadecane (40 mg) and the oil-soluble initiator V59 (25 mg) in styrene (995 µL). After combination of aqueous and organic phase, the system was stirred for 1 h at 1000 rpm and then sonicated (¼" tip, 70 % intensity, 1 min, 30 s pulse/10 s pause). The emulsion was polymerized for 17 h at 72 °C.

5.5.2. Particles Stabilized by Ludox TMA Silica

The silica-stabilized particles were prepared by dispersing the commercial 34 wt.% Ludox TMA dispersion (435 µL) in water (16.6 mL, 15.6 mL or 14.6 mL). Afterwards, sodium chloride (0.9 g, 1.8 g or 2.7 g) was dissolved in the dispersion. After addition of the organic phase, consisting of styrene (1.989 mL), hexadecane (103 µL) and V59 (50 mg), the mixture was stirred for 1 h at 1000 rpm. The samples were sonified (Branson W 450 digital sonifier; ½" tip, 70 % intensity, 3 min, 30 s pulse/10 s pause, ice cooling) and polymerized at 72 °C for 17 h.

5.6. Experimental Details for Section 4.6¹⁰

5.6.1. Functionalization of Silica Particles

The particles were functionalized according to the method described in section 5.1.2.

5.6.2. Preparation of Nanocapsules in Inverse Miniemulsion

The silica nanoparticles (450 mg) were dispersed in cyclohexane (9 mL). The aqueous phase consisting of 1,6-hexanediol (45 mg) and water (850 µL) was prepared separately. For some

¹⁰This section is based on the publication "Surfactant-Free Polyurethane Nanocapsules via Inverse Pickering Miniemulsion" by Alexander Schoth, Katharina Landfester and Rafael Muñoz-Espí, published in 2015 in *Langmuir*, volume 31 on pages 3784 to 3788. © 2015, with kind permission from American Chemical Society.

samples, varying amounts of sodium chloride, sodium sulfate or SR101 were added. The two phases were combined, stirred and sonicated in the ultrasound bath until the cyclohexane phase was clear. Ultrasonication took place for 180 s at 70 % intensity with a pulse/pause interval of 30 s and 20 s (Branson W 450 digital sonifier; ¼" tip). Afterwards, a solution of TDI (90 mg) in cyclohexane (2 mL) was added dropwise under stirring.

5.6.3. Sample Preparation for Fluorescence Measurements

1 mL of the nanocapsule dispersion was dispersed in 5 mL of a 0.1 wt.% solution of SDS in water. For evaporation of the cyclohexane and to enable the release of the dye, the dispersion was allowed to stir for 24 h. The nanocapsules were then removed in a centrifuge at 4000 rpm for 2 min. The supernatant solutions as well as the non-centrifuged dispersions were measured in the plate reader.

5.7. Analytical Tools

5.7.1. Transmission Electron Microscopy (TEM)

For sample preparation, 5 µL of the sample dispersion was put on a carbon coated 300-mesh copper grid. To avoid degradation under the electron beam, the samples containing PMMA were afterwards coated by a thin carbon layer, using a Leica EM Med020 Vacuum Coating System (Leica Micro Systems, Germany).

The samples were measured in a JEOL 1400 Electron Microscope (JEOL Ltd., Japan), using a LaB₆ cathode at an acceleration voltage of 120 kV. The images were recorded by a GATAN Ultrascan 1000 CCD camera (Gatan Inc., USA).

5.7.2. Scanning Electron Microscopy (SEM)

The diluted dispersions were drop-casted on a silicon wafer. The images were taken on a Zeiss 1530 Gemini Leo field emission Microscope (Carl Zeiss, Germany), operated at different voltages.

5.7.3. Dynamic Light Scattering (DLS)

The average hydrodynamic diameter as well as the size distribution of the nanomaterials was determined by means of dynamic light scattering (DLS) with a Nicomp 380 Submicron Particle Sizer (Nicomp PSS, USA). The detection angle was fixed at 90° and the measurements were carried out at room temperature.

5.7.4. Thermogravimetric Analysis (TGA)

The amount of functionalization agent on the inorganic particles as well as the composition of hybrid materials were measured by thermogravimetric analysis (TGA), using a Mettler Toledo ThermoSTAR TGA/SDTA 851 thermobalance (Mettler-Toledo, Switzerland). The measurements cover a temperature range between 40–1000 °C at a heating rate of 10 °C min⁻¹.

5.7.5. Differential Scanning Calorimetry (DSC)

The thermal properties of the nanomaterials were characterized by Differential Scanning Calorimetry (DSC) with a PerkinElmer DSC 823 (PerkinElmer Inc., USA). For the experiments described in section 4.3, the samples were measured in a temperature range of -40 °C to 200 °C at a heating/cooling rate of 10 °C min⁻¹. For the experiments in section 4.6, the temperature range was -50 °C to 90 °C at the same heating/cooling rate.

5.7.6. Reaction Calorimetry

The calorimetric measurements were carried out on a μ RC-micro-reaction calorimeter (Thermal Hazard Technology, UK).

5.7.7. Isothermal Titration Calorimetry (ITC)

Isothermal Titration Calorimetry (ITC) was performed using a MicroCal VP-ITC equipment (GE Healthcare, USA).

5.7.8. Gel Permeation Chromatography (GPC)

The molar weight distributions of the polymers were determined via gel permeation chromatography (GPC) in an Agilent PCC SECurity SEC. The samples were eluted through three SDV columns with particles of 10 μ m and pore sizes of 106 Å, 104 Å and 500 Å. As detectors, a S-3702 UV detector (254 nm) and a DRI shodex RI-101 detector (ECR) were used. The molecular weights were calculated by comparison with a PMMA standard provided by Polymer Standards Service.

5.7.9. Infrared Spectroscopy

For Fourier Transform Infrared Spectroscopy (FTIR), the dried sample was pressed with KBr to form a pellet and the absorption in the range of 4000–500 cm⁻¹ was determined in a Spectrum BX spectrometer (PerkinElmer Inc., USA).

5.7.10. UV/Vis Spectroscopy

Fluorescence was measured with a Tecan M1000 Microplate Reader (Tecan Group Ltd., Switzerland). For the detection of the fluorescent dye SR101, an excitation wavelength of 585 nm was used and the fluorescence was recorded in the range of 595–700 nm.

6. Summary and Outlook

Within this thesis, new strategies for the synthesis of polymer/inorganic hybrid nanomaterials with a controlled structure were described. Different parameters that influence the structure of the hybrids as well as ways to tune them were presented. The strategies for structure control were transferred to different material combinations and show the versatility of the applied miniemulsion techniques.

In the first part (section 4.1), hybrid nanoparticles consisting of silica and poly(methyl methacrylate) (PMMA) were synthesized as a model system for polymer/inorganic hybrid nanomaterials in general. Different surface functionalization agents for silica have been tested, like cetyl trimethylammonium chloride (CTMA-Cl) as example for surface functionalization with a cationic surfactant. The CTMA-Cl desorbed from the particle surface during emulsification and acted as additional surfactant in the system. The silica particles were not sufficiently hydrophobic to stay inside the monomer droplets, so addition of 4-vinylpyridine (4VP) as comonomer was necessary in order to enhance the interaction between inorganic material and organic phase. The second strategy for surface functionalization was the use of the trimethoxysilane compounds 3-methacryloyloxypropyl trimethoxysilane (MPS) and octadecyl trimethoxysilane (ODTMS). The trimethoxysilane groups bind to the silica surface in a condensation reaction and form a covalent connection. Encapsulation in PMMA using miniemulsion polymerization was successful and gave hybrid particles with different structures. While the MPS-functionalized silica was distributed homogeneously inside the polymer, the ODTMS-functionalized particles aggregated inside the polymer, which resulted in a Janus-like structure. Particles with the same compositions were synthesized by using the solvent evaporation technique, where the droplets consist of a dissolved, pre-formed polymer. Here, the particles were not formed by a polymerization reaction, but by evaporation of the solvent from the droplets. In this case, both types of silica particles could be found on the surface of the hybrids. The MPS-functionalized particles were distributed homogeneously over the surface, while the ODTMS-functionalized silica formed aggregates. The structural differences between the samples could be explained by regarding polarity and reactivity of the functionalization agents, as it was explained in detail in section 4.7.

In the next set of experiments, silica was replaced by magnetite, as it was described in section 4.2. While oleic acid (OA) is the most common functionalization agent for magnetite nanoparticles, it offers only poor control over the structure of the hybrids. As an alternative, MPS and ODTMS were applied for surface functionalization. The functionalized particles were encapsulated in PMMA, polystyrene and a copolymer of styrene and 4VP, using the miniemulsion polymerization technique. For all experiments, the encapsulation efficiency was around 50 %. By increasing the concentration of highly magnetic particles using a strong magnet, the magnetite content of the samples could be increased up to 60 wt.%. The structures of

the hybrids were comparable to the results obtained for silica and PMMA. MPS-functionalized particles were distributed homogeneously inside the polymers, while particles functionalized with ODTMS or OA gave a Janus structure. It is notable that no significant difference could be found for the different polymers. This is a good example that thermodynamic control of the structure can be overcome by using chemical fixation.

Section 4.3 gave an example for possible applications of the systems described before. Hybrid particles containing MPS- and ODTMS-functionalized silica were prepared in different copolymers of methyl methacrylate (MMA) and butyl methacrylate (BMA). Structures and encapsulation efficiencies of these systems were comparable to the results with pure PMMA. Determination of the glass transition temperature T_g by differential scanning calorimetry (DSC) showed that silica particles have no influence on the thermal properties. The molar weight distribution of the polymers was also not affected. However, it could be shown that around 50 % of the polymer copolymerized with the MPS-functionalized particles. The dispersions were used to prepare translucent films, which were investigated by scanning electron microscopy (SEM). The structures of the hybrid particles could be preserved during film formation. While the MPS-functionalized silica was distributed homogeneously in the films, ODTMS-functionalized silica forms big aggregates.

The strategies for structure control in hybrid nanoparticles could also be transferred to systems with a liquid core, as shown in section 4.4. By increasing the amount of hexadecane, nanocapsules with a PMMA shell and a liquid hexadecane core could be obtained in the presence of functionalized silica nanoparticles. The synthesis using miniemulsion polymerization was possible, but the samples were very heterogeneous, the capsules were not very stable and a lot of free silica could be found. Solvent evaporation gave nanocapsules with stable shells and a narrow size distribution. Again, significant differences in the structures could be observed. While MPS-functionalized particles assembled in the PMMA shell, the ODTMS-functionalized silica could be found in the hexadecane core. This result could be explained by regarding the different polarities of the particles and the chemical similarity to the surrounding materials.

A different approach was the use of Pickering emulsions. In Pickering emulsions, droplets are not stabilized by surfactants, but by a layer of solid particles. Therefore, the droplets act as templates for a core-shell structure. In section 4.5, the synthesis of PMMA particles stabilized by unfunctionalized silica particles in direct miniemulsion was described. Salt was added to destabilize the dispersed silica particles and to force them to assemble at the liquid/liquid interface. The resulting particles were quite large with diameters of several microns, but it could be shown that the silica particles were able to stabilize the emulsions.

The Pickering strategy was also applied to inverse miniemulsions, as described in section 4.6. In these experiments, water droplets in cyclohexane were stabilized by silica nanoparticles. The particles had to be functionalized in order to meet the suitable polarity to assemble

at the liquid/liquid interface. The emulsions were sufficiently stable to perform interfacial polymerization and obtain a polyurethane shell. Encapsulation of an organic dye as well as of high loads of inorganic salts demonstrated the versatility of the system. With this approach, the encapsulation of any water-soluble substance should be possible.

The techniques discussed above provide plenty of possibilities to control the structure of polymer/inorganic hybrid nanomaterials. Combinations of different inorganic materials and polymers can be transformed into hybrid particles and capsules using direct and inverse miniemulsion systems. Possible candidates for applications are coatings, as described in section 4.3. By using UV-active materials such as zinc oxide or titania, translucent films for UV protection can be produced. Another possibility is the encapsulation of catalytically active substances with a controlled interfacial area to the surrounding medium. Generally, the basic principles developed for the structure control by surface functionalization can be easily transferred to other systems and offer a broad variety of possible applications.

7. Zusammenfassung und Ausblick

Im Rahmen dieser Doktorarbeit wurden verschiedene neue Strategien zur Synthese polymerer/anorganischer Hybridmaterialien mit kontrollierter Struktur vorgestellt. Verschiedene Parameter, die diese Strukturen beeinflussen, wurden beschrieben. Die Strategien zur Strukturkontrolle wurden auf verschiedene Materialkombinationen übertragen und zeigen die Vielseitigkeit der hier angewandten Miniemulsionstechnik.

Im ersten Teil der Arbeit (Abschnitt 4.1) wurden, als Modellsystem für polymere/anorganische Hybridmaterialien im Allgemeinen, Hybridnanopartikel aus Silica und Polymethylmethacrylat (PMMA) hergestellt. Dabei wurden verschiedene Funktionalisierungsreagenzien für Silica untersucht, u.a. Cetyltrimethylammoniumchlorid (CTMA-Cl) als Beispiel für die Oberflächenfunktionalisierung durch kationische Tenside. Das CTMA-Cl desorbierte während der Emulgierung von der Partikeloberfläche und wirkte im System als zusätzliches Tensid. Die Silicapartikel waren nicht mehr ausreichend hydrophob, um im Inneren der Monomertropfen zu bleiben. Um die Wechselwirkung zwischen anorganischen Partikeln und der organischen Phase zu erhöhen, war daher die Zugabe von 4-Vinylpyridin (4VP) als Comonomer notwendig. Die zweite Strategie zur Oberflächenfunktionalisierung war der Einsatz der Trimethoxysilane 3-Methacryloyloxypropyltrimethoxysilan (MPS) sowie Octadecyltrimethoxysilan (ODTMS). Die Trimethoxysilangruppe kondensiert auf die Silicaoberfläche und bildet eine kovalente Bindung aus. Die Verkapselung der so funktionalisierten Partikel in PMMA war erfolgreich und lieferte Hybridpartikel mit unterschiedlichen Strukturen. Während MPS-funktionalisierte Silicapartikel homogen im Polymer verteilt vorlagen, aggregierten die ODTMS-funktionalisierten Partikel im Polymer und bildeten Janus-artige Strukturen. Mit dem Lösungsmittelverdampfungsverfahren (Solvent Evaporation Process) wurden Hybridpartikel mit der gleichen Zusammensetzung hergestellt. Hierbei bestanden die Tropfen allerdings nicht aus Monomer, sondern aus einem vorgefertigten Polymer, das in einem organischen Lösungsmittel gelöst war. Die Partikel wurden somit nicht durch Polymerisation, sondern durch das Verdampfen des Lösungsmittels aus den Miniemulsionstropfen gebildet. Hierbei befanden sich sowohl MPS- als auch ODTMS-funktionalisiertes Silica auf der Oberfläche der Hybridpartikel. Während die MPS-funktionalisierten Partikel homogen auf der Oberfläche verteilt waren, bildeten die ODTMS-funktionalisierten Silicapartikel Aggregate. Die strukturellen Unterschiede zwischen den Proben konnte durch eine Betrachtung der Funktionalisierungsreagenzien hinsichtlich Reaktivität und Polarität erklärt werden. Diese Betrachtungen sind in Abschnitt 4.7 zusammengefasst.

Im nächsten Schritt wurde Silica durch Magnetit ersetzt. Diese Experimente sind in Abschnitt 4.2 beschrieben. Obwohl Ölsäure das gebräuchlichste Funktionalisierungsreagenz für Magnetitnanopartikel ist, bietet es nur wenig Kontrolle über die Struktur von Hybridpartikeln. Als Alternative wurden daher MPS und ODTMS als Funktionalisierungsreagenzien

verwendet. Die funktionalisierten Magnetitpartikel wurden mittels Miniemulsionspolymerisation in PMMA, Polystyrol sowie einem Copolymer aus Styrol und 4VP verkapselt. Bei all diesen Experimenten lag die Verkapselungseffizienz bei rund 50 %. Durch eine Erhöhung des Anteils stark magnetischer Partikel mittels eines Magneten konnte der Magnetitgehalt der Proben auf bis zu 60 Gew.% gesteigert werden. Die Strukturen der Hybridpartikel waren in allen Fällen vergleichbar mit denen von Silica in PMMA. Während MPS-funktionalisierte Partikel homogen in den Polymeren verteilt waren, bildeten ODTMS- und OA-funktionalisiertes Magnetit Janus-Strukturen. Hierbei ist bemerkenswert, dass kein signifikanter Unterschied zwischen den Polymeren festgestellt werden konnte. Dieses System ist damit ein gutes Beispiel, dass thermodynamische Strukturkontrolle durch chemische Fixierung umgangen werden kann.

In Abschnitt 4.3 wurde eine mögliche Anwendung für die hier beschriebenen Systeme vorgestellt. Hybridpartikel wurden mit MPS- und ODTMS-funktionalisiertem Silica in verschiedenen Copolymeren von Methylmethacrylat (MMA) und Butylmethacrylat (BMA) hergestellt. Strukturen und Verkapselungseffizienzen dieser Systeme waren vergleichbar mit den Ergebnissen in reinem PMMA. Die Bestimmung der Glasübergangstemperatur T_g mittels dynamischer Differenzkalorimetrie (DSC) zeigte, dass die Anwesenheit der Silicapartikel keinerlei Einfluss auf die thermischen Eigenschaften der Polymere hat. Die Molmassenverteilung der Polymere wurde ebenfalls nicht beeinflusst, obwohl gezeigt werden konnte, dass 50 % des Polymers mit den MPS-funktionalisierten Partikeln copolymerisiert und somit kovalent an sie gebunden war. Aus den Dispersionen wurden anschließend durchsichtige Filme hergestellt und mittels Rasterelektronenmikroskopie (SEM) untersucht. Die Strukturen der Hybridpartikel blieben während der Filmbildung erhalten. Während MPS-funktionalisierte Partikel homogen in den Filmen verteilt waren, formten die ODTMS-funktionalisierten Silicapartikel große Aggregate.

Die Strategien zur Strukturkontrolle in Hybridnanopartikeln konnten außerdem auf Systeme mit flüssigem Kern übertragen werden, wie in Abschnitt 4.4 beschrieben. Durch eine Erhöhung des Hexadekangehalts konnten Nanokapseln bestehend aus einer PMMA-Hülle und einem flüssigen Hexadekan-Kern in Gegenwart funktionalisierter Silicapartikel hergestellt werden. Die Synthese mittels Miniemulsionspolymerisation war möglich, jedoch waren die Proben sehr heterogen. Die Kapseln waren nicht stabil und viel freies Silica befand sich außerhalb der Kapseln. Das Lösungsmittelverdampfungsverfahren lieferte hingegen Kapseln mit stabilen Hüllen und einer engen Größenverteilung. Wiederum konnten erhebliche Unterschiede hinsichtlich der Strukturen beobachtet werden. Während sich MPS-funktionalisierte Partikel bevorzugt in der PMMA-Schale einlagerten, befanden sich die ODTMS-funktionalisierten Partikel vor allem im flüssigen Hexadekankern. Diese Beobachtungen konnten durch Betrachtung der Polaritäten der funktionalisierten Partikel sowie der chemischen Ähnlichkeit zu den sie umgebenden Materialien erklärt werden.

Ein weiterer Ansatz zur Strukturkontrolle war die Verwendung von Pickering-Emulsionen. In Pickering-Emulsionen werden die Tropfen nicht durch Tenside, sondern durch eine Schicht fester Partikel stabilisiert. Durch diese Geometrie wirken die Tropfen als Vorlage für eine Kern-Schale-Morphologie. In Abschnitt 4.5 wurde die Stabilisierung direkter Miniemulsionen durch unfunktionalisierte Silicapartikel sowie die Synthese von PMMA-Partikeln in diesen Systemen beschrieben. Durch die Zugabe von Salz zur wässrigen Phase wurden die Silicapartikel destabilisiert und so zur Anlagerung an der flüssig/flüssig-Phasengrenze gedrängt. Obwohl die resultierenden Hybridpartikel mit Durchmessern von mehreren Mikrometern sehr groß waren, konnte gezeigt werden, dass Silicapartikel in der Lage sind, Emulsionen zu stabilisieren.

Die Pickering-Stabilisierung wurde, wie in Abschnitt 4.6 beschrieben, ebenfalls in inversen Miniemulsionen angewandt. In diesen Experimenten wurden Wassertropfen in Cyclohexan durch Silicananopartikel stabilisiert. Um die passende Polarität für eine Anordnung an der flüssig/flüssig-Phasengrenze zu erreichen, musste die Oberfläche der Silicapartikel funktionalisiert werden. Die so erhaltenen Emulsionen waren ausreichend stabil, um mittels Grenzflächenpolymerisation Polyurethanhüllen herzustellen. Die Vielseitigkeit dieses Systems wurde durch die Verkapselung eines organischen Farbstoffs sowie großer Mengen anorganischer Salze unter Beweis gestellt. Mit diesem Ansatz sollte somit die Verkapselung jeder wasserlöslichen Substanz möglich sein.

Die zuvor diskutierten Techniken bieten zahlreiche Möglichkeiten zur Strukturkontrolle in polymeren/anorganischen Hybridnanomaterialien. Kombinationen verschiedener anorganischer Materialien und Polymere können mittels direkter und inverser Miniemulsionssysteme in Hybridpartikel und -kapseln überführt werden. Mögliche Anwendungen für diese Systeme sind z.B. Beschichtungen, wie in Abschnitt 4.3 beschrieben. Durch die Verwendung UV-aktiver Materialien wie beispielsweise Zinkoxid oder Titandioxid ist die Herstellung durchsichtiger, aber UV-absorbierender Filme möglich. Eine weitere Möglichkeit ist die Verkapselung katalytisch aktiver Substanzen mit kontrollierbarer Grenzfläche zum umgebenden Medium. Die hier entwickelten Prinzipien zur Strukturkontrolle mittels Oberflächenfunktionalisierung lassen sich leicht auf eine Vielzahl anderer Systeme übertragen und sind daher für ein breites Anwendungsspektrum geeignet.

8. References

- [1] M. I. Siponen, P. Legrand, M. Widdrat, S. R. Jones, W.-J. Zhang, M. C. Y. Chang, D. Faivre, P. Arnoux, D. Pignol, *Nature* **2013**, *502*, 681–684.
- [2] C. S. Young, H. Abukawa, R. Asrican, M. Ravens, M. J. Troulis, L. B. Kaban, J. P. Vacanti, P. C. Yelick, *Tissue Eng.* **2005**, *11*, 1599–1610.
- [3] H.-D. Dörfler, *Grenzflächen und kolloid-disperse Systeme*, Springer, Berlin, **2002**.
- [4] C. Xu, S. Sun, *Adv. Drug Delivery Rev.* **2013**, *65*, 732–743.
- [5] J. Kim, Y. Lee, S. Sun, *J. Am. Chem. Soc.* **2010**, *132*, 4996–4997.
- [6] J. L. Vivero-Escoto, Y.-D. Chiang, K. C.-W. Wu, Y. Yamauchi, *Sci. Technol. Adv. Mater.* **2012**, *13*, 013003.
- [7] E. J. Henderson, A. J. Shuhendler, P. Prasad, V. Baumann, F. Maier-Flaig, D. O. Faulkner, U. Lemmer, X. Y. Wu, G. A. Ozin, *Small* **2011**, *7*, 2507–2516.
- [8] C. Xu, B. Wang, S. Sun, *J. Am. Chem. Soc.* **2009**, *131*, 4216–4217.
- [9] E. Bourgéat-Lami, J. Lang, *J. Colloid Interface Sci.* **1998**, *197*, 293–308.
- [10] W. Stöber, A. Fink, E. Bohn, *J. Colloid Interface Sci.* **1968**, *26*, 62–69.
- [11] H.-J. Butt, K. Graf, M. Kappl, *Physics and Chemistry of Interfaces*, Wiley-VCH, Weinheim, 3rd ed., **2013**.
- [12] K. Landfester, M. Willert, M. Antonietti, *Macromolecules* **2000**, *33*, 2370–2376.
- [13] C. Mora-Huertas, H. Fessi, A. Elaissari, *Int. J. Pharm.* **2010**, *385*, 113–142.
- [14] R. Strey, *Colloid Polym. Sci.* **1994**, *272*, 1005–1019.
- [15] J. Ugelstad, M. S. El-Aasser, J. W. Vanderhoff, *J. Polym. Sci. Part C: Polym. Lett.* **1973**, *11*, 503–513.
- [16] K. Landfester, *Macromol. Rapid Commun.* **2001**, *22*, 896–936.
- [17] M. J. Rosen, *Surfactants and Interfacial Phenomena*, Wiley, Hoboken, 3rd ed., **2004**.
- [18] D. Schaeffel, R. H. Staff, H.-J. Butt, K. Landfester, D. Crespy, K. Koynov, *Nano Lett.* **2012**, *12*, 6012–6017.
- [19] H. Schubert, *Emulgiertechnik*, Behrs Verlag, Hamburg, 3rd ed., **2012**.
- [20] M. Antonietti, K. Landfester, *Prog. Polym. Sci.* **2002**, *27*, 689–757.
- [21] P. A. Lovell, M. S. El-Aasser, *Emulsion Polymerization and Emulsion Polymers*, J. Wiley, **1997**.
- [22] S. U. Pickering, *J. Chem. Soc. Trans.* **1907**, *91*, 2001–2021.

-
- [23] R. Aveyard, B. P. Binks, J. H. Clint, *Adv. Colloid Interface Sci.* **2003**, *100–102*, 503–546.
- [24] A. Schrade, K. Landfester, U. Ziener, *Chem. Soc. Rev.* **2013**, *42*, 6823–6839.
- [25] B. P. Binks, J. H. Clint, *Langmuir* **2002**, *18*, 1270–1273.
- [26] W. C. Moore, *J. Am. Chem. Soc.* **1919**, *41*, 940–946.
- [27] B. P. Binks, S. O. Lumsdon, *Phys. Chem. Chem. Phys.* **1999**, *1*, 3007–3016.
- [28] J. H. Schulman, J. Leja, *T. Faraday Soc.* **1954**, *50*, 598–605.
- [29] B. P. Binks, *Curr. Opin. Colloid Interface Sci.* **2002**, *7*, 21–41.
- [30] P. Finkle, H. D. Draper, J. H. Hildebrand, *J. Am. Chem. Soc.* **1923**, *45*, 2780–2788.
- [31] F. Jansen, J. Harting, *Phys. Rev. E* **2011**, *83*, 046707.
- [32] S. Torza, S. G. Mason, *J. Colloid Interface Sci.* **1970**, *33*, 67–83.
- [33] J. Berg, D. Sundberg, B. Kronberg in *Proceedings of the ACS Division of Polymeric Materials*, Vol. 54, **1986**, pp. 367–369.
- [34] S. Theisinger, K. Schoeller, B. Osborn, M. Sarkar, K. Landfester, *Macromol. Chem. Phys.* **2009**, *210*, 411–420.
- [35] R. H. Staff, P. Rupper, I. Lieberwirth, K. Landfester, D. Crespy, *Soft Matter* **2011**, *7*, 10219–10226.
- [36] P. B. Cardoso, P. H. H. Araujo, C. Sayer, *Macromol. Symp.* **2013**, *324*, 114–123.
- [37] N. Jagielski, S. Sharma, V. Hombach, V. Mailänder, V. Rasche, K. Landfester, *Macromol. Chem. Phys.* **2007**, *208*, 2229–2241.
- [38] D. Crespy, M. Stark, C. Hoffmann-Richter, U. Ziener, K. Landfester, *Macromolecules* **2007**, *40*, 3122–3135.
- [39] E. Marie, K. Landfester, M. Antonietti, *Biomacromolecules* **2002**, *3*, 475–481.
- [40] D. Wu, C. Scott, C.-C. Ho, C. C. Co, *Macromolecules* **2006**, *39*, 5848–5853.
- [41] Z. Cao, U. Ziener, *Nanoscale* **2013**, *5*, 10093–10107.
- [42] M. A. Hood, U. Paiphansiri, D. Schaeffel, K. Koynov, M. Kappl, K. Landfester, R. Muñoz-Espí, *Chem. Mater.* **2015**, *27*, 4311–4318.
- [43] M. Hajir, P. Dolcet, V. Fischer, J. Holzinger, K. Landfester, R. Muñoz-Espí, *J. Mater. Chem.* **2012**, *22*, 5622–5628.
- [44] I. Singh, A. K. Nigam, K. Landfester, R. Muñoz-Espí, A. Chandra, *Appl. Phys. Lett.* **2013**, *103*, 182902.
- [45] B. L. Cushing, V. L. Kolesnichenko, C. J. O’Connor, *Chem. Rev.* **2004**, *104*, 3893–3946.
-

- [46] B. Aslibeiki, P. Kameli, H. Salamati, *J. Magn. Magn. Mater.* **2012**, *324*, 154–160.
- [47] K. Y. van Berkel, C. J. Hawker, *J. Polym. Sci. Part A: Polym. Chem.* **2010**, *48*, 1594–1606.
- [48] T. Trindade, P. O’Brien, N. L. Pickett, *Chem. Mater.* **2001**, *13*, 3843–3858.
- [49] U. Schubert, N. Hüsing, *Synthesis of Inorganic Materials*, Wiley-VCH, Weinheim, 2nd ed., **2005**.
- [50] J. Park, K. An, Y. Hwang, J.-G. Park, H.-J. Noh, J.-Y. Kim, J.-H. Park, N.-M. Hwang, T. Hyeon, *Nat. Mater.* **2004**, *3*, 891–895.
- [51] L. P. Ramírez, K. Landfester, *Macromol. Chem. Phys.* **2003**, *204*, 22–31.
- [52] M. B. Bannwarth, S. W. Kazer, S. Ulrich, G. Glasser, D. Crespy, K. Landfester, *Angew. Chem. Int. Ed.* **2013**, *52*, 10107–10111.
- [53] A. Petri-Fink, H. Hofmann, *IEEE T. Nanobiosci.* **2007**, *6*, 289–297.
- [54] F. Tiarks, K. Landfester, M. Antonietti, *Langmuir* **2001**, *17*, 5775–5780.
- [55] S. Garabagiu, I. Bratu, *Appl. Surf. Sci.* **2013**, *284*, 780–783.
- [56] Y. Kadoma, S. Fujisawa, *Molecules* **2008**, *13*, 2488–2499.
- [57] I. Fuchs, D. Avnir, *Langmuir* **2013**, *29*, 2835–2842.
- [58] A. H. Gröchel, A. Walther, T. I. Löbbling, F. H. Schacher, H. Schmalz, A. H. E. Müller, *Nature* **2013**, *503*, 247–251.
- [59] P. Akcora, H. Liu, S. K. Kumar, J. Moll, Y. Li, B. C. Benicewicz, L. S. Schadler, D. Acehan, A. Z. Panagiotopoulos, V. Pryamitsyn, V. Ganesan, J. Ilavsky, P. Thiyyagarajan, R. H. Colby, J. F. Douglas, *Nat. Mater.* **2009**, *8*, 354–359.
- [60] R. P. Bagwe, L. R. Hilliard, W. Tan, *Langmuir* **2006**, *22*, 4357–4362.
- [61] E. Bourgéat-Lami, N. N. Herrera, J.-L. Putaux, S. Reculosa, A. Perro, S. Ravaine, C. Mingotaud, E. Duguet, *Macromol. Symp.* **2005**, *229*, 32–46.
- [62] J. Fickert, P. Rupper, R. Graf, K. Landfester, D. Crespy, *J. Mater. Chem.* **2012**, *22*, 2286–2291.
- [63] R. Ghosh Chaudhuri, S. Paria, *Chem. Rev.* **2012**, *112*, 2373–2433.
- [64] A. Philipse, A. Vrij, *J. Colloid Interface Sci.* **1989**, *128*, 121–136.
- [65] H. Wang, P. Xu, S. Meng, W. Zhong, W. Du, Q. Du, *Polym. Degrad. Stab.* **2006**, *91*, 1455–1461.
- [66] V. I. Klimov, A. A. Mikhailovsky, S. Xu, A. Malko, J. A. Hollingsworth, C. A. Leatherdale, H.-J. Eisler, M. G. Bawendi, *Science* **2000**, *290*, 314–317.

-
- [67] H. C. Leventis, S. P. King, A. Sudlow, M. S. Hill, K. C. Molloy, S. A. Haque, *Nano Lett.* **2010**, *10*, 1253–1258.
- [68] G. H. Gao, G. H. Im, M. S. Kim, J. W. Lee, J. Yang, H. Jeon, J. H. Lee, D. S. Lee, *Small* **2010**, *6*, 1201–1204.
- [69] Y. Mori, H. Kawaguchi, *Colloids Surf. B* **2007**, *56*, 246–254.
- [70] H. Zou, S. Wu, J. Shen, *Chem. Rev.* **2008**, *108*, 3893–3957.
- [71] Y.-L. Liu, C.-Y. Hsu, K.-Y. Hsu, *Polymer* **2005**, *46*, 1851–1856.
- [72] M. M. Demir, G. Wegner, *Macromol. Mater. Eng.* **2012**, *297*, 838–863.
- [73] N. Steiert, K. Landfester, *Macromol. Mater. Eng.* **2007**, *292*, 1111–1125.
- [74] F. Tiarks, K. Landfester, M. Antonietti, *Macromol. Chem. Phys.* **2001**, *202*, 51–60.
- [75] M. Klapper, C. G. Clark Jr, K. Müllen, *Polym. Int.* **2008**, *57*, 181–202.
- [76] A. Jordan, P. Wust, R. Scholz, B. Tesche, H. Fahling, T. Mitrovics, T. Vogl, J. Cervos-Navarro, R. Felix, *Int. J. Hyperthermia* **1996**, *12*, 705–722.
- [77] Y. Jiao, N. Ubrich, M. Marchand-Arvier, C. Vigneron, M. Hoffman, T. Lecompte, P. Maincent, *Circulation* **2002**, *105*, 230–235.
- [78] D. Wang, J. Zhu, Q. Yao, C. A. Wilkie, *Chem. Mater.* **2002**, *14*, 3837–3843.
- [79] E. Duguet, M. Abboud, F. Morvan, P. Maheu, M. Fontanille, *Macromol. Symp.* **2000**, *151*, 365–370.
- [80] X. Huang, W. J. Brittain, *Macromolecules* **2001**, *34*, 3255–3260.
- [81] F. Corcos, E. Bourgéat-Lami, C. Novat, J. Lang, *Colloid Polym. Sci.* **1999**, *277*, 1142–1151.
- [82] A. R. Mahdavian, M. Ashjari, A. B. Makoo, *Eur. Polym. J.* **2007**, *43*, 336–344.
- [83] P. J. Colver, C. A. L. Colard, S. A. F. Bon, *J. Am. Chem. Soc.* **2008**, *130*, 16850–16851.
- [84] S. Reculosa, C. Poncet-Legrand, S. Ravaine, C. Mingotaud, E. Duguet, E. Bourgéat-Lami, *Chem. Mater.* **2002**, *14*, 2354–2359.
- [85] J. M. Asua, *Macromol. Chem. Phys.* **2014**, 458–464.
- [86] K. Landfester, N. Bechthold, F. Tiarks, M. Antonietti, *Macromolecules* **1999**, *32*, 5222–5228.
- [87] A. Schoth, C. Wagner, L. L. Hecht, S. Winzen, R. Muñoz-Espí, H. P. Schuchmann, K. Landfester, *Colloid Polym. Sci.* **2014**, *292*, 2427–2437.
- [88] A. Bonnefond, M. Micusik, M. Paulis, J. R. Leiza, R. F. A. Teixeira, S. A. F. Bon, *Colloid Polym. Sci.* **2012**, *291*, 167–180.
-

- [89] N. Nabih, U. Herrmann, G. Glasser, I. Lieberwirth, K. Landfester, A. Taden, *Prog. Org. Coat.* **2013**, *76*, 555–562.
- [90] H. Dong, V. Mantha, K. Matyjaszewski, *Chem. Mater.* **2009**, *21*, 3965–3972.
- [91] T. Fröschl, U. Hörmann, P. Kubiak, G. Kucerova, M. Pfanzelt, C. K. Weiss, R. J. Behm, N. Hüsing, U. Kaiser, K. Landfester, M. Wohlfahrt-Mehrens, *Chem. Soc. Rev.* **2012**, *41*, 5313–5360.
- [92] Y. Gao, Y. Song, Q. Zheng, *Colloids Surf. A* **2012**, *411*, 40–49.
- [93] L. L. Hecht, M. Winkelmann, C. Wagner, K. Landfester, W. Gerlinger, B. Sachweh, H. P. Schuchmann, *Chem. Eng. Technol.* **2012**, *35*, 1670–1676.
- [94] T. Staudt, T. O. Machado, N. Vogel, C. K. Weiss, P. H. H. Araujo, C. Sayer, K. Landfester, *Macromol. Chem. Phys.* **2013**, *214*, 2213–2222.
- [95] X. Qiao, M. Chen, J. Zhou, L. Wu, *J. Polym. Sci. Part A: Polym. Chem.* **2007**, *45*, 1028–1037.
- [96] M. Urban, A. Musyanovych, K. Landfester, *Macromol. Chem. Phys.* **2009**, *210*, 961–970.
- [97] Z. Z. Xu, C. C. Wang, W. L. Yang, Y. H. Deng, S. K. Fu, *J. Magn. Magn. Mater.* **2004**, *277*, 136–143.
- [98] K. Wormuth, *J. Colloid Interface Sci.* **2001**, *241*, 366–377.
- [99] Y.-D. Luo, C.-A. Dai, W.-Y. Chiu, *J. Polym. Sci. Part A: Polym. Chem.* **2008**, *46*, 8081–8090.
- [100] S. Abdolbaghi, S. Pourmahdian, Y. Saadat, *Colloid Polym. Sci.* **2014**, *292*, 1091–1097.
- [101] A. P. Romio, H. H. Rodrigues, A. Peres, A. Da Cas Viegas, E. Kobitskaya, U. Ziener, K. Landfester, C. Sayer, P. H. H. Araujo, *J. Appl. Polym. Sci.* **2013**, *129*, 1426–1433.
- [102] A. Hamberger, U. Ziener, K. Landfester, *Macromol. Chem. Phys.* **2013**, *214*, 691–699.
- [103] R. H. Staff, I. Lieberwirth, K. Landfester, D. Crespy, *Macromol. Chem. Phys.* **2012**, *213*, 351–358.
- [104] C. Kaewsaneha, P. Tangboriboonrat, D. Polpanich, M. Eissa, A. Elaissari, *J. Colloid Interface Sci.* **2013**, *409*, 66–71.
- [105] G. Mistlberger, A. L. Medina-Castillo, S. M. Borisov, T. Mayr, A. Fernández-Gutiérrez, J. F. Fernandez-Sanchez, I. Klimant, *Microchim. Acta* **2011**, *172*, 299–308.
- [106] Y.-Y. Yu, C.-Y. Chen, W.-C. Chen, *Polymer* **2003**, *44*, 593–601.
- [107] L. L. Hecht, A. Schoth, R. Muñoz-Espí, A. Javadi, K. Köhler, R. Miller, K. Landfester, H. P. Schuchmann, *Macromol. Chem. Phys.* **2013**, *214*, 812–823.

-
- [108] L. L. Hecht, T. Merkel, A. Schoth, C. Wagner, K. Köhler, R. Muñoz-Espí, K. Landfester, H. P. Schuchmann, *Chem. Eng. J.* **2013**, *229*, 206–216.
- [109] L. J. Gonzalez-Ortiz, J. M. Asua, *Macromolecules* **1995**, *28*, 3135–3145.
- [110] T. Gong, D. Yang, J. Hu, W. Yang, C. Wang, J. Q. Lu, *Colloids Surf. A* **2009**, *339*, 232–239.
- [111] M. J. Percy, C. Barthet, J. C. Lobb, M. A. Khan, S. F. Lascelles, M. Vamvakaki, S. P. Armes, *Langmuir* **2000**, *16*, 6913–6920.
- [112] D. Dupin, A. Schmid, J. A. Balmer, S. P. Armes, *Langmuir* **2007**, *23*, 11812–11818.
- [113] F. F. Fang, J. H. Kim, H. J. Choi, C. A. Kim, *Colloid Polym. Sci.* **2009**, *287*, 745–749.
- [114] Z. Xu, A. Xia, C. Wang, W. Yang, S. Fu, *Mater. Chem. Phys.* **2007**, *103*, 494–499.
- [115] J. H. Chen, C.-Y. Cheng, W.-Y. Chiu, C.-F. Lee, N.-Y. Liang, *Eur. Polym. J.* **2008**, *44*, 3271–3279.
- [116] J. Jeng, T.-Y. Chen, C.-F. Lee, N.-Y. Liang, W.-Y. Chiu, *Polymer* **2008**, *49*, 3265–3271.
- [117] X. Song, Y. Zhao, H. Wang, Q. Du, *Langmuir* **2009**, *25*, 4443–4449.
- [118] Y. Zhao, G. Yin, Z. Zheng, H. Wang, Q. Du, *J. Polym. Sci. Part A: Polym. Chem.* **2011**, *49*, 5257–5269.
- [119] M. J. Percy, S. P. Armes, *Langmuir* **2002**, *18*, 4562–4565.
- [120] F. F. Fang, H. J. Choi, Y. Seo, *J. Nanosci. Nanotechnol.* **2010**, *10*, 285–289.
- [121] J. Zhang, X. Ge, M. Wang, J. Yang, Q. Wu, M. Wu, N. Liu, Z. Jin, *Chem. Commun.* **2010**, *46*, 4318–4320.
- [122] A. Walther, M. Hoffmann, A. H. E. Müller, *Angew. Chem. Int. Ed.* **2008**, *47*, 711–714.
- [123] T. Li, H. Liu, L. Zeng, W. Miao, Y. Wu, *Colloid Polym. Sci.* **2011**, *289*, 1543–1551.
- [124] M. Chen, S. Zhou, B. You, L. Wu, *Macromolecules* **2005**, *38*, 6411–6417.
- [125] Z. Yuhong, Z. Qichao, S. Xingwang, T. Qingqiong, C. Min, W. Limin, *J. Colloid Interface Sci.* **2009**, *336*, 544–550.
- [126] D. J. Voorn, W. Ming, A. M. van Herk, *Macromolecules* **2006**, *39*, 2137–2143.
- [127] S. A. F. Bon, P. J. Colver, *Langmuir* **2007**, *23*, 8316–8322.
- [128] E. T. A. van den Dungen, J. Galineau, P. C. Hartmann, *Macromol. Symp.* **2012**, *313–314*, 128–134.
- [129] A. Schrade, Z. Cao, K. Landfester, U. Ziener, *Langmuir* **2011**, *27*, 6689–6700.
- [130] B. Kang, A. Schrade, Y. Xu, Y. Chan, U. Ziener, *Langmuir* **2012**, *28*, 9347–9354.
-

- [131] K. González-Matheus, G. P. Leal, C. Tollan, J. M. Asua, *Polymer* **2013**, *54*, 6314–6320.
- [132] Z. Cao, A. Schrade, K. Landfester, U. Ziener, *J. Polym. Sci. Part A: Polym. Chem.* **2011**, *49*, 2382–2394.
- [133] N. Zgheib, J.-L. Putaux, A. Thill, F. Agosto, M. Lansalot, E. Bourgéat-Lami, *Langmuir* **2012**, *28*, 6163–6174.
- [134] S. C. Thickett, N. Wood, Y. H. Ng, P. B. Zetterlund, *Nanoscale* **2014**, 8590–8594.
- [135] S. A. F. Bon, T. Chen, *Langmuir* **2007**, *23*, 9527–9530.
- [136] K. González-Matheus, G. P. Leal, J. M. Asua, *Part. Part. Syst. Char.* **2014**, *31*, 94–100.
- [137] R. Miller, V. B. Fainerman, V. I. Kovalchuk, D. O. Grigoriev, M. E. Leser, M. Michel, *Adv. Colloid Interface Sci.* **2006**, *128–130*, 17–26.
- [138] S. Simovic, C. A. Prestidge, *Langmuir* **2008**, *24*, 7132–7137.
- [139] B. P. Binks, J. H. Clint, C. P. Whitby, *Langmuir* **2005**, *21*, 5307–5316.
- [140] L. Duan, M. Chen, S. Zhou, L. Wu, *Langmuir* **2009**, *25*, 3467–3472.
- [141] K. Zhang, W. Wu, K. Guo, J. Chen, P. Zhang, *Langmuir* **2010**, *26*, 7971–7980.
- [142] J. Goldstein, D. E. Newbury, D. C. Joy, C. E. Lyman, P. Echlin, E. Lifshin, L. Sawyer, J. R. Michael, *Scanning Electron Microscopy and X-ray Microanalysis*, Springer, New York, 3rd ed., **2007**.
- [143] S. L. Flegler, J. W. Heckman, *Scanning and Transmission Electron Microscopy: An Introduction*, Oxford University Press, Oxford, 2nd ed., **1997**.
- [144] W. Schärtl, *Light Scattering from Polymer Solutions and Nanoparticle Dispersions*, Springer, Berlin, **2007**.
- [145] A. Schoth, Diploma Thesis, Johannes Gutenberg-Universität, Mainz, **2012**.
- [146] S. P. Stodghill, A. E. Smith, J. H. O’Haver, *Langmuir* **2004**, *20*, 11387–11392.
- [147] P. Somasundaran, T. W. Healy, D. W. Fuerstenau, *J. Phys. Chem.* **1964**, *68*, 3562–3566.
- [148] J. H. Harwell, J. C. Hoskins, R. S. Schechter, W. H. Wade, *Langmuir* **1985**, *1*, 251–262.
- [149] K. Teshima, H. Sugimura, Y. Inoue, O. Takai, *Langmuir* **2003**, *19*, 8331–8334.
- [150] J.-J. Max, C. Chapados, *J. Chem. Phys.* **2009**, *131*, 184505.
- [151] J. M. Ramos-Fernández, C. Guillem, A. Lopez-Buendia, M. Paulis, J. M. Asua, *Prog. Org. Coat.* **2011**, *72*, 438–442.

- [152] L. L. Hecht, C. Wagner, K. Landfester, H. P. Schuchmann, *Langmuir* **2011**, *27*, 2279–2285.
- [153] L. L. Hecht, C. Wagner, Ö. Özcan, F. Eisenbart, K. Köhler, K. Landfester, H. P. Schuchmann, *Macromol. Chem. Phys.* **2012**, *213*, 2165–2173.
- [154] H. P. Grace, *Chem. Eng. Commun.* **1982**, *14*, 225–277.
- [155] N. Bechthold, K. Landfester, *Macromolecules* **2000**, *33*, 4682–4689.
- [156] Y. T. Choi, M. S. El-Aasser, E. D. Sudol, J. W. Vanderhoff, *J. Polym. Sci. Part A: Polym. Chem.* **1985**, *23*, 2973–2987.
- [157] P. J. Blythe, A. Klein, J. A. Phillips, E. D. Sudol, M. S. El-Aasser, *J. Polym. Sci. Part A: Polym. Chem.* **1999**, *37*, 4449–4457.
- [158] A. Ziegler, K. Landfester, A. Musyanovych, *Colloid Polym. Sci.* **2009**, *287*, 1261–1271.
- [159] W. D. Harkins, *J. Am. Chem. Soc.* **1947**, *69*, 1428–1444.
- [160] N. Bechthold, PhD thesis, Universität Potsdam, Golm, **2000**.
- [161] T. Kietzke, D. Neher, K. Landfester, R. Montenegro, R. Güntner, U. Scherf, *Nat. Mater.* **2003**, *2*, 408–412.
- [162] K. G. Neoh, E. T. Kang, *Polym. Chem.* **2011**, *2*, 747–759.
- [163] A. Schoth, E. S. Adurahim, M. A. Bahattab, K. Landfester, R. Muñoz-Espí, *Macromol. React. Eng.* **2015**, DOI 10.1002/mren.201500029.
- [164] N. P. Ashby, B. P. Binks, *Phys. Chem. Chem. Phys.* **2000**, *2*, 5640–5646.
- [165] S. L. Tawari, D. L. Koch, C. Cohen, *J. Colloid Interface Sci.* **2001**, *240*, 54–66.
- [166] A. Schoth, K. Landfester, R. Muñoz-Espí, *Langmuir* **2015**, *31*, 3784–3788.
- [167] M. M. Farid, A. M. Khudhair, S. A. K. Razack, S. Al-Hallaj, *Energ. Convers. Manage.* **2004**, *45*, 1597–1615.
- [168] A. Abhat, *Sol. Energy* **1983**, *30*, 313–332.

A. List of Figures

2.1. Coalescence and Ostwald ripening lead to a growth of the average droplet diameter and diminish the number of droplets.	4
2.2. Surfactants prevent the collision of droplets by electrostatic and steric stabilization.	5
2.3. Suppression of Ostwald ripening by the addition of an osmotic agent.	6
2.4. The contact angle of particles at the oil/water interface is crucial for their ability to stabilize oil-in-water (O/W) or water-in-oil (W/O) emulsions. . . .	8
2.5. Resulting morphologies for different combinations of spreading coefficients s_i . . .	10
2.6. Functionalization of silica nanoparticles with trimethoxysilanes	16
2.7. Scheme for the preparation of polymer/silica hybrid particles by the miniemulsion polymerization technique.	17
2.8. Scheme for the preparation of polymer/silica hybrid particles by the miniemulsion solvent evaporation technique.	19
2.9. Influence of the interfacial tensions on the morphology of polymer/inorganic hybrid nanoparticles synthesized in miniemulsion.	20
3.1. Schematic description of an isothermal titration calorimeter.	26
4.1. Isothermal titration curve of added CTMA-Cl solution to a Ludox TMA silica particles dispersion.	29
4.2. Thermogravimetric analyses of differently modified Ludox TMA particles. . .	30
4.3. Thermogravimetric analyses of CTMA-Cl- and MPS-modified Ludox TMA particles before and after purification.	31
4.4. FTIR spectra of Ludox TMA particles before and after functionalization with MPS.	31
4.5. TEM images of miniemulsion dispersions containing CTMA-Cl-modified Ludox TMA particles in PMMA and PMMA- <i>co</i> -4VP.	33
4.6. DLS measurements of hybrid nanoparticles with differently functionalized Ludox TMA particles.	34
4.7. TEM and SEM images of PMMA/MPS-silica composite particles, synthesized with a silica content of 20 wt.% and 40 wt.%.	35
4.8. TEM and SEM images of PMMA/ODTMS-silica composite particles, synthesized with a silica content of 20 wt.%.	35
4.9. Calorimetric curves of the polymerization of PMMA miniemulsions containing different amounts of MPS- and ODTMS-functionalized Ludox TMA particles. .	37
4.10. TEM and SEM images of PMMA/silica composite particles, synthesized via the solvent evaporation approach.	38
4.11. Schematic description of oleic acid-functionalized magnetite nanoparticles. . .	40

4.12. Thermogravimetric analysis of magnetite nanoparticles with different surface functionalizations.	41
4.13. Thermogravimetric analysis of magnetite nanoparticles functionalized by different carboxylic acids.	41
4.14. TGA traces of hybrid nanoparticles containing differently functionalized magnetite nanoparticles and different polymers.	43
4.15. Transmission and scanning electron micrographs of differently functionalized magnetite nanoparticles in PMMA before and after magnetic purification. . .	46
4.16. Transmission and scanning electron micrographs of differently functionalized magnetite nanoparticles in polystyrene before and after magnetic purification. .	47
4.17. Transmission and scanning electron micrographs of differently functionalized magnetite nanoparticles in poly(styrene- <i>co</i> -4VP) before and after magnetic purification.	48
4.18. Schematic description of the preparation of hybrid films by miniemulsion polymerization.	50
4.19. Thermogravimetric analyses of hybrid particles with different polymer compositions and differently functionalized silica particles.	51
4.20. Transmission electron micrographs of hybrid nanoparticles with a BMA/MMA ratio of 1:2 and differently functionalized silica particles.	52
4.21. Particle size of hybrid particles with different compositions as determined by DLS.	53
4.22. Scanning electron micrographs of hybrid particles with a BMA:MMA ratio of 1:2 and differently functionalized silica particles before and after tempering. .	55
4.23. Photographs of hybrid particles with a BMA:MMA ratio of 1:2 as dispersions and as dry films after tempering.	56
4.24. TEM and SEM images of PMMA/silica hybrid nanocapsules containing hexadecane as liquid core, synthesized via miniemulsion polymerization.	58
4.25. TEM and SEM images of PMMA/silica hybrid nanocapsules containing hexadecane as liquid core, synthesized via solvent evaporation.	60
4.26. Scanning electron micrograph of clay-stabilized polystyrene nanoparticles. . .	62
4.27. Scanning electron micrographs of particles stabilized with Ludox TMA. . . .	63
4.28. Thermogravimetric analyses of differently functionalized Ludox TMA silica nanoparticles.	64
4.29. Preparation of Pickering miniemulsions consisting of water, NaCl, silica particles and cyclohexane.	66
4.30. TEM and SEM images of PU nanocapsules containing water without and with 2.5 wt.% sodium chloride.	67

4.31. Size distribution of salt-free PU capsules compared to capsules containing 2.5 wt.% NaCl.	67
4.32. Thermogravimetric analyses of PU/silica nanocapsules without and with 2.5 wt.% of sodium chloride.	67
4.33. Fluorescence intensities of the fluorescent dye SR101 in a redispersed nanocapsule dispersion and the supernatant solution after centrifugation.	68
4.34. TEM and SEM images of PU nanocapsules containing 5 wt.% of sodium sulfate.	69
4.35. TEM image and size distribution of PU nanocapsules containing 20 wt.% of sodium sulfate.	69
4.36. Thermal analyses of PU nanocapsules containing 20 wt.% of sodium sulfate. .	70

B. List of Tables

4.1. Compositions of polymer/silica hybrid nanoparticles via the miniemulsion polymerization process.	32
4.2. Solid contents of the dispersions, magnetite contents of the hybrid particles and particle diameters of differently synthesized hybrid particles before and after magnetic purification.	43
4.3. Physical properties of hybrid particles with different compositions.	52
4.4. Compositions and sizes of nanocapsules synthesized via miniemulsion polymerization.	57
4.5. Compositions and sizes of nanocapsules synthesized via solvent evaporation. .	59
4.6. Compositions of Pickering-stabilized nanoparticles.	62
4.7. Compositions of Pickering-stabilized nanocapsules.	70
4.8. Structures of hybrid nanomaterials achievable in miniemulsion systems by using different surface functionalization agents.	71
4.9. Structures of hybrid nanomaterials via Pickering-stabilized miniemulsions. . .	73

C. Abbreviations and Symbols

γ	Interfacial tension
Π_{osm}	Osmotic pressure
Θ	Contact angle
A	Interfacial area
c	Concentration
M	Molecular weight
p_L	Laplace pressure
R	Universal gas constant
r	Radius
T	Temperature
4-VP	4-Vinylpyridine
BMA	Butyl methacrylate
cmc	Critical micellar concentration
CTMA-Cl	Cetyl trimethylammonium chloride
DLS	Dynamic light scattering
DSC	Differential scanning calorimetry
FTIR	Fourier transform infrared spectroscopy
GPC	Gel permeation chromatography
ITC	Isothermal titration calorimetry
MA	Methacrylic acid
MMA	Methyl methacrylate
MPS	3-Methacryloyloxypropyl trimethoxysilane
OA	Oleic acid
ODTMS	Octadecyl trimethoxysilane
PCM	Phase change material
PMMA	Poly(methyl methacrylate)
PTMS	Propyl trimethoxysilane
PU	Poly urethane
SDS	Sodium dodecyl sulfate
SEM	Scanning electron microscopy
SR101	Sulforhodamine 101
TDI	Toluene diisocyanate
TEM	Transmission electron microscopy
TGA	Thermogravimetric analysis
V59	2,2'-Azobis(2-methylbutyronitrile)

D. Acknowledgments

E. Curriculum Vitae

F. Scientific Contributions

F.1. Publications

- **Structure Control in PMMA/Silica Hybrid Nanoparticles by Surface Functionalization**
A. Schoth, C. Wagner, L. L. Hecht, S. Winzen, R. Muñoz-Espí, H. P. Schuchmann, K. Landfester
Colloid Polym. Sci. **2014**, *292*, 2427–2437
- **Surfactant-Free Polyurethane Nanocapsules via Inverse Pickering Miniemulsion**
A. Schoth, K. Landfester, R. Muñoz-Espí
Langmuir **2015**, *31*, 3784–3788
- **Waterborne Polymer/Silica Hybrid Nanoparticles and their Structure in Coatings**
A. Schoth, E.S. Adurahim, M.A. Bahattab, K. Landfester, R. Muñoz-Espí
Macromol. React. Eng. **2015**, DOI: 10.1002/mren.201500029
- **Silanization as a Versatile Functionalization Method for the Synthesis of Polymer/Magnetite Hybrid Nanoparticles with Controlled Structure**
A. Schoth, A.D. Keith, K. Landfester, R. Muñoz-Espí
in preparation
- **Determination of the Ideal Surfactant Concentration in Miniemulsion Polymerization**
L. L. Hecht, A. Schoth, R. Muñoz-Espí, A. Javadi, K. Köhler, R. Miller, K. Landfester, H. P. Schuchmann
Macromol. Chem. Phys. **2013**, *214*, 812–823
- **Emulsification of Particle Loaded Droplets with Regard to Miniemulsion Polymerization**
L. L. Hecht, T. Merkel, A. Schoth, C. Wagner, K. Köhler, R. Muñoz-Espí, K. Landfester, H. P. Schuchmann
Chem. Eng. J. **2013**, *229*, 206–216

- **Continuous Preparation of Polymer/Inorganic Composite Nanoparticles via Miniemulsion Polymerization**

T. Merkel, L. L. Hecht, A. Schoth, C. Wagner, R. Muñoz-Espí, K. Landfester, H. P. Schuchmann

in *Colloid Process Engineering* (Eds.: M. Kind, W. Peukert, H. Rehage, H.P. Schuchmann), Springer International Publishing, **2015**, 345–370

F.2. Presentations

- **Universidade Federal de Santa Catarina**

Oral presentation

“Morphology Control in Polymeric/Inorganic Hybrid Nanoparticles”

November 2013, Florianópolis, Brazil

- **10th Zsigmondy Colloquium of the German Colloid Society**

Oral presentation

“Tailoring the Structure of Inorganic/Polymeric Hybrid Nanoparticles”

April 2014, Konstanz, Germany

- **15th Conference of the International Association of Colloid and Interface Scientists (IACIS)**

Poster presentation

“Polymer/Inorganic Hybrid Materials: Structure Control in Miniemulsion”

May 2015, Mainz, Germany

Awarded the “Best Poster Award”

- **Advanced Materials World Congress**

Oral presentation

“Tailoring the Structure of Polymer/Inorganic Hybrid Nanoparticles”

August 2015, Stockholm, Sweden